

A systems biology approach to dynamic modelling of the AMP-activated kinase pathway

Dissertation

zur

Erlangung des akademischen Grades

Doktor-Ingenieur (Dr.-Ing.)

Promotionsgebiet Systembiologie

Fakultät für Informatik und Elektrotechnik

Universität Rostock

**Universität
Rostock**



Traditio et Innovatio

vorgelegt von

Simone Frey, geboren am 31. August 1980 in Köln, wohnhaft in Rostock

Rostock, April 2011

urn:nbn:de:gbv:28-diss2011-0135-1

Gutachter:

Prof. Olaf Wolkenhauer (PhD) (Universität Rostock)

Prof. Dr. Ursula Kummer (Universität Heidelberg)

Prof. Dr. Mattias Goksör (University of Gothenburg)

Tag der Verteidigung: 12. Juli 2011

Abstract

Responding to changes in the intra and extracellular environment is a fundamental property of living organisms enabling them to adapt and survive. The information transfer in cells is accomplished through complex networks of interacting proteins. Dysfunctions in the transmission process can lead to various diseases, such as obesity or cancer. Thus, gaining information on the interrelations of the components of signalling pathways has become a focus in biomedical and drug development. The focus of this work is on cell signalling in the context of energy sensing, which is linked to glucose uptake and metabolism.

One pathway, which is an important energy sensor, is the AMPK signalling pathway controlling various metabolic processes. In this work, a systems biology approach is presented that consists of iterative cycles between data-driven modelling and model-driven experimentation. A mathematical model composed of ordinary differential equations is established to investigate the AMPK pathway homologue in the yeast *Saccharomyces cerevisiae*, the Snf1 pathway. Therefore, at first the definition of a glucose-regulated stimulus is derived requiring information of the mechanisms of glucose transport across the membrane. The data of the Snf1 pathway component Mig1 is generated by fluorescent microscopy, which suffers from bleaching effects and background noise. The processing of this data is realised through the development of a mathematical approach, which extracts the GFP-tagged Mig1 data from background noises while taking account for bleaching effects and predicting the dynamics of Mig1. The extracted information of the processed fluorescent data, the derived glucose-regulated signal, and the Snf1 Western blot data are then combined in order to compare those data to the simulations of the alternative network structures suggested to underly the Snf1 pathway. The simulations indicate that certain network structures can be excluded from the list of candidate structures describing the dynamics of the Snf1 pathway.

In the second part of this thesis, signalling pathways are considered in a more general setting using quantitative measures to characterise them. Quantitative measures have become a useful tool to describe the dynamic properties of the components of signalling pathways, such as the average time until activation or the average duration of remaining in an activated state. An optimality criterion is defined, based on quantitative measures, to analyse the characteristic design of a MAPK pathway and to compare the consequences of model approximations. Comparisons with single and triple phosphorylated structures showed that the design of a MAPK pathway is favourable for pathways that realise the transmission of fast signals with short duration.

Zusammenfassung

Ein wichtiges Merkmal aller Lebensformen ist ihre Fähigkeit, intra- und extrazelluläre Veränderungen in Form von Signalen, zum Beispiel in Ionenkonzentrationen, Hormonen oder Nährstoffen, zu erfassen und sich ihnen anpassen zu können. Dieser Prozess wird durch biochemische Reaktionsnetzwerke bestehend aus interagierenden Proteinen realisiert. Ein Beispiel für ein solches Netzwerk ist der AMPK Signalweg, der eine bedeutende Rolle im Gleichgewicht des Energiehaushalts spielt, indem er bei Energiemangel katabolische Vorgänge mobilisiert, anabolische hingegen versucht einzusparen. Fehlfunktionen dieses Signalwegs können zu Diabetes Typ 2 und Fettleibigkeit führen.

In dieser Arbeit wurde ein systembiologischer Ansatz, bestehend aus mehreren Iterationen aus Modellierung und Experimenten, zur Untersuchung des Snf1 Signalwegs verwendet. Dabei wurde zuerst ein glukoseinduziertes Eingangssignal zur Snf1 Regulation hergeleitet. Zur Aufbereitung von Fluoreszenzmikroskopiedaten der Snf1 Signalwegkomponente Mig1, wurde ein mathematisches Modell erstellt. Fluoreszenzmikroskopiedaten sind mit unerwünschten Nebeneffekten, wie Leuchten von Hintergrundmolekülen und Ausbleicheffekten behaftet. Das erstellte mathematische Modell ermöglicht es, die Fluoreszenzintensität der Hintergrundmoleküle abzuziehen und die Ausbleichrate der Hintergrundmoleküle und die der Mig1-GFP-Proteine zu bestimmen und zu kompensieren, so dass Vorhersagen über die Dynamik von Mig1 gemacht werden können, wie sie ohne diese Nebeneffekte auftreten würden. Die aufbereiteten Daten wurden zusammen mit dem hergeleiteten Eingangssignal und Snf1 Western Blot Daten zur Analyse mehrerer alternativer Snf1 Netzwerkstrukturen verwendet. Dabei wurde gezeigt, dass ein zusätzlicher glukoseregulierender Schritt für die Regulation des Snf1 Signalwegs erforderlich ist.

Quantitative Maße können zur Charakterisierung der Dynamik von Komponenten eines Signalwegs angewendet werden. Beispiel sind die mittlere Dauer, die eine Komponente aktiviert bleibt oder die mittlere Zeit, die sie braucht, um aktiviert zu werden. Die Beschreibung solcher Eigenschaften ist nützlich, um Konsequenzen unterschiedlicher Netzwerkstrukturen aufdecken zu können. Bei Krankheit der Zelle sind solche Eigenschaften unter Umständen verändert. Im zweiten Teil dieser Arbeit werden ausgehend von der charakteristischen Kaskadenstruktur eines MAPK Signalweges, bestehend aus drei Ebenen und zwei Doppelphosphorylierungen, Signalwegsstrukturen mit Hilfe von quantitativen Maßen untersucht und verglichen. Dabei wurde unter Berücksichtigung der MAPK spezifischen Verstärkung gezeigt, dass die Struktur der MAPK Kaskade daraufhin ausgerichtet sein könnte, ein Eingangssignal mit schneller Aktivitätszeit und kurzer Dauer zu übertragen.

Contents

Abstract	i
List of Figures	ix
List of Tables	xi
Acronyms	xii
List of Symbols	xv
1. Introduction	1
1.1. Signal transduction pathways	1
1.1.1. The AMP-activated kinase pathway	3
1.1.2. The AMPK counterpart in <i>Saccharomyces cerevisiae</i> : Snf1	3
1.1.3. MAPK cascades	4
1.2. Mathematical modelling of signal transduction pathways	4
1.3. Technologies for data generation	6
1.3.1. Western blotting	7
1.3.2. Fluorescence microscopy	7
1.4. Glucose uptake and metabolism in yeast	7
1.4.1. Hexose transport	8
1.4.2. Respiration and fermentation	8
1.5. Quantitative measures	9
1.6. Aims and objectives	9
1.7. Outline of this thesis	10
2. Biological background of the AMP-activated kinase pathway	13
2.1. The adenosine monophosphate activated protein kinase (AMPK)	14
2.2. Malfunctions of the AMPK pathway	17
2.3. The AMPK counterpart in <i>Saccharomyces cerevisiae</i> : Snf1	19
2.4. Glucose consumption in yeast: Hexose transporters	22
2.5. Summary	24

3. Mathematical modelling of the Snf1 pathway	27
3.1. Dynamics of hexose transporters in <i>S. cerevisiae</i> upon glucose pulses	27
3.1.1. Materials and methods	28
3.1.2. The carrier model for glucose transport	30
3.1.3. Dynamic contribution of hexose transporters	32
3.1.4. Dynamic contribution of high and low affinity transporters	33
3.1.5. Applications of the model	38
3.1.6. Conclusions	39
3.2. Data processing for the Snf1 pathway component Mig1	42
3.2.1. Materials and methods	43
3.2.2. Results	48
3.2.3. Discussion	55
3.3. Snf1 pathway modelling	57
3.3.1. Alternative Snf1 pathway models	57
3.3.2. Snf1 pathway models	59
3.3.3. Snf1 pathway models with a two-step regulation for Snf1	64
3.3.4. Snf1 pathway models with a two-step regulation for Mig1	66
3.4. Summary	72
4. Quantitative measures for signalling pathways	75
4.1. The need for quantitative measures	75
4.2. Quantitative measures for general systems	77
4.3. Extension to signals with a non-zero basal level	79
4.4. Quantitative measures for weakly activated systems	82
4.5. Restrictions for weakly activated systems	83
4.6. An optimality criterion	86
4.7. Consequences of approximations	87
4.8. Summary	90
5. Application of quantitative measures to the MAPK cascade	91
5.1. The two double phosphorylations within the MAPK cascade	91
5.2. Applying quantitative measures to the MAPK cascade	92
5.3. Summary	95
6. Conclusions	97
Appendix	100
A. Parameters for the Snf1 models	101

B. Models of the MAPK cascade	105
B.1. Huang and Ferrell	105
B.2. Kholodenko	106
B.3. Heinrich et al.	106
B.4. Relation between the kinetic parameters	107
B.5. Properties of the external stimulus	109
Publications	132
Selbständigkeitserklärung	133
Theses for the doctoral research	134

List of Figures

1.1. Scheme of a signal transduction pathway	2
1.2. MAPK cascade	5
2.1. AMPK network	14
2.2. Snf1 network	19
2.3. Glucose sensing and signalling in <i>S. cerevisiae</i>	24
3.1. Carrier model	31
3.2. Consolidated contribution model	32
3.3. High and low affinity transporter model	35
3.4. Simulations of glucose consumptions for all batch experiments	36
3.5. High and low affinity transporters at steady-state conditions	37
3.6. Simulations of Snf1	41
3.7. Schematic representation of the microfluidic flow system	44
3.8. <i>S. cerevisiae</i> cells expressing Mig1-GFP and Nrd1-mCherry	46
3.9. Experiments with a changing environment	47
3.10. Contributions to the fluorescent signal of the nucleus	49
3.11. Simulation of background experiments	50
3.12. Simulation of the background bleaching experiments	51
3.13. Simulation of environmental change experiments	54
3.14. Simulation of Mig1 and Mig1P	55
3.15. Mig1 model validation	56
3.16. Snf1 pathway network structure	59
3.17. Glucose profiles for Snf1-pathway models	60
3.18. Snf1 data and simulations of Snf1 pathway models	63
3.19. Kinase and phosphatase rates of Snf1 models	64
3.20. Simulations and data for nuclear intensities (Snf1 model)	65
3.21. Two-step Snf1 network structure	66
3.22. Simulations and data for nuclear intensities (two-step Snf1 models)	68
3.23. Two-step Mig1 network structure	69
3.24. Simulations and data for nuclear intensities (two-step Mig1 models)	71

4.1. A three level cascade	77
4.2. Quantitative measures	79
4.3. Simulation of a sequential phosphorylation cascade	80
4.4. Amplification in a Hg and Hw model	84
4.5. Comparing model approaches with τ and ϑ	89
5.1. Optimality criterion for MAPK cascade	93
5.2. Comparison of cascades differing in lengths	94

List of Tables

3.1. Glucose pulse experiments	29
3.2. Parameters of the transporter models	40
3.3. Parameters for Mig1-GFP data processing	53
3.4. List of ODEs for Snf1 models	62
3.5. List of ODEs for the two-step models for Snf1 regulation	67
3.6. List of ODEs for the two-step models for Mig1 regulation	70
4.1. Three model approximations	88
A.1. Parameters for Snf1 models	101
A.2. Parameters for the two-step Snf1 models	102
A.3. Parameters for the two-step Mig1 models	103

Acronyms

ACC	Acetyl-CoA carboxylase
ADP	Adenosine diphosphate
AICAR	5-Aminoimidazole-4-carboxamide-1- β -D-ribofuranoside
AMP	Adenosine monophosphate
AMPK	Adenosine monophosphate activated protein kinase
ATP	Adenosine triphosphate
Ca	Calcium
CaMKK	calmodulin-dependent kinase kinase
CoA	Coenzyme A
CPT1	CholinePhosphoTransferase
eEF-2K	Eukaryotic Elongation Factor 2 Kinase
EF-2K	Elongation Factor 2 Kinase
Elm1	ELongated Morphology
ERK	extracellular signal regulated kinase
G-6-P	Glucose-6-phosphate
Gal1	GALactose metabolism
Gal83	GALactose metabolism
Glc7	GLyCogen
Glk1	GLucoKinase
GLUT	Glucose transporter
Hxk1	Hexokinase isoenzyme
Hxt	HeXose Transporter
IR	Insulin receptor
IRS	Insulin receptor substrate
LKB1	Serine/threonine kinase 11 (STK11)
MAPK	Mitogen Activated Protein Kinase
MAPKK	Mitogen Activated Protein Kinase Kinase
MAPKKK	Mitogen Activated Protein Kinase Kinase Kinase

Mig1	Multicopy Inhibitor of GAL gene expression
Msn5	Multicopy suppressor of SNF1 mutation
Mth1	MSN Three Homolog
mTOR	mammalian Target of Rapamycin
NADH	Nicotinamide adenine dinucleotide
ODE	Ordinary differential equation
PFK	Phosphofructokinase
PP1	Type 1 protein phosphatase
Reg1	REsistance to Glucose repression
Rgt1	Restores Glucose Transport
Rgt2	Restores Glucose Transport
Sak1	Snf1 Activating Kinase
Sip1	SNF1-Interacting Protein
Sip2	SNF1-Interacting Protein
Snf1	Sucrose NonFermenting
Snf4	Sucrose NonFermenting
Snf3	Sucrose NonFermenting
Std1	Suppressor of Tbp Deletion
Suc2	SUCrose fermentation
Tos3	Target Of Sbf
TSC	tuberous sclerosis 2
UK	Upstream kinase
Yck1/2	Palmitoylated plasma membrane-bound casein kinase
ZMP	5-Aminoimidazole-4-carboxamide-1- β -D-ribofuranoside monophosphate

List of Symbols

τ	average time until a signal is activated
ϑ	average time that a signal remains activated
S	signal strength
λ	rate constant

1. Introduction

All cells, whether they live as individuals or in multicellular organisms, are exposed to a diversity of signals, such as light, odours, nutrients, temperature, hormones, or changes in ion concentrations [Hancock 2010]. The potential to sense and to respond to them in an appropriate manner is crucial to survival. Therefore, cells must be able to detect signals and to transmit that information, a process termed cellular signalling or signal transduction [Asthagiri and Lauffenburger 2000]. The focus of this work lies in signalling in the context of energy sensing, which is linked to glucose uptake and metabolism. The AMPK pathway acts as a main energy sensor controlling metabolic pathways and appears to be highly conserved between vertebrates, plants, and yeasts [Woods *et al.* 1994; Mitchelhill *et al.* 1994; Carling 2004; Hedbacker and Carlson 2008]. In this thesis, the mathematical modelling is accomplished on the level of the AMPK counterpart in the yeast *Saccharomyces cerevisiae*, the Snf1 pathway. The mathematical modelling of the Snf1 pathway comprised at first the definition of a glucose regulated stimulus. For this reason, also the process of glucose transport into the yeast cell is discussed. Furthermore, the proceeding of fluorescence microscopy data of a Snf1 pathway component is discussed, separating the information of interest from bleaching effects and background noises. The processed data is then compared to the model simulations. In the second part of this work, quantitative measures, which define properties such as the average time until a pathway component is activated, are used to elucidate deviations between different model approximations as well as to quantify differences between different pathway structures.

1.1. Signal transduction pathways

Cells realise and control the sensing, transduction, and response to a diversity of signals via networks of interacting proteins, groups of which are organised into signalling pathways. The specificity of the cellular response to a certain stimulus is encoded by the spatial and temporal dynamics of signalling networks [Kholodenko 2006]. By this means, cellular processes are regulated, e.g. development, tissue function, and immune response [Asthagiri and Lauffenburger 2000; Wolkenhauer 2007]. Figure 1.1 illustrates the main steps of cellular signalling. The first step in cellular signalling is the recognition of the signal by signal specific plasma membrane receptors, such as G protein-coupled receptors (GPCRs) and receptor tyrosine kinases (RTKs). The specificity of the signal is a precon-

1. Introduction

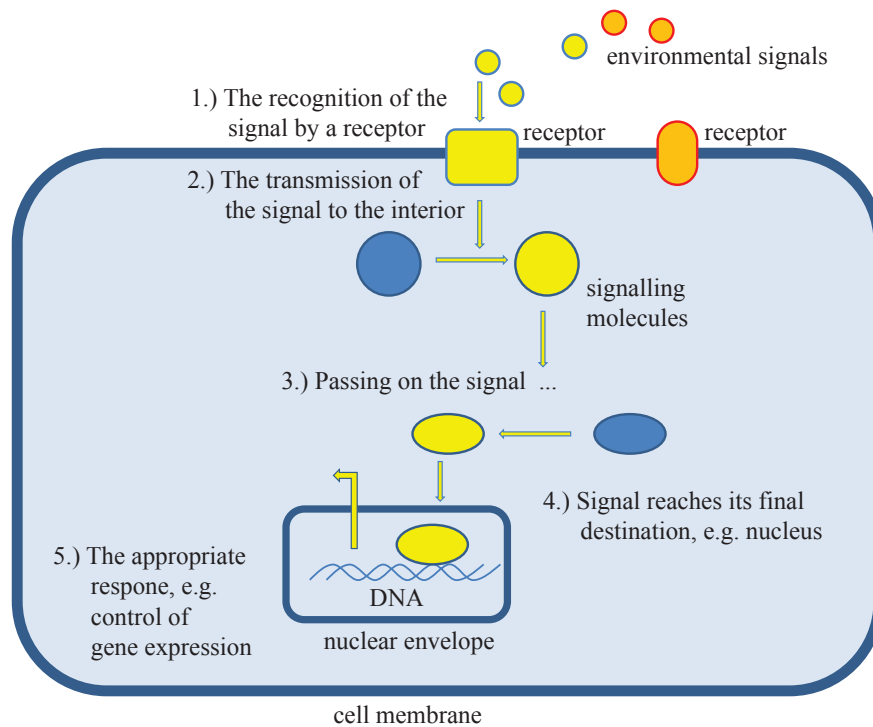


Figure 1.1.: Simplification summarising the main steps of signal transduction: An extracellular stimulus is transduced by a membrane receptor into the intracellular environment. The signal is translated and passed on in a series of biochemical reactions towards its destination to precipitate the appropriate response, for example the transcription of certain genes.

dition to ensure the correct cellular response. The second step comprises the transmission of the signal to cytoplasmic proteins. In a third step, the signal is passed on to a series of complex biochemical circuits of protein interactions and modifications, often referred to as cascades, that leads the signal to a defined place within the cytosol or nucleus [Kholodenko 2006; Hancock 2010]. The transfer and processing of a signal can be accomplished through biochemical reactions such as (de)phosphorylation, (de)methylation, ubiquitination, or complex associations and dissociations. The final step includes the arrival of the signal at its destination resulting in the appropriate cellular response. In the simplest case, regulatory signalling pathways are of linear structure, but more often, their structure include feedback and feedforward mechanisms allowing for complex responses, e.g. sigmoidal switches, transient responses, hysteretic switches, and oscillators [Tyson *et al.* 2003]. The different outcomes are determined by the kinetic parameters of the components, the network structure, and the input signal. For example, a sustained (long duration) activation of ERK leads to differentiation, whereas a transient (short duration) activation of ERK leads to proliferation [Marshall 1995]. The investigation of signal transduction pathways is important to understand the functioning of intact cells and hence, to understand the malfunctions of cells that lead to diseases, such as cancer or diabetes [Hancock 2010]. Accordingly, the medical and drug developing research increasingly focus on gathering

information on the dynamic interactions between the components of signalling pathways [Levitzki 1996].

Three examples of signal transduction pathways, analysed in this thesis, will be introduced in the following.

1.1.1. The AMP-activated kinase pathway

Given that most biological processes such as cell growth, division or movement require energy, it is not surprising that cells and organisms have the ability to sense energy levels in order to adapt their energy household to their current demands [Cantó and Auwerx 2010]. The adenosine monophosphate activated protein kinase (AMPK) is a key energy sensor in cells and well conserved among almost all eukaryotes [Carling *et al.* 1994; Woods *et al.* 1994; Mitchelhill *et al.* 1994; Carling 2004]. In multicellular organisms, AMPK regulates a variety of cellular and physiological responses including carbohydrate and lipid metabolism and appetite regulation [Hardie *et al.* 2003; Carling 2004; Gruzman *et al.* 2009]. Activated by a low energy status, AMPK switches cellular metabolism from anabolic to catabolic mode by turning on ATP-producing catabolic pathways (e.g. glycolysis, fatty acid oxidation, and glucose uptake) and switches off ATP-consuming anabolic pathways (e.g. lipogenesis, gluconeogenesis, and protein synthesis) [Hardie 2007; Cantó and Auwerx 2010].

Malfunctions of the AMPK pathway have been associated with diabetes type two [Gruzman *et al.* 2009] and obesity [Kola *et al.* 2008], which are some of the presently most prevalent diseases [Viollet *et al.* 2007; Steinberg and Kemp 2009], and more recently, also with cancer [Zadra *et al.* 2010].

1.1.2. The AMPK counterpart in *Saccharomyces cerevisiae*: Snf1

The yeast *S. cerevisiae* is highly amenable to genetic, biochemical, and cell biological studies, and was the first eukaryote to have its entire genome sequenced [Chen and Thorner 2007]. Thereon, it has been used as a reference for comparison to sequences of humans and animals. Many pathways are conserved between eukaryotes, hence allowing for studies of pathways in model organisms that are easier to manipulate than in mammalian systems [Petranovic *et al.* 2010]. For this reason, the investigation of interrelations between the components of the Snf1 pathway, which is the AMPK counterpart in yeast, are of huge interest.

The enzyme kinase Snf1 plays a crucial role in regulating cellular metabolism under changing glucose conditions by controlling gene expression and regulating metabolic enzymes [Celenza and Carlson 1986; Gancedo 2008; Hedbacker and Carlson 2008]. Upon glucose limitation, Snf1 is activated adapting gene expression to provide the metabolic equipment for the usage of other carbon sources than glucose [Gancedo 1998; Carlson 1999;

1. Introduction

McCartney and Schmidt 2001; Santangelo 2006; Hong and Carlson 2007]. Upon glucose presence, the Snf1 pathway is inhibited [Wilson *et al.* 1996; McCartney and Schmidt 2001].

Snf1 is activated by other stress signals as well, e.g. sodium ion stress, alkaline pH, and oxidative stress [Hong and Carlson 2007], which leads to its involvement in various processes, such as thermotolerance, sporulation, phospholipid synthesis, aging, and meiosis [Thompson-Jaeger *et al.* 1991; Hedbacker and Carlson 2008; Smets *et al.* 2010] adapting the cell to the corresponding type of stress.

Cells lacking Snf1 are unable to use sucrose, galactose, or nonfermentable carbon sources, and display sporulation defects [Carlson *et al.* 1981; Celenza and Carlson 1986]. Cells overproducing Snf1 have been shown to display accelerated aging [Hedbacker and Carlson 2008].

1.1.3. MAPK cascades

Ubiquitous among eukaryotes, mitogen-activated protein kinase (MAPK) pathways relay extra- or intracellular stimuli to the nucleus controlling a plethora of cellular processes, such as growth, proliferation, differentiation, migration and apoptosis [Rubinfeld and Seger 2005; Shaul and Seger 2007]. There are at least six groups of MAPKs identified in mammals [Dhillon *et al.* 2007]. The central intracellular building blocks of all MAPK cascades are composed of three to five tiers of protein kinases, which sequentially activate each other by phosphorylation [Shaul and Seger 2007]. Three tiers (i.e. MAPK, MAPKK, and MAPKKK) are considered to be the core cascade, whereas the components in the other tiers are not always involved [Rubinfeld and Seger 2005]. Such a simple sequential kinase cascade allows for sensitive responses towards a signal [Kholodenko 2000]. MAPK cascades can also be embedded in positive or negative feedback loops [Kholodenko 2000]. An example for the structure of a MAPK pathway is depicted in Figure 1.2. The ERK kinase was the first MAP kinase to be elucidated [Seger and Krebs 1995]. Their ability to regulate a wide range of cellular processes is due to different mechanisms including signal duration and strength, interaction with scaffold proteins, subcellular localisation, and crosstalk [Shaul and Seger 2007].

Dysfunctions of these pathways contribute to the development of cancer [Dhillon *et al.* 2007] and various metabolic disorders, such as insulin resistance, obesity, and hypertension, which are collectively known as metabolic syndrome [Gehart *et al.* 2010].

1.2. Mathematical modelling of signal transduction pathways

Systems biology [Ideker *et al.* 2001; Kitano 2002; Wolkenhauer *et al.* 2003; Kohl *et al.* 2010] aims at understanding cellular functioning as a well organised system of dynamic processes. Combining experimental data with mathematical models is a promising approach to gain

1.2. Mathematical modelling of signal transduction pathways

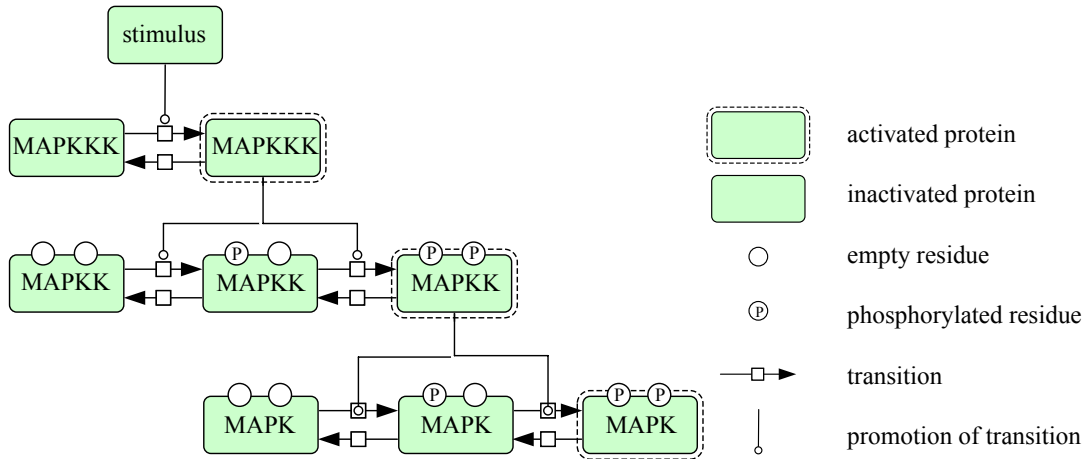


Figure 1.2.: Schematic representation of a three level MAPK cascade. Upon activation via an extracellular stimulus, sequential phosphorylation/activation is conducted: MAPKKK phosphorylates its downstream target MAPKK at two phosphorylation sites. The activated MAPKK thereon acts by double phosphorylating MAPK, which initiates diverse responses involving cell growth, differentiation, and stress responses. Kinase cascades allow for sensitive responses towards a signal [Kholodenko 2000]. The activated MAPK protein is denoted the most downstream component. This figure was designed using CellDesigner [Funahashi *et al.* 2003].

insights into those complex systems. This so called systems biology approach [Kohl *et al.* 2010] provides a powerful foundation from which to address critical scientific questions that are fundamental to our understanding of living cells [Materi and Wishart 2007; Voit and Kemp 2011].

Systems are called ‘complex’ if their behaviour cannot be understood from the laws that govern their subsystems. According to Voit *et al.* [Voit *et al.* 2008], this mainly is due to three reasons: i) a large number of components that are either unknown or only partly understood, ii) the network structure, allowing for several different interactions among the components, and iii) the occurrence of invisible thresholds, i.e. strikingly different behaviour of the system as the parameter values change. Hence, modelling is needed where we cannot make reliable predictions about the biological system with intuition alone.

One of the first steps of the modelling process is the determination of the mathematical framework. This decision depends on practical or experimental considerations, such as the goal and purpose of the model, the available experimental data, mathematical conveniences, and personal preferences [Materi and Wishart 2007; Voit *et al.* 2008]. For choosing the appropriate framework, one should consider the following aspects: Do we seek to establish a

- dynamic model (e.g. a signalling pathway model) or a static model (e.g. a metabolic pathway model that is restricted to a steady-state)
- a deterministic model (e.g. a model describing the average behaviour is sufficient) or a stochastic model (e.g. a model determining how far the system could deviate from

1. Introduction

its normal value) [Voit *et al.* 2008]?

A common approach for deterministic models is based on ordinary differential equations, denoted ODEs [de Jong 2002]. Thereby, it is assumed that the components are present in large amounts and that fluctuations do not generate a different behaviour. In other words, the average value is a sufficiently good description of the components' behaviour.

In contrast to stochastic approaches, simulations can be conducted with less computational time, and the tools of analyses, such as parameter estimations, are better developed. However, eventually, the question that is to be addressed will be pivotal in deciding about the mathematical framework. If the average behaviour is a sufficient description for the dynamics of the components, a deterministic model may comply with the requirements while allowing for less technical effort [Voit *et al.* 2008]. Focusing on a dynamic system with transient continuous changes and assuming that the average value is sufficient to describe the system's behaviour, we use a deterministic approach for our mathematical models.

Once the model, based on a certain framework and assumptions about the biological system, has been defined, values for rate constants and other parameters have to be determined. This can be achieved by fitting the model to experimental data. Thereby, for a predictive character of the model, identifiability of the parameters should be guaranteed [Balsa-Canto *et al.* 2010]. The next step is to test and analyse the model. Due to its simplified nature, a model will never be able to respond to all possible scenarios correctly. It is only defined to respond reasonably in relevant situations.

Experimental techniques, which generate data on the spatio-temporal interactions of cellular components, are essential in order to allow for identification, selection, and characterisation of the components of a pathway [Wolkenhauer 2007]. In the following paragraphs, technologies used for experimental data generation of this thesis will be presented.

1.3. Technologies for data generation

Systems biology is on the rise because of developments in molecular biology and biophysics, i.e. techniques to isolate, sequence, or manipulate proteins, characterise their biochemical activities, and determine their structural properties [Vidal 2009]. Thus, experimental data are generated in diverse forms ranging from quantitative dynamic time series data to qualitative static data.

To generate the data for the experimental system in this thesis (i.e. the Snf1 pathway), the well established technologies Western blotting and fluorescence microscopy were used. They are explained in the following paragraphs.

1.3.1. Western blotting

The technique of Western blotting provides measurements of relative changes of protein levels detecting the protein of interest by means of separation by gel electrophoresis and antibody labeling [Alberts *et al.* 2002]. In some cases there exist antibodies that are specific to an antigenic region in the protein structure allowing for direct detection of different proteins. More often, the antibody is specific towards a tag that is attached to the protein of interest. For these experiments presented in this thesis, a protein specific antibody for Snf1 and a second antibody that specifically recognises the phosphorylated Snf1 were commercially available. However, for another protein of interest, Mig1, no protein specific antibody for phosphorylated Mig1 was available. Thus, another way of data generation had to be chosen as is introduced in the next part.

1.3.2. Fluorescence microscopy

Fluorescence microscopy in combination with optical tweezers and microfluidics has become a powerful tool to assay biological structures and processes in the physiological context of intact living cells [Pepperkok and Ellenberg 2006; Fujioka *et al.* 2006; Ishii *et al.* 2010]. It can be used to acquire images with high spatial and temporal resolution that allow quantitative information regarding the response of single cells to environmental changes to be extracted as demonstrated in [Eriksson 2009].

The data generated using this technique and presented in this thesis are intensity data of the protein Mig1 in the nucleus under changing glucose concentrations. Tagging the brightly glowing green fluorescent protein GFP to the invisible protein of interest (Mig1) allowed the observation of the movements and positions of Mig1-GFP.

1.4. Glucose uptake and metabolism in yeast

The Snf1 kinase is essential for the yeast cell to adapt to glucose limiting conditions and to utilise other carbon sources than glucose, e.g. sucrose. The identity of the glucose signal as well as the mechanisms, by which it is transduced to Snf1, have remained elusive [Rubenstein *et al.* 2008]. However, it is assumed that the signal is related to the first step of glycolysis, converting intracellular glucose into glucose-6-phosphate. For describing the Snf1 dynamics, a glucose-regulated stimulus needs to be derived. As a basis for this derivation, the rate of glucose consumption of yeast cells needs to be taken into account. This rate depends on the extracellular glucose concentrations and the hexose transporters composition within the cell membrane.

1. Introduction

1.4.1. Hexose transport

Lipid bilayers, such as cell membranes, allow for the passage of water and nonpolar molecules (CO_2 , O_2 , etc.) down their concentration gradients due to random thermal movements, a process termed diffusion [Elliott and Elliott 2005]. In contrast to that, the passage of various polar molecules, such as sugars and ions, is accomplished by special membrane transport proteins classified into ion channels and carrier proteins [Alberts *et al.* 2002]. Channel proteins form a pore across the membrane through which specific molecules can diffuse down their concentration gradient, a process termed passive transport or facilitated diffusion [Alberts *et al.* 2002]. Carrier proteins, unlike ion channels, undergo a series of conformational changes in order to transport a molecule across the membrane. Some carrier proteins do so by passive transport, but there are also special carrier proteins (pumps) to transport molecules actively against their concentration gradient, a process called active transport. Active transport requires a source of energy such as ATP to catalyse these energetically unfavourable movements [Alberts *et al.* 2002].

The yeast *S. cerevisiae* preferably subsists on glucose and fructose, which are transported into the cell by passive, energy-independent facilitated diffusion [Romano 1982; Bisson and Fraenkel 1984; Zaman *et al.* 2008] mediated by a large hexose transporters family [Boles and Hollenberg 1997]. In its natural habitat, yeast is exposed to wide ranges of glucose levels. Due to that, not only the sensing of the presence or absence of glucose is a crucial property but also to determine the amount [Bisson and Kunathigan 2003]. Equipped with several kinds of hexose transporter proteins, which differ in their affinity towards glucose [Lagunas 1993], yeast is able to grow under variable conditions from approximately 0.1% to over 40% glucose [Greatrix and Vuuren 2006]. The glucose induction pathway transmits a signal in the presence of glucose that eventually leads to the induction of hexose transporter genes [Johnston 1999; Özcan and Johnston 1999; Özcan 2002]. Thereby, in response to certain glucose concentrations, yeast cells express hexose transporters that are of low, mediate, or high affinity towards glucose, allowing for a highly specialised and efficient glucose transport system [Kruckeberg 1996; Boles and Hollenberg 1997]. The family of hexose transporters has been defined on the basis of sequence similarity and consists of at least 20 members including Hxt1-Hxt17, Gal2, Snf3, and Rgt2.

1.4.2. Respiration and fermentation

S. cerevisiae utilises glucose as main carbon and energy source for biosynthesis. Glycolysis is the metabolic pathway to break down glucose into pyruvate, thereby generating the nucleotide ATP and the coenzyme NADH. *S. cerevisiae* is able to utilise pyruvate in different ways [Zaman *et al.* 2008; Smets *et al.* 2010]. At high glucose concentrations, it prefers fermentation with the release of ethanol and CO_2 rather than respiration. This process allows rapid cell growth [Bisson and Kunathigan 2003]. At low glucose concentra-

tions and in the presence of oxygen, *S. cerevisiae* uses the most efficient way to generate ATP molecules at the expense of the maximal speed of yeast cell growth. This is accomplished in the process of respiration, which includes as the first step the conversion of pyruvate into acetyl CoA (coenzyme A), followed by the citric acid cycle and the oxidative phosphorylation.

1.5. Quantitative measures

As recent experimental and theoretical studies have shown, key parameters for the cellular response are timing and order of events [Rensing *et al.* 2001; Murphy and Blenis 2006], signal duration [Marshall 1995; Ferrell Jr. 1996; Sabbagh *et al.* 2001; Vaudry *et al.* 2002; Millat *et al.* 2008] as well as signal strength (thresholds) [Behar *et al.* 2008]. On the one hand for example, cells that do not react quickly enough to changing nutrient conditions risk being overgrown by competitors that are more efficient on the uptake rates. On the other hand, cells that respond too quickly risk wasting energy on the response itself and being overgrown by more efficient competitors [Kalisky *et al.* 2007]. Additionally, the duration should be long enough to be distinguishable from noise, while not expanding the duration of signal transmission longer than needed. For example, it was observed in cells of the neuroendocrine cell line PC12 that the duration of signalling through ERK may hold the key to the very different outcomes of EGF and NGF stimulation [Sabbagh *et al.* 2001; Vaudry *et al.* 2002]. As reported in [Marshall 1995], the duration of ERK activation determines whether cells can trigger either proliferation or differentiation. The characterisation of dynamic features of signal transduction pathways is therefore crucial to describe cellular adaptation.

The meaningful determination of quantitative properties for dynamic signals is not simple. In this work, the definitions by Heinrich *et al.* [Heinrich *et al.* 2002] are applied. They defined measures to quantify the average signalling time, average signal duration, and the signal amplitude using three different integrals over a dynamic signal.

1.6. Aims and objectives

In the first part of this thesis, the biological background and the mathematical modelling of the Snf1 pathway is discussed (Chapters 2 and 3, respectively). To gain deeper understanding of the interrelations within the Snf1 pathway components, coincided with the need for derivation of a glucose-regulated input signal controlling Snf1 regulation and the processing of fluorescent microscopy data. Thereafter, several alternative ODE-based models were established describing different hypotheses about the underlying network structures. The simulations were compared to experimental time course data generated

1. Introduction

by the groups of Stefan Hohmann¹, Mattias Goksör², and Goutham Vemuri³ from the University of Gothenburg. The questions of focus are as follows:

- i) How can the still unknown signal, which leads to the regulation of the Snf1 pathway, be described and incorporated into the Snf1 pathway model?
- ii) How can fluorescent microscopy data, exposed to bleaching and affected by background noise, be processed to extract the information of the protein of interest?
- iii) Is the regulation of Mig1, which is a target of Snf1, controlled by glucose, or could it be constitutive?
- iv) Is the involvement of the Snf4-subunit required for explaining the experimental observations?
- v) Is the regulation of Snf1 mediated by a glucose-regulated kinase or a glucose-regulated phosphatase, or even both?

The second part of this thesis comprises the introduction and application of quantitative measures to signalling pathways (Chapters 4 and 5, respectively). Here, the questions of focus are:

- i) Which parameter values do still allow for a sensible description of the biological system while applying a weakly activated system?
- ii) How to define a plausible optimisation criterion for comparing different pathway structures?
- iii) What are the consequences of three different model approximations with respect to time and duration describing the same pathway structure?
- iv) Is the characteristic structure of a MAPK pathway, comprising two double phosphorylations, of advantage for signal transmission with respect to the average time and average duration of active signal?

1.7. Outline of this thesis

This work is structured as follows:

Chapter 2 reviews the biological background of this thesis by introducing the AMPK pathway and its homologue pathway in *S. cerevisiae*, the Snf1 pathway. This information

¹Department of Cell and Molecular Biology, University of Gothenburg, SE-40530 Göteborg, Sweden.

²Department of Physics, University of Gothenburg, SE-41296 Göteborg, Sweden.

³Department of Chemical and Biological Engineering, Chalmers University of Technology, SE-41296 Göteborg, Sweden.

provides the basis to follow the assumptions of network structures, which lead to a stepwise Snf1 model development in Chapter 3. Moreover, the importance for investigating the interrelations of the Snf1 pathway components for medical research is emphasised.

Chapter 3 comprises the steps of data processing and Snf1 pathway model development. First, the derivation for a suitable definition of the glucose-regulated signal, which leads to the regulation of Snf1, is discussed. This work has been submitted for publication [Frey *et al.* 2011a]. Then, the processing of fluorescent microscopy data for the Snf1 pathway component Mig1-GFP is presented. The data suffer from bleaching effects and background noises. A mathematical model is established that allows for the extraction of Mig1-GFP intensities by taking bleaching effects and background noises into account. This work has been published in [Frey *et al.* 2011b]. In a final step, those results are combined with Snf1 Western blot data and compared to alternative network structures underlying Snf1 pathway.

Chapter 4 begins by introducing quantitative measures, as defined by Heinrich *et al.* [Heinrich *et al.* 2002]. These definitions build the basis for the onward analyses. An optimality criterion is defined as a measure for the optimal cascade length (i.e. the number of tiers) concerning average time and average duration of active cascade components. This is followed by an analysis of limits for a weakly activated system by determining those parameter value sets that lead to biological nonsensical results, exemplarily for a cascade with one phosphorylation cycle as published in [Frey *et al.* 2008].

In **Chapter 5**, the optimality criterion of Chapter 4 is applied to three MAPK pathway models, which differ in their underlying approximations, discussing consequences of approximations. These models are extended for hypothetical cascade structures varying in tiers and number of phosphorylations in order to address the question of focus: Is the characteristic structure of a MAPK pathway, comprising two double phosphorylations, of advantage for signal transmission with respect to time and duration? This chapter includes the main contents published in [Frey *et al.* 2008] and [Frey *et al.* 2009].

Chapter 6 concludes this work by summarising the main results and by giving an outlook on future research topics.

2. Biological background of the AMP-activated kinase pathway

In this chapter, a review of the biological background of this thesis is given by introducing the AMPK pathway and its homologue in yeast, the Snf1 pathway. This information provides the basis to follow the assumptions of network structures, which lead to a stepwise Snf1 model development discussed in Chapter 3. Moreover, malfunctions of the AMPK pathway are briefly discussed. At the end, a summary of glucose transport into the yeast cell is given.

Given that most biological processes such as cell growth, division, or movement require energy, it is not surprising that cells and organisms have the potential to sense energy levels in order to adapt their energy household to their current demands [Cantó and Auwerx 2010]. The adenosine monophosphate activated protein kinase (AMPK) is a key energy sensor of the cell controlling metabolic pathways and appears to be highly conserved between vertebrates, plants, and yeasts [Carling *et al.* 1994; Woods *et al.* 1994; Mitchelhill *et al.* 1994; Carling 2004]. In yeast, AMPK regulates gene expression under changing glucose conditions [Gancedo 1998; Carlson 1999; Johnston 1999; Gancedo 2008; Hedbacker and Carlson 2008]. In multicellular organisms, it is involved in maintaining whole body energy balance [Hardie *et al.* 2003; Carling 2004; Cantó and Auwerx 2010]. Therefore, it is not surprising that defects in this pathway are responsible for the development of metabolic diseases. In particular, the malfunction of the AMPK pathway has been associated with some of the presently most rapidly advancing diseases, such as diabetes type two and obesity [Towler and Hardie 2007; Viollet *et al.* 2007; Kola *et al.* 2008; Gruzman *et al.* 2009; Steinberg and Kemp 2009]. Recent findings implicate malfunctions in the AMPK pathway in cancer [Huang *et al.* 2008; Shackelford and Shaw 2009; Zadra *et al.* 2010; Fogarty and Hardie 2010]. Gathering information on the dynamic interactions between the components of signalling pathways has become a focus of the medical and drug developing research [Levitzki 1996], in particular, gaining insights into the AMPK/Snf1 pathway aims at tackling diabetes type two and obesity.

A detailed overview of the involvement of AMPK in cellular processes and its regulation is depicted in Figure 2.1 and described in the following section.

The AMPK complex: The mammalian AMPK is a heterotrimeric serine/threonine

2. Biological background of the AMP-activated kinase pathway

kinase, which is composed of a catalytic subunit (α) and two regulatory subunits (β and γ) [Davies *et al.* 1994; Hardie 2007]. Each subunit is encoded by at least two genes, i.e. there are two isoforms for the α -subunit (denoted $\alpha 1$ and $\alpha 2$), two for β -subunits ($\beta 1$ and $\beta 2$), and three for γ -subunits ($\gamma 1$, $\gamma 2$, and $\gamma 3$), yielding 12 heterotrimeric combinations [Carling 2004]. The different isoforms display tissue-specific expression and activity [Steinberg and Kemp 2009].

2.1. The adenosine monophosphate activated protein kinase (AMPK)

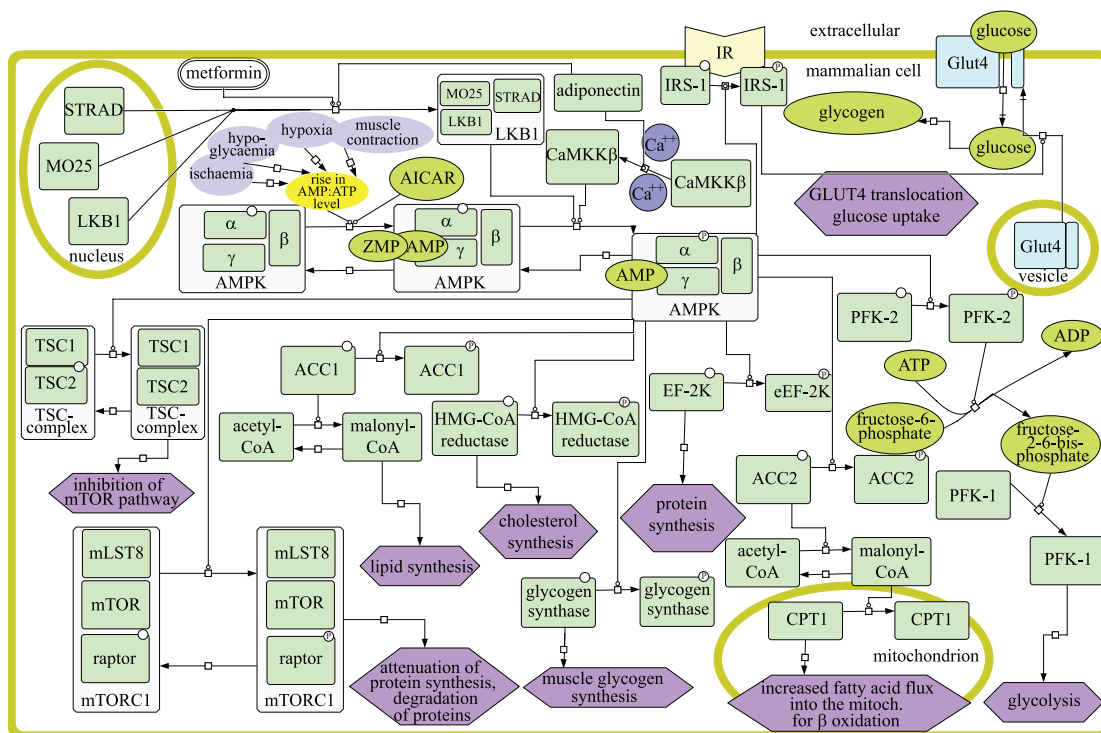


Figure 2.1.: Overview of the involvement of AMPK into metabolic and signalling processes. For further explanation please see Section 2.1. This figure was designed using the software *CellDesigner* [Funahashi *et al.* 2008] and Adobe Illustrator Cs5.

Regulation of AMPK activation: Phosphorylation of the threonine residue 172 (Thr-172) within the catalytic α -subunit is essential for AMPK activation [Hawley *et al.* 1996; Stein *et al.* 2000]. Furthermore, the enzyme activity is affected by post-translational modification of the β -subunit through myristoylation¹ and phosphorylation at three serine residues (Ser-24 or Ser-25, Ser-108, and Ser-182) [Warden *et al.* 2001; Hamilton *et al.* 2002]. The β -subunit acts as a scaffold bridging the α - with the γ -subunit [Woods *et al.* 1996]. One of the critical features of the enzyme is contained in its regulatory γ -subunit

¹Myristoylation is a protein modification binding a myristoyl group.

2.1. The adenosine monophosphate activated protein kinase (AMPK)

[Xiao *et al.* 2007] comprising an interface for interaction with two AMP or ATP molecules in a mutually exclusive way and a third AMP molecule in a non-exchangeable fashion [Xiao *et al.* 2007; Cantó and Auwerx 2010]. The exchange of ATP for AMP promotes an approximately five-fold activation of AMPK via an allosteric mechanism [Hawley *et al.* 1996]. The mechanisms of rising AMP levels triggering AMPK phosphorylation are not completely understood yet [Oakhill *et al.* 2010]. However, it was shown that AMP binding to the γ -subunit stimulates phosphorylation of AMPK (at Thr-172), provided that the β -subunit is myristoylated [Oakhill *et al.* 2010] and protects the enzyme against dephosphorylation [Sanders *et al.* 2007; Xiao *et al.* 2011]. AMP binding also causes allosteric activation [Sanders *et al.* 2007; Xiao *et al.* 2011]. Both AMP-promoted effects, i.e. the allosteric and phosphorylation effects, increase the activation of AMPK approximately 1000-fold [Suter *et al.* 2006; Cantó and Auwerx 2010]. The compound AICAR can be used as an experimental tool to activate AMPK. Upon intake into the cell, it is converted to an AMP analogue called ZMP. ZMP mimics the effects of AMP on AMPK.

Once activated by metabolic stresses, e.g. hypoxia, ischaemia, muscle contraction, or simply glucose deprivation causing depletion of ATP [Corton *et al.* 1994], AMPK changes the mode of metabolism by switching off ATP-consuming anabolic processes that are not essential for the immediate survival of the cell and by stimulating catabolic processes that generate ATP [Corton *et al.* 1994; Hardie 2007]. It thus keeps an appropriate balance between the energy-producing catabolic and energy-consuming anabolic processes.

So far, two upstream kinases of AMPK are identified, LKB1 [Hawley *et al.* 2003; Woods *et al.* 2003; Shaw *et al.* 2004] and CaMKK β [Hawley *et al.* 2005; Woods *et al.* 2005; Hurley *et al.* 2005], whereas the exact identity of the phosphatase remains elusive [Cantó and Auwerx 2010]. LKB1 activity requires the formation of a complex with two additional proteins, STRAD and MO25 [Hawley *et al.* 2003; Boudeau *et al.* 2003]. Upon complex formation, it is transported from the nucleus to the cytosol, where it performs its biological function [Boudeau *et al.* 2003]. Whereas the LKB1 complex is constitutively active [Sakamoto *et al.* 2004; Lizcano *et al.* 2004], the LKB1 subunit achieves only weak activation [Hawley *et al.* 2003]. LKB1 serves as an upstream kinase for different AMPK-related kinases [Lizcano *et al.* 2004]. Substrate specificity for AMPK is created through binding of AMP to AMPK making it a better substrate for LKB1 [Hawley *et al.* 2003]. The other upstream kinase of AMPK identified yet is the Ca²⁺/calmodulin-dependent kinase kinase (CaMKK) [Hawley *et al.* 2005; Woods *et al.* 2005; Hurley *et al.* 2005]. Phosphorylation of AMPK by CaMKK β is stimulated by a rise in Ca²⁺-ions, independent of a rise in AMP levels [Hawley *et al.* 2005; Hurley *et al.* 2005; Woods *et al.* 2005; Suter *et al.* 2006]. Tak1 (transforming growth factor- β -activated kinase 1) has been reported to be capable of phosphorylating AMPK *in vitro* and is thus suggested to be a candidate for a third AMPK kinase [Momcilovic *et al.* 2006; Cantó and Auwerx 2010].

2. Biological background of the AMP-activated kinase pathway

AMPK is a multisubstrate enzyme. Targets of activated AMPK range from lipid- and carbohydrate- to protein-metabolism.

Targets of activated AMPK in lipid-metabolism: The first targets for AMPK to be identified were acetyl-CoA carboxylase (denoted ACC) [Carlson and Kim 1974] and 3-hydroxy-3-methylglutaryl-CoA (denoted HMG-CoA) reductase [Beg *et al.* 1973], which play a key role in fatty acid synthesis and cholesterol synthesis, respectively. AMPK inhibits by phosphorylation both isoforms of the acetyl-CoA carboxylase, denoted ACC1 (cytoplasmic) and ACC2 (primarily mitochondrial) [Hardie and Pan 2002]. Both isoforms of ACC catalyse the reaction forming malonyl-CoA from acetyl-CoA. Malonyl-CoA produced by ACC1 is used in lipid synthesis, malonyl-CoA produced by ACC2 is exclusively involved in regulation of fatty acid oxidation [Hardie and Pan 2002]. Thus, the inactivation of ACC1 through AMPK leads to inhibition of fatty acid synthesis conserving ATP under cellular stress. Inactivation of ACC2 leads to increasing the uptake of fatty acids into mitochondria via the carrier CPT-1b, which is no longer blocked by ACC2 [Mills *et al.* 1983]. Thus, AMPK induces β -oxidation stimulating ATP synthesis [Merrill *et al.* 1997].

Targets of activated AMPK in carbohydrate-metabolism: Animals compensate for long periods of fasting by converting sugars (and also fats) into special forms of storage such as glycogen in a process called glycogenesis [Alberts *et al.* 2002]. Glycogen is a short-term energy storage composed of glucose subunits. AMPK deactivates glycogen synthase, the enzyme that mediates the production of glycogen. This results in the inhibition of glycogenesis [Carling and Hardie 1989; Jørgensen *et al.* 2004]. Thus, glucose is available for energy production. On the other hand, the AMPK-induced phosphorylation of PFK-2 (6-phosphofructo-2-kinase) results in an increased synthesis of fructose-2-6-bisphosphate, a potent stimulator of PFK1 (phosphofructokinase 1), which has a key role in the regulation of glycolysis. Thus, AMPK promotes ATP production also via the metabolic pathway glycolysis [Marsin *et al.* 2000].

In skeletal muscles, AMPK stimulates glucose uptake [Merrill *et al.* 1997] by translocation of the glucose transporter GLUT4 to the plasma membrane [Kurth-Kraczek *et al.* 1999] and by increasing its expression [Holmes *et al.* 1999] in order to provide ATP as a fuel. However, the exact events that link AMPK activation to GLUT4 translocation are not fully understood yet [Cantó and Auwerx 2010]. In contrast to that, in adipocytes (fat cells), AMPK stimulation inactivates insulin-stimulated glucose transport, inhibiting triacylglycerol synthesis, to conserve ATP under conditions of cellular stress [Salt *et al.* 2000].

Binding of the hormone insulin to an insulin receptor (IR) is followed by the binding and phosphorylation of an insulin receptor substrate (IRS-1) that trigger various mechanisms,

2.2. Malfunctions of the AMPK pathway

such as activation of the glycogen synthase and the translocation of a glucose transporter (GLUT4) to the cell membrane [Muoio and Newgard 2008].

Targets of activated AMPK in protein-metabolism: Protein synthesis utilises cellular energy. Thus, in order to maintain sufficient cellular ATP levels under metabolic stress, inhibition of translation of proteins, which are evitable for the immediate survival of the cell, is a crucial property. The phosphorylation and inactivation of eEF-2K (eukaryotic elongation factor 2 kinase) by AMPK leads to a temporary pausing of translation at elongation [Horman *et al.* 2002]. Translation can resume quickly upon normal ATP levels [Horman *et al.* 2002]. AMPK also inhibits translation by phosphorylation of TSC2 (tuberous sclerosis 2) [Inoki *et al.* 2003] that functions as a key player in the regulation of the mTOR pathway. The mTOR (mammalian target of rapamycin) pathway controls protein synthesis, glucose homeostasis, and fat metabolism [Steinberg and Kemp 2009]. It can also be inhibited through direct phosphorylation of the raptor subunit of the mTOR complex by AMPK [Gwinn *et al.* 2008]. The inhibition of the mTOR pathway leads to attenuation of protein biosynthesis and to the induction of protein degradation [Polak and Hall 2009].

2.2. Malfunctions of the AMPK pathway

Malfunctions of the AMPK pathway, i.e. AMPK is not activated upon metabolic stress, are associated with the metabolic syndrome, which comprises diseases as diabetes type two, insulin resistance, cardiovascular disease and fatty liver disease [Winder and Hardie 1999; Steinberg and Kemp 2009; Fogarty and Hardie 2010]. However, it is still unclear whether they are causes or consequences of the pathological conditions [Kola *et al.* 2008]. In addition to the metabolic syndrome, it increasingly is becoming clear that AMPK represents a link between energy homeostasis and cancer, in particular, prostate cancer [Zadra *et al.* 2010]. Thus, treatments applying AMPK activators are a promising target in the medical research [Zadra *et al.* 2010].

Whereas diabetes type one is characterised by the complete absence of insulin, due to autoimmune destruction of the pancreatic islet β -cells, the primary factors causing diabetes type two are poorly understood [Savage *et al.* 2007; Muoio and Newgard 2008]. Due to the presence of insulin sensitivity in patients with diabetes type two several years before the onset of diabetes type two and its consistent occurrence, it is assumed to play a major role in the development of diabetes type two [Shulman 2000]. Insulin resistance is characterised by an impaired insulin secretion or a non-insulin-dependent defect (i.e. insulin is present while not effective). In consequence, insulin might be present or even

2. Biological background of the AMP-activated kinase pathway

elevated, but cells do not respond to it due to insensitivity caused by the downregulation of the insulin receptors. Hence, blood glucose cannot be transported into the cells to be stored for energy. Insulin resistance might be caused by lipotoxicity, which describes the accumulation of lipids in other cell types than the target adipose tissue [Schaffer 2003; Savage *et al.* 2007]. Whereas adipose tissues have a high capacity for storing lipids, cells of non-adipose tissues have limited capacity. Thus, exceeded capacity leads to cellular dysfunctions or even cell death [Schaffer 2003]. Adiponectin is a plasma protein exhibiting anti-diabetic properties [Zhou *et al.* 2009]. Promoting LKB1 translocation out of the nucleus into the cytosol, it stimulates the activation of AMPK, enhancing fatty-acid oxidation, and therefore decreasing insulin resistance [Yamauchi *et al.* 2001; Zhou *et al.* 2009]. It also activates CaMKK by subsequently inducing Ca^{2+} -release from the endoplasmic reticulum [Zhou *et al.* 2009].

Metformin is a widely used drug for reducing the blood glucose levels in diabetes type two mainly through inhibiting hepatic gluconeogenesis [Towler and Hardie 2007; Fogarty and Hardie 2010]. The mechanism by which it leads to AMPK activation is still being debated [Fogarty and Hardie 2010]. Positive effects of AMPK on insulin sensitivity can be explained by findings that AMPK might be a potential modifier of insulin signalling through phosphorylation of IRS-1 *in vitro* [Jakobsen *et al.* 2001]. AMPK also appears as a promising target for cancer prevention and therapy [Luo *et al.* 2011]. AMPK performs its function in various organs, especially in skeletal muscles (stimulation of glucose transport and fatty acid oxidation) and liver (increase of fatty acid oxidation and decrease of glucose output, decrease of cholesterol and triglyceride synthesis) [Gruzman *et al.* 2009]. The widespread cellular functioning of AMPK, ranging from metabolic effects through appetite regulation, cell growth and differentiation to vascular functions [Gruzman *et al.* 2009], hamper drug target specificity and might cause unwanted and harmful side effects, e.g. the biguanide phenformin was withdrawn as anti-diabetic drug due to the emergence of lactic acidosis [Fogarty and Hardie 2010]. Furthermore, negative effects of consistent AMPK activation include glycogen accumulation in the heart, inhibition of insulin secretion, and increases in body weight due to appetite stimulation [Viollet *et al.* 2007; Kola *et al.* 2008]. Accordingly, an ideal drug agent would only affect AMPK activity in peripheral tissues, such as the liver, while at the same time, not affect AMPK activity in the hypothalamus, a portion of the brain which controls appetite. Thus, the agent enhances fatty acid oxidation and glucose uptake and prevents cholesterol and triglycerides biosynthesis, while reducing food intake and body weight [Viollet *et al.* 2007]. In addition to side effects, resistance towards a drug agent due to genetic variations, which may alter responsiveness, is a widely known challenge.

2.3. The AMPK counterpart in *Saccharomyces cerevisiae*: Snf1

An introduction into the characteristics and functioning of Snf1 is given below and can be retraced in Figure 2.2.

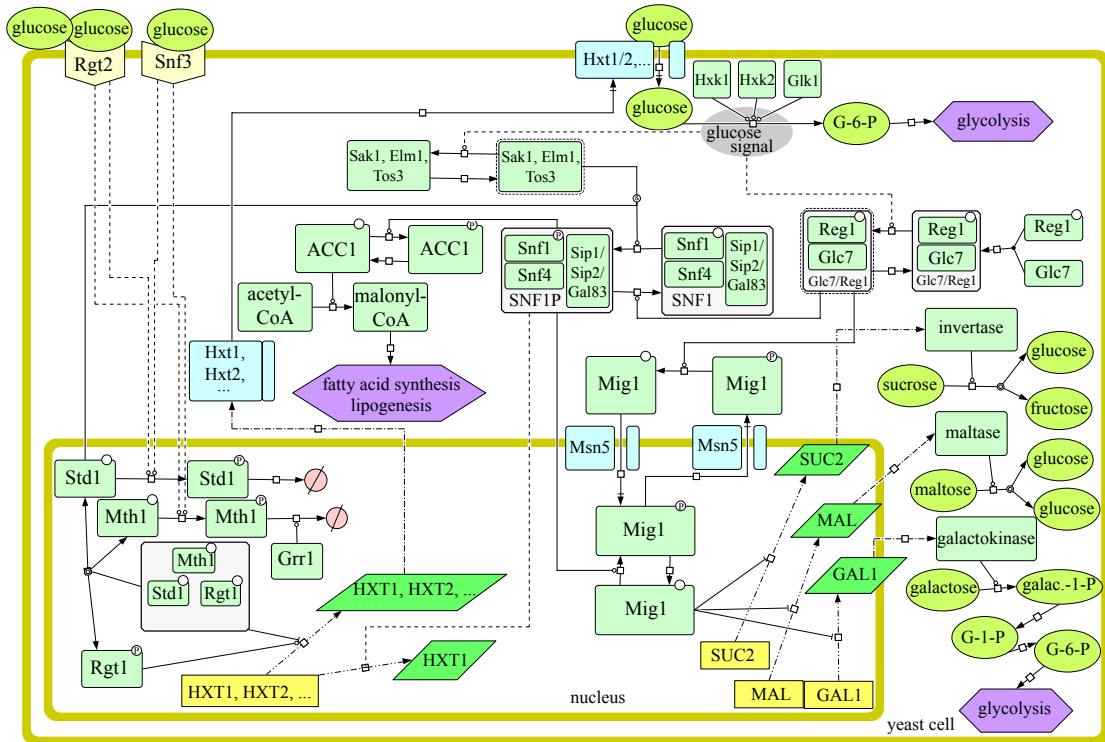


Figure 2.2.: Overview of the Snf1 pathway and crosstalk to the Rgt2/Snf3 and PKA signalling pathways. For further explanation see Section 2.3. The images were designed using the software *CellDesigner* [Funahashi *et al.* 2008].

The Snf1 complex: Like AMPK, Snf1 is a heterotrimeric enzyme complex comprising a catalytic α -subunit Snf1, a regulatory γ -subunit Snf4 [Celenza and Carlson 1989; Celenza *et al.* 1989], and either of three alternative regulatory β -subunits Sip1-, Sip2-, and Gal83-subunit [Erickson and Johnston 1993; Yang *et al.* 1994]. The proteins Sip1, Sip2, and Gal83 serve as alternate members of the kinase complex [Erickson and Johnston 1993; Yang *et al.* 1994] leading to three possible alternative isoforms of the complex. The β -subunit determines the localisation of the complex within the cell: in a glucose rich medium, all three subunits are cytosolic, while in poor glucose conditions, Sip1 changes its location to the vacuole, and Gal83 to the nucleus [Vincent *et al.* 2001], Sip2 staying cytosolic [Vincent *et al.* 2001]. All three β -subunits are essential for the response to starvation for nutrients, such as glucose [Schmidt and McCartney 2000]. In homology to the mammalian β -subunit, also the Sip1/Sip2/Gal83-subunit acts as a scaffold in the complex and bridges Snf1 and Snf4 via two distinct conserved domains [Jiang and Carlson 1997].

2. Biological background of the AMP-activated kinase pathway

Furthermore, a crucial role performed by the β -subunit lies in targeting Snf1 to specific substrates [Schmidt and McCartney 2000].

Regulation and stimulation of Snf1: Snf1 is activated by glucose limitation through phosphorylation of the threonine residue 210 (Thr-210) located in the activation loop segment [Jiang and Carlson 1996; Wilson *et al.* 1996; McCartney and Schmidt 2001]. Unlike the mammalian counterpart, Snf1 does not bind AMP *in vitro* [Woods *et al.* 1994; Mitchelhill *et al.* 1994; Stapleton *et al.* 1994; Wilson *et al.* 1996] and allosteric activation by AMP binding to Snf1 could not be detected [Woods *et al.* 1994; Steinberg and Kemp 2009]. The Snf1 complex undergoes glucose-regulated conformational changes: Interaction of the Snf1- and Snf4-subunit is inhibited by high levels of glucose and induced in low levels of glucose [Jiang and Carlson 1996]. When glucose is depleted, Snf4 binds to Snf1 and counteracts an autoinhibitory interaction among the catalytic and the regulatory domain of Snf1 [Celenza and Carlson 1989; Jiang and Carlson 1996]. In addition to this mechanism, the protein Std1 has been implicated in regulatory functions on Snf1 [Kuchin *et al.* 2003]. It stimulates Snf1 activity by interacting with the catalytic domain promoting an active conformation of Snf1 [Kuchin *et al.* 2003]. The involvement of Std1 in the glucose induction pathway is described in Section 2.4 and in Figure 2.3.

Snf1 is phosphorylated by the kinases Sak1 [Nath *et al.* 2003; Momcilovic *et al.* 2008], Elm1 [Sutherland *et al.* 2003], and Tos3 [Hong *et al.* 2003], and dephosphorylated by the phosphatase complex Glc7/Reg1 [Tu and Carlson 1995; Sanz *et al.* 2000]. The three kinases have overlapping functions *in vivo*, and all three genes must be deleted to abolish Snf1 catalytic function [Hong *et al.* 2003; Sutherland *et al.* 2003]. They do not show a preference to specific isoforms of the Snf1 complex [McCartney *et al.* 2005]. Instead, the different isoforms of the Snf1 complex display stress-dependent preferences for the kinases [McCartney *et al.* 2005]. The three activating kinases make distinct contributions to Snf1 activation in response to different type of stress, e.g. Sak1 is the major activating kinase under glucose-limiting conditions [McCartney *et al.* 2005].

The phosphatase complex Glc7/Reg1 functions antagonistically to the upstream kinases of Snf1 [Tu and Carlson 1994]. In response to a glucose signal, it dephosphorylates and thus inactivates Snf1 [Ludin *et al.* 1998; Sanz *et al.* 2000]. Apart from its role in glucose repression, the subunit Glc7 also fulfills tasks in the regulation of translation, cell cycle progression, chromosome segregation, and glycogen accumulation [De Wever *et al.* 2005]. Thereby, it achieves substrate specificity through binding to a certain regulatory subunit [Tu and Carlson 1995; Tu *et al.* 1996]. Cells lacking the Reg1-subunit showed constitutive phosphorylation of Snf1 [McCartney and Schmidt 2001]. There is still uncertainty concerning the regulatory mechanisms of the phosphatase and kinases of Snf1. It is unknown, whether they are constitutively active or whether they are (de)activated in response to

2.3. The AMPK counterpart in *Saccharomyces cerevisiae*: Snf1

glucose availabilities. Upon glucose uptake into the cell, the enzymes Hxk1, Hxk2 (hexokinase 1 and 2), and Glk1 (glucokinase 1) catalyse the phosphorylation of glucose into glucose-6-phosphate (G-6-P). It is assumed that the signal leading to glucose-induced Snf1 inactivation is related to the rate of this first step of glycolysis, but more details on the molecular signals responsible for Snf1 regulation still remain elusive [Rubenstein *et al.* 2008; Hedbacker and Carlson 2008]. In general, Snf1 activity is negatively regulated by glucose [Jiang and Carlson 1996], i.e. Snf1 is activated upon glucose limitation and inhibited upon glucose presence [Wilson *et al.* 1996; McCartney and Schmidt 2001]. In glucose presence, inactivation of Snf1 is essential for the repression of those genes that are not needed during fermentative growth on glucose, such as genes encoding enzymes involved in gluconeogenesis, respiration, Citric acid cycle, and metabolism of alternative carbon sources [Santangelo 2006; Smets *et al.* 2010]. Snf1 is also activated by other stress signals, such as salt stress, alkaline pH, or oxidative stress [Hong and Carlson 2007; Ye *et al.* 2008] leading to its involvement in various processes, such as thermotolerance, sporulation, phospholipid synthesis, aging, and meiosis [Thompson-Jaeger *et al.* 1991; Hedbacker and Carlson 2008].

Targets of activated Snf1 in lipid-metabolism: The Snf1 protein kinase complex and its mammalian counterpart AMPK have at least one substrate in common: both can directly inactivate ACC1 (acetyl-CoA carboxylase) by phosphorylation inhibiting fatty acid synthesis during glucose-limiting conditions [Mitchellhill *et al.* 1994; Woods *et al.* 1994].

Targets of activated Snf1 in carbohydrate-metabolism: The primary role of Snf1 is to relieve the repression mediated by Mig1 and other regulators of genes that are not required for fermentative growth on glucose. In response to glucose stress, Snf1 is activated through phosphorylation and thereon phosphorylates Mig1 at four sites [Treitel *et al.* 1998; Östling and Ronne 1998; Smith *et al.* 1999]. Mig1 binds promoters of many glucose-repressed genes, such as GAL1, SUC2, and MAL [Klein *et al.* 1998; Carlson 1999] encoding the enzymes galactose, sucrose and maltose, respectively, for utilisation of alternative carbon sources. Mig1 activity is controlled by a glucose-regulated nuclear import-export-mechanisms [DeVit *et al.* 1997]. The phosphorylation of Mig1 promotes its recognition by the nuclear exportin Msn5 and thereon, the transport of Mig1 into the cytosol [DeVit *et al.* 1997; DeVit and Johnston 1999]. In *msn5* mutants, it was shown that Mig1 was constitutively located to the nucleus, while gene expression was derepressed. Thus, Msn5 only partially regulates Mig1 function [DeVit and Johnston 1999]. The export of Mig1 to the cytosol relieves transcriptional repression, leading to expression of the target genes described above. Inversely, dephosphorylation of Mig1 might be the signal for the transport back into the nucleus [Tu and Carlson 1995; DeVit *et al.* 1997]. Cells lacking the γ -subunit of the Snf1 complex exhibit normal regulation of Thr-210 phosphorylation in response to

2. Biological background of the AMP-activated kinase pathway

glucose limitation, but are unable to efficiently phosphorylate Mig1, both *in vitro* [Elbing *et al.* 2006] and *in vivo* [McCartney and Schmidt 2001]. Nevertheless, deletion of Snf4 results in a partially active Snf1, able to phosphorylate Mig1 to some extent [McCartney and Schmidt 2001]. In the absence of Snf4, cells are unable to grow on alternative carbon sources, such as ethanol or raffinose, despite the partially active Snf1. In response to salt stress, Snf1 is phosphorylated but phosphorylation of Mig1 could not be observed [Ye *et al.* 2008].

Glc7/Reg1 is suggested to be the phosphatase not only for Snf1 but also for Mig1 [Treitel *et al.* 1998; McCartney and Schmidt 2001]. There are also other phosphatases, e.g. Sit4, which function in dephosphorylating Mig1 [Jin *et al.* 2007].

Snf1 activates glycogen synthase [Thompson-Jaeger *et al.* 1991] and is required for the accumulation of glycogen [Hedbacker and Carlson 2008] for glucose storage.

Similarities between the AMPK and the Snf1 pathway: Mammalian AMPK and yeast Snf1 are structurally and functionally related [Woods *et al.* 1994; Mitchelhill *et al.* 1994].

Both are heterotrimeric enzyme complexes sharing 59% identity in their amino acid sequences within the catalytic domains [Carling *et al.* 1994; Mitchelhill *et al.* 1994]. The similarity among the catalytic domains of the three kinases Elm1, Sak1, and Tos3 to those of CaMKKs and LKB1 led to the identification of LKB1 as a candidate kinase of AMPK [Hong *et al.* 2003] and its verification [Woods *et al.* 2003].

Both regulate gene expression, and both affect the activity of metabolic enzymes and transporters in response to metabolic stress [Hong *et al.* 2005]. For example, Snf1 and AMPK inhibit fatty acid synthesis through targeting ACC1 during glucose-limiting conditions [Mitchelhill *et al.* 1994; Woods *et al.* 1994; Hardie and Pan 2002] and control glycogenesis [Carling and Hardie 1989; Jørgensen *et al.* 2004]. As activity of Snf1 in *S. cerevisiae* is regulated by glucose [Jiang and Carlson 1996], also AMPK in pancreatic β -cells of multicellular eukaryotes responds to a glucose signal: activated by glucose and inhibited by high glucose concentrations to control hormone release and feeding behaviour [Salt *et al.* 1998].

The kinases display cross-species functionality, LKB1 and CaMKK functioning in yeast cells as Snf1-activating kinases [Woods *et al.* 2005; Hong *et al.* 2005] and Tos3 and Elm1 were shown to activate AMPK *in vitro* [Hong *et al.* 2003; Sutherland *et al.* 2003].

2.4. Glucose consumption in yeast: Hexose transporters

The glucose-sensing mechanisms for Snf1 regulation are poorly understood [Rubenstein *et al.* 2008; Hedbacker and Carlson 2008], but it is assumed that it is related to the rate of

2.4. Glucose consumption in yeast: Hexose transporters

the first step in glycolysis. However, its proper derivation is crucial for modelling Snf1 regulation. To provide the biological background for the mathematical representation of the glucose-regulated stimulus, a summary of glucose transport into the cell of *S. cerevisiae* is given. The derivation of a glucose-regulated stimulus will then be shown in Section 3.1.

Glucose is the main energy and carbon source for the yeast *S. cerevisiae*. The abundance of this sugar is carefully monitored by the cells, adapting the mode of metabolism accordingly. In addition to initiating metabolism, glucose also triggers a signal that regulates gene expression via two different pathways, known as the glucose repression and the glucose induction pathways [Santangelo 2006]. At high glucose availabilities, yeast mainly ferments sugars, while repressing utilisation of alternative carbon and energy sources, a phenomenon named glucose repression. The repression pathway inhibits a large group of genes involved in catabolism of alternative carbon sources, respiration, and mitochondrial functioning. In addition, another group of genes is strongly upregulated (e.g. encoding glycolytic enzymes, glucose transporters, etc.) [Santangelo 2006]. Concomitantly, the induction pathway ensures that the genes and proteins required for glucose metabolism are activated. Those genes comprise the family of hexose transporters, which consists of at least 20 members, including Hxt1-Hxt17, Gal2, Snf3, and Rgt2 [Kruckeberg 1996].

In yeast, glucose is transported into the cell by passive, energy-independent facilitated transport [Romano 1982; Bisson and Fraenkel 1984]. In its natural habitat, baker's yeast is exposed to a wide range of glucose levels from approximately 0.1% to extreme conditions of over 40% glucose [Gretchen and Vuuren 2006]. Yeast possesses a number of transporters with different affinities in order to operate optimally in this broad range of extracellular glucose concentrations [Lagunas 1993; Boles and Hollenberg 1997]. They can be classified as transporters of low (*HXT1* and *HXT3*), high (*HXT2*, *HXT6*, and *HXT7* [Kruckeberg and Bisson 1990]), and medium (*HXT5* [Diderich *et al.* 2001]) affinity towards glucose [Kruckeberg 1996; Boles and Hollenberg 1997]. In the presence of low glucose concentrations (of about 0.1 % to 0.5 %), high affinity transporters are most abundant, while low affinity transporters are not expressed [Bisson and Fraenkel 1984]. At high glucose concentrations (of more than 1 %), the reverse situation has been observed. In that case, low affinity transporters are widely expressed [Reifenberger *et al.* 1997; Özcan and Johnston 1999].

The presence of extracellular glucose is sensed by two membrane-bound sensors, Rgt2 with low, and Snf3 with high affinity for glucose [Özcan *et al.* 1996, 1998; Santangelo 2006]. They initiate a signalling cascade that regulates expression of the hexose transporter genes [Özcan and Johnston 1999; Johnston 1999; Özcan 2002] involving the proteins Std1 and Mth1 [Flick *et al.* 2003; Moriya and Johnston 2004] via the transcription factor Rgt1 [Johnston and Kim 2005], as shown in Figure 2.3. During glucose presence, Rgt1 dis-

2. Biological background of the AMP-activated kinase pathway

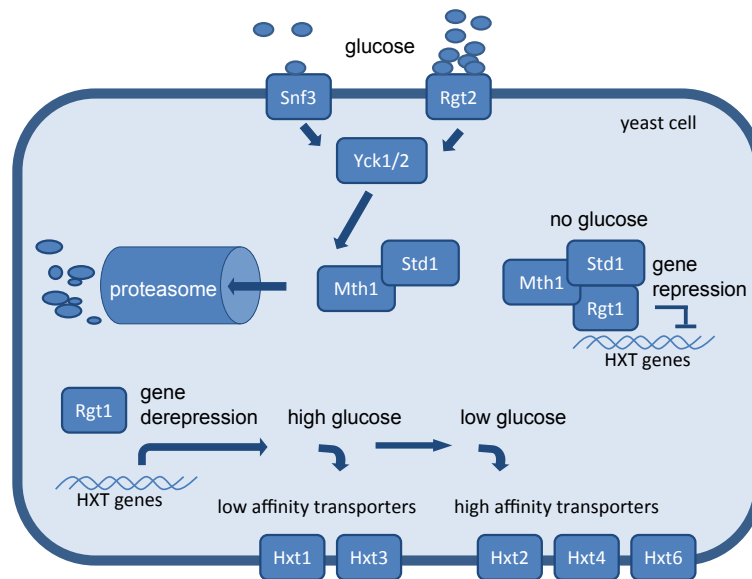


Figure 2.3.: Glucose sensing and signalling in *S. cerevisiae*. Snf3 is responsible for the regulation of high affinity sugar transporters, e.g. *HXT2*, *HXT4*, and *HXT6*, whereas Rgt2 regulates the low affinity transporters, e.g. *HXT1* and *HXT3*. In the presence of glucose, Rgt1 dissociates from the repressor complex with Mth1 and Std1 and acts as a transcriptional activator for expression of low affinity transporter genes. During glucose absence, Rgt1 associates with the repressor complex and acts as a transcriptional repressor for *HXT* genes by binding their promoters [Özcan and Johnston 1996, 1999; Mosley *et al.* 2003]. Yck1/2 provides an essential function in triggering the degradation of Mth1 and Std1.

sociates from the repressor complex including Mth1 and Std1 while activated Yck1/2 phosphorylates Mth1 and Std1, which are thereon recognised by the SCF^{Grr1} complex for degradation via a proteasome [Gancedo 2008]. The phosphorylation of Rgt1 in response to glucose converts it to an activator by inhibiting its DNA-binding ability, thereby relieving repression of *HXT* gene expression [Flick *et al.* 2003; Kim *et al.* 2003; Moriya and Johnston 2004]. During glucose absence, Rgt1 associates with Mth1 and Std1 in a complex acting as a transcriptional repressor for the *HXT1* to *HXT4* genes by binding their promoters [Özcan and Johnston 1996, 1999; Mosley *et al.* 2003]. It is assumed that Snf3 and Rgt2 generate the same signal regulating HXT gene expression and that their different roles in high and low affinity glucose receptors is due to their affinity towards glucose [Özcan and Johnston 1999].

2.5. Summary

Mammalian AMPK and yeast Snf1 are structurally and functionally related proteins that play a crucial role in energy homeostasis of the cell. Activated by any stress that depletes cellular ATP, AMPK switches off ATP-consuming biosynthetic pathways, while switching on ATP-producing catabolic pathways. Snf1 regulates transcription of genes encoding

2.5. *Summary*

enzymes for the use of alternative carbon sources to adapt to glucose limiting conditions. A large family of hexose transporters with different affinities to glucose, allows yeast to carefully monitor glucose in its environment and to control glucose uptake. Investigating dysfunctions in the AMPK and Snf1 signalling pathways is a promising approach to tackle one of the most prevalent diseases diabetes type two and obesity.

3. Mathematical modelling of the Snf1 pathway

This chapter comprises the steps of model development for the Snf1 pathway. In Section 3.1, the derivation of a glucose-regulated signal, which leads to the regulation of the Snf1 pathway, is discussed. The experimental data were generated by Goutham Vemuri¹ and the group of Stefan Hohmann². This work has been submitted for publication [Frey *et al.* 2011a]. In Section 3.2, a mathematical approach is presented that allows for the processing of fluorescent microscopy data of Mig1-GFP (a downstream Snf1 pathway component) generated by the group of Mattias Goksör³. This work was published in [Frey *et al.* 2011b]. In Section 3.3, the results of Sections 3.1 and 3.2 are then combined with Snf1 Western blot data, generated by the group of Stefan Hohmann, University of Gothenburg, to enter an iterative cycle between data-driven modelling and model-driven experimentation to investigate the interrelations of Snf1 pathway components, which is part of unpublished collaborative work (Manuscript in preparation [Garcia Salcedo 2009]). In a final part (Section 3.4), the overall results are summarised.

3.1. Dynamics of hexose transporters in *S. cerevisiae* upon glucose pulses

The research in the following section is motivated by the question:

How can the still unknown signal, which leads to the regulation of the Snf1 pathway, be described and incorporated into the Snf1 pathway model?

It is assumed that the signal leading to glucose-induced Snf1 inactivation is connected to the rate of the first step of glycolysis, but more details on the molecular signals responsible for Snf1 regulation still remain elusive [Rubenstein *et al.* 2008; Hedbacker and Carlson 2008]. In order to investigate the dynamics of Snf1 (de)phosphorylations upon glucose availabilities, the derivation of a glucose-regulated input function is essential.

¹Department of Chemical and Biological Engineering, Chalmers University of Technology, SE-41296 Göteborg, Sweden.

²Department of Cell and Molecular Biology, University of Gothenburg, SE-40530 Göteborg, Sweden.

³Department of Physics, University of Gothenburg, SE-41296 Göteborg, Sweden.

3. Mathematical modelling of the Snf1 pathway

S. cerevisiae utilises glucose as its main carbon and energy sources. Its glucose uptake transport system consists of a family of hexose transporters, able to ensure efficient uptake in a wide range of concentrations. Pulsing glucose to exponentially growing yeast cells, we measured and modelled the dynamics of glucose consumption. We find that the carrier model, which assumes a constant contribution of glucose transporters, is not able to reproduce the experimentally observed dynamics of glucose consumption. We attribute this discrepancy between the simulations and the experimental data to the overly simplified model. We therefore established an advanced model that considers the dynamic contribution of low and high affinity glucose transporters. Our results show that the model, which describes the dynamic contribution of high and low affinity transporters appropriately, leads to an improved agreement of the simulations and the experimental data of glucose consumption. Our findings reveal substantial changes in the degree of utilization of the membrane transporters upon pulsing with nutrients in order to maintain an efficient uptake. Our model is suitable to study glucose triggered signalling pathways, in this work demonstrated for the Snf1 pathway.

Various studies of sugar transport across the plasma membrane have resulted in a deeper understanding of its mechanisms [Bisson *et al.* 1993; Boles and Hollenberg 1997; Özcan and Johnston 1999; Carlson 1999; Diderich *et al.* 1999]. Modelling approaches for transmembrane glucose transport comprised carrier models [Steinmeyer and Shuler 1989; Rizzi *et al.* 1996; Teusink *et al.* 2000; Hynne *et al.* 2001; Bertilsson *et al.* 2008], which are formally identical to the Michaelis-Menten equation for enzyme kinetic reactions. Carrier models describe the glucose uptake by facilitated diffusion [Hoppe *et al.* 1983; Teusink *et al.* 2000] and include the following properties: i) Transport of glucose to the interior of the cell occurs only in the presence of a concentration gradient. ii) The transport is substrate selective. iii) For high glucose concentrations, a maximal flow of glucose into the cell is reached and saturation occurs [Hoppe *et al.* 1983; Weiss 1996].

3.1.1. Materials and methods

Yeast strains and growth conditions

The yeast strain used in this work is YSH1715 (MATa ura3-52 snf1::KanMX), derived from W303-1A (MATa ade2-1 can1-100 his3- Δ 1 leu2-3,112 trp1-289 ura3-52) [Wallis *et al.* 1989] and made prototrophic by transformation with the plasmid pRS316-SNF1-HA [McCartney and Schmidt 2001]. Cultivations were conducted in a Braun Biostat A fermentor (Braun, Melsungen, Germany), using 2x concentrated defined minimal medium [Verduyn *et al.* 1992] containing 2 % or 4 % glucose as carbon source (see Table 3.1) and 0.1mL/L polypropylene glycol as anti-foaming agent. The medium (2 L) was inoculated with an overnight culture to an optical density (OD_{600nm}) of 0.05 and cells were grown with an aeration of 0.5L/min, at 30°C, 1000 rpm and pH 5. In some of the fermentations, two hours

3.1. Dynamics of hexose transporters in *S. cerevisiae* upon glucose pulses

after sugar depletion the cultivation was pulsed with glucose to a final concentration of 2% or 4 % (Table 3.1). Carbon Dioxide production was measured on-line (one measurement per minute) using a photoacoustic gas analyser (type 1308; Brüel and Kjaerum, Denmark). Samples were withdrawn during the experiment for the determination of extracellular glucose and the measurement of the optical density. For our analysis, we included data from eight different experiments. An overview of the experiments is given in Table 3.1.

Experiment	A	B	C	D	E	F	G	H
Glucose concentration [g/L] at 16 hours before time zero	40	20	20	40	40	40	-	-
Initial glucose concentration [g/L] at time zero	32.99	0	0	28.41	36.1	19	24	10.82
Amount of glucose pulse [g/L]	34.89	40.59	43.18	19.09	34.46	-	87.32	88.55
Time of added glucose pulse	8.55[h]	1.13[h]	1 [h]	6.36[h]	9.30[h]	-	1[min]	1[min]
Duration of glucose depletion	3.18[h]	1.13[h]	1 [h]	2.02[h]	2.61[h]	-	-	-

Table 3.1.: Overview of the different glucose pulse experiments. Cells were inoculated in a medium with initial glucose concentration as listed. After sugar depletion, some of the fermentors were pulsed with glucose (denoted as ‘Amount of glucose pulse’).

Determination of extracellular glucose

Duplicate samples of 1 ml were sterile-filtered (0.22 μm pore size), frozen in liquid nitrogen and stored at $-40^{\circ}C$. Glucose was determined using an enzyme kit (Boehringer-Mannheim GmbH, Mannheim, Germany).

Numerical simulations

Numerical simulations were carried out in Matlab (MathWorks, Inc.). Parameter estimation was done with the *Systems Biology Toolbox2* [Schmidt and Jirstrand 2006] using the *pswarm-algorithm* [Vaz and Vicente 2007].

3. Mathematical modelling of the Snf1 pathway

3.1.2. The carrier model for glucose transport

S. cerevisiae thrives in environments with wide variations of glucose concentrations due to a family of hexose transporters specialised in uptake through their affinities towards glucose [Özcan and Johnston 1999]. In order to explain our experimental data from batch cultivations, we present different models. To begin with, we use the established carrier model and show its inadequacy in Section 3.1.2. Then, we extend this model in Section 3.1.3 and 3.1.4 to improve the agreement of the model simulations with the experimental data. In Section 3.1.5, we apply our model to derive a glucose-regulated stimulus to model the dynamics of Snf1 (de-)phosphorylation.

Yeast consumes glucose using facilitated transport [Fuhrmann *et al.* 1976], mediated by several hexose transporters [Boles and Hollenberg 1997]. It incorporates a saturation that rises from a limited number of transporters in the membrane. Hence, there is a threshold rate beyond which the cells cannot consume glucose any faster. The uptake of glucose from the extracellular to the intracellular medium can thus formally be described by a carrier model

$$\frac{d}{dt}Glc_{\text{ext}} = -\frac{V_{\text{max}} \cdot Glc_{\text{ext}}}{K_{\text{M}} + Glc_{\text{ext}}} \cdot \text{OD} \cdot k_{\text{OD}} \quad (3.1)$$

with $V_{\text{max}} = k \cdot Hxt^{\text{total}}$ comprising all hexose transporters of a cell, thereby k denoting a rate of transport efficiency. Due to the assumption that internal glucose is rapidly transformed into glucose-6-phosphate and hence, cannot cross the membrane again [Becker and Betz 1972], we consider only the influx of glucose not the efflux, as suggested in [Rizzi *et al.* 1996]. The parameters $V_{\text{max}} = k \cdot Hxt^{\text{total}}$ denoting the limiting rate of glucose uptake and K_{M} denoting the affinity constant, are estimated from our experimental data using the *SBToolbox2* [Schmidt and Jirstrand 2006]. The glucose consumption rate $d/dt Glc_{\text{ext}}$ considers the overall number of cells within the fermentor. Therefore, the right hand side of Eq. (3.1) needs the incorporation of the factor $\text{OD} \cdot k_{\text{OD}}$. The OD denotes the optical density (OD_{600}) and k_{OD} is a factor to convert the optical density to the number of cells per litre. Since one unit of OD_{600} corresponds to approximately 10^{10} cells per litre, we approximate $k_{\text{OD}} \cdot \text{OD} \approx 10^{10} \cdot \text{OD}$. In order to restrict the intervals for reasonable parameter values, we use information from the literature: The limiting transport rate V_{max} of cells that are fermenting glucose rapidly was measured in ranges up to 10^7 glucose molecules per cell per second [Kruckeberg 1996]. We relate this value properly for our experimental data of extracellular glucose, since it is measured in hours and g/L. Then, it results in approximately $36 \cdot 10^9$ glucose molecules per cell per hour, which is approximately equal to 10^{-11} gram per cell per hour. The model described above is not sufficient to describe the data of glucose consumption under the experimental conditions studied (Figure 3.1(a)). There is no unique set of V_{max} and K_{M} values, which

3.1. Dynamics of hexose transporters in *S. cerevisiae* upon glucose pulses

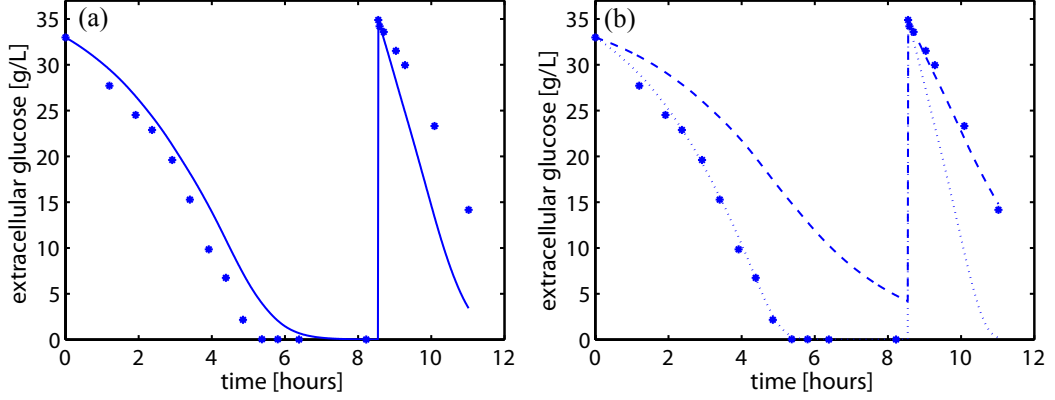


Figure 3.1.: Simulation of glucose consumption Eq. (3.1) compared to experimental data from Experiment A (see Table 3.1). (a) The simulation is too slow for the first consumption (\approx hour 0 to hour 6) and too fast for the second consumption (\approx hour 8 to end of experiment). The estimated parameters are: $V_{\max} = 1.9 \cdot 10^{-10}$ gram per litre per hour and $K_M = 8.3$ g/L. (b) It is possible to simulate the experimental data of the first glucose consumption or the second, but not both at the same time. Fitting the first glucose consumption curve (\approx hour 0 to hour 6) is possible through changing, e.g. the value for K_M to 3.2 g/L (dotted line), fitting the second glucose consumption curve (\approx hour 8 to end of experiment) is possible through changing, e.g. the value for K_M to 36 g/L (dashed line), but there is no unique set of parameters to fit both at the same time.

explains the time course of the whole experiment. Considering two different value sets of the parameters, we can either reproduce the first glucose consumption (within the first six hours of Figure 3.1(b)), or the second glucose consumption (time after the given pulse in Figure 3.1(b)). This clearly suggests the need to include at least one additional factor to account for the deviations between the experimental data and the simulation of Eq. (3.1). A summary of all parameter values is given in Table 3.2.

So far, the glucose consumption rate has been described assuming a constant contribution of transporters (Eq. (3.1)). However, in the course of our experiments, the yeast cells face extreme glucose conditions, varying from 0 % up to 4 % glucose concentrations. The sudden exposure to high glucose concentrations is accomplished by adding a pulse. We reason that the composition of high and low affinity transporters in the cell membrane differs significantly, comparing cells in high to cells in low glucose concentrations. Hence, the consequence is a different glucose uptake rate. Thus, we hypothesise that the deviation between simulation and experimental data is due to the neglected dynamic contribution of high and low affinity transporters in the cell membrane. Consequently, we now establish a model that considers the contribution of the transporters in response to glucose availabilities in the following section.

3. Mathematical modelling of the *Snf1* pathway

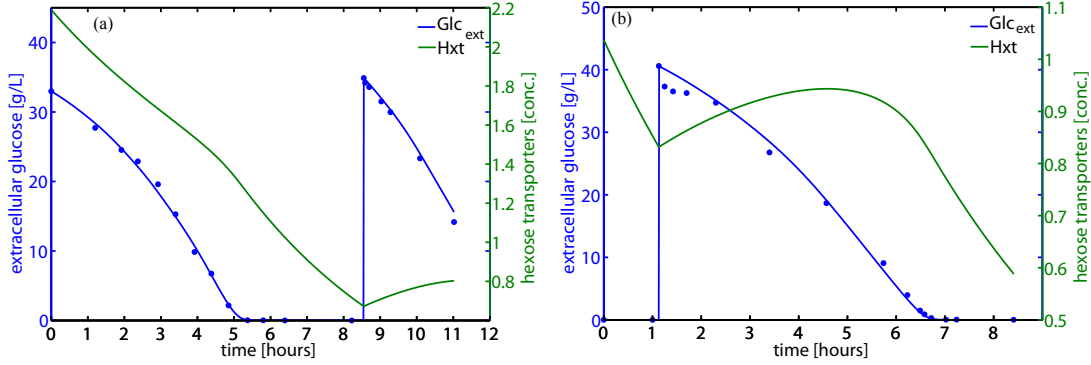


Figure 3.2.: Simulations of glucose consumption (blue line) and the consolidated contribution of hexose transporters (green line). (a) Simulation of Eq. (3.2) for glucose consumption (blue line) compared to experimental data for glucose (blue dots) and simulation of Eq. (3.3) for the hexose transporters in the membrane (green line), for Experiment A. (b) Analogous to (a) for Experiment B, respectively. Experiments are listed in Table 3.1. Parameter values are shown in Table 3.2.

3.1.3. Dynamic contribution of hexose transporters

Since the model assuming a constant contribution of hexose transporters, as described in Eq. (3.1), does not simulate the experimental data accurately, we consider the contribution of transporters that varies with glucose availabilities. We therefore extend Eq. (3.1) to incorporate the contribution of the hexose transporters

$$\frac{d}{dt}Glc_{\text{ext}} = -\frac{k \cdot Hxt(t) \cdot Glc_{\text{ext}}}{K_M + Glc_{\text{ext}}} \cdot OD \cdot k_{OD} \quad (3.2)$$

In contrast to the constant contribution of hexose transporters in Eq. (3.1), the term $Hxt(t)$ captures their dynamic contribution on glucose transport. Since V_{max} is denoted as the limiting transport rate for a constant total amount of transporters, we replace V_{max} with $k \cdot Hxt(t)$ to emphasise the dynamics. The rate of change of the hexose transporters is formalised as

$$\frac{d}{dt}Hxt = k_{\text{synth}} \cdot \frac{Glc_{\text{ext}}}{K + Glc_{\text{ext}}} - k_{\text{degr}} \cdot Hxt \quad (3.3)$$

In this equation, the synthesis term comprises the increase of the hexose transporters in the presence of extracellular glucose [Özcan and Johnston 1999]. The synthesis includes among others also the expression and the recruitment of the transporters into the cell membrane. Analogously, the degradation term is composed of the removal from the membrane and the degradation within the cytosol. In addition, we define a limit upon which the rate of synthesis of transporters is saturated. The estimated values of the parameters of Eqs. (3.2) and (3.3) are listed in Table 3.2. This amendment results in a significant improvement for explaining the experimental data of glucose consumption as shown in Figure 3.2.

3.1. Dynamics of hexose transporters in *S. cerevisiae* upon glucose pulses

However, as can be seen in Figure 3.2(b) for Experiment B (specified in Table 3.1), rapidly after the glucose pulse (time 1.5 hours), glucose is first consumed faster, and then slowed down. This can also be observed for Experiment A (Figure 3.2(a)) but to a much less extent. This behaviour cannot be described assuming transporters with a single affinity (K_M) to glucose as in Eq. (3.2). This difference between the two experiments might be a consequence of different experimental setups. Prior to starting the experimental measurements of Experiment B (Table 3.1), the cells were exposed to low and zero glucose concentrations before the beginning of the experiment (from time 16 hours before the start of the experiment until time zero). Furthermore, the duration of glucose repression in Experiment A was much shorter (from time five to time eight, shown in Figure 3.2(a)) than in Experiment B. Taken the observation and the different experimental setup together, this might indicate that the composition of high and low affinity transporters in Experiment B (after several hours exposed to glucose poor medium) is highly adapted to transport glucose in glucose poor conditions, whereas their composition in Experiment A (after only ≈ 3 hours exposed to glucose poor medium) has not yet reached the same level. Thus the deviation immediately after the glucose pulse might be interpreted as an abundance of high affinity transporters that were produced and recruited by the cells during the glucose poor condition. During glucose absence that precedes the pulse, the high affinity transporters were active, while the low affinity transporters were repressed. Upon pulsing with glucose, the low affinity transporters need to be synthesised and transported to the cell membrane. Through the addition of the glucose pulse, the high affinity transporters, still located within the cell membrane, face high glucose concentrations. This leads to a too fast uptake and consumption of glucose by the cells, which results in the accumulation of waste products of the electronic transport chain, glycolysis and fermentation. Those waste products include toxic molecules, e.g. super oxide ions, or oxygen peroxides. Thus, to maintain a healthy intracellular environment, the cells have to slow down the uptake rate by adapting the transporters composition.

Based on our analysis and the discussion above, we further improve the model by considering both, high and low affinity transporters, in a more detailed manner. This is accomplished by using two separate differential equations instead of just one for the hexose transporters.

3.1.4. Dynamic contribution of high and low affinity transporters

There is previous evidence [Bisson and Fraenkel 1983] that glucose uptake in yeast involves at least two different types of systems, which differ in their affinities to glucose. For the high affinity uptake system, K_M values of ca. 1 mM (≈ 0.2 g/L) for glucose were measured and for the low affinity uptake system, K_M values of ca. 20 mM (≈ 5 g/L) [Bisson and Fraenkel 1983; Özcan and Johnston 1999]. The high affinity transporters

3. Mathematical modelling of the *Snf1* pathway

are repressed in cells grown with high glucose concentrations and are derepressed in cells grown on low glucose concentrations, whereas the low affinity transporters appear to be largely constitutive [Özcan and Johnston 1999]. Extending Eq. (3.1), we now define two terms for the consumption of glucose: one responsible for the glucose transport in glucose rich medium, the other dominating the transport process in glucose poor medium. In contrast to Rizzi *et al.* [Rizzi *et al.* 1996], we consider the dynamics of high and low affinity transporters as shown in the following three equations:

$$\frac{d}{dt}Glc_{\text{ext}} = - \left(\frac{k^{\text{low}} \cdot Hxt^{\text{low}}(t) \cdot Glc_{\text{ext}}}{K_M^{\text{low}} + Glc_{\text{ext}}} + \frac{k^{\text{high}} \cdot Hxt^{\text{high}}(t) \cdot Glc_{\text{ext}}}{K_M^{\text{high}} + Glc_{\text{ext}}} \right) \cdot OD \cdot k_{\text{OD}}. \quad (3.4)$$

The degradation of the transporters occurs on the one hand to be constitutively and on the other hand to be influenced by the availability of affinity transporters of the opposite type. Hence, we establish the rate of change for low affinity transporters

$$\frac{d}{dt}Hxt^{\text{low}} = k_{\text{synth}}^{\text{low}} \cdot \frac{Glc_{\text{ext}}}{K^{\text{low}} + Glc_{\text{ext}}} - k_{\text{degr1}}^{\text{low}} \cdot Hxt^{\text{low}} - k_{\text{degr2}}^{\text{low}} \cdot Hxt^{\text{low}} \cdot Hxt^{\text{high}} \quad (3.5)$$

and for high affinity transporters

$$\frac{d}{dt}Hxt^{\text{high}} = k_{\text{synth}}^{\text{high}} \cdot \frac{1}{K^{\text{high}} + Glc_{\text{ext}}} - k_{\text{degr1}}^{\text{high}} \cdot Hxt^{\text{high}} - k_{\text{degr2}}^{\text{high}} \cdot Hxt^{\text{high}} \cdot Hxt^{\text{low}} \quad (3.6)$$

For high affinity transporters, we define an inhibition term for the synthesis depending on glucose concentrations. The inhibition term ensures high affinity transporters to be available in glucose poor conditions. The simulations of glucose consumption are in good agreement with the experimental data as shown in Figure 3.3(a). The simulations of Eqs. (3.5) and (3.6) for low and high affinity transporters, respectively, are shown in Figure 3.3(b). During glucose absence, the sensitive high affinity transporters increase and eventually approach their maximum (Figure 3.3(b)). With the addition of the glucose pulse, an instant reorganisation of the transporters composition begins, in order to adapt to the new extreme glucose conditions and to avoid an accumulation of waste products. Consequently, before this reorganisation has been completed, a noticeably faster consumption rate of glucose is observed (Figure 3.3(a)). This result points towards a significant reorganisation of the membrane transporters upon pulsing with nutrients in order to maintain an efficient uptake. Note that the simulations of glucose consumption for all other experiments of Table 3.1 are shown in Figure 3.4.

Given the model of high and low affinity transporters, we show the changes in their composition with respect to changes in glucose concentrations in Figure 3.5. A reciprocal relationship between the high and low affinity transporters as reported in [Ramos *et al.* 1988] is supported by our simulations (Figure 3.3(b) and Figure 3.5). As glucose

3.1. Dynamics of hexose transporters in *S. cerevisiae* upon glucose pulses

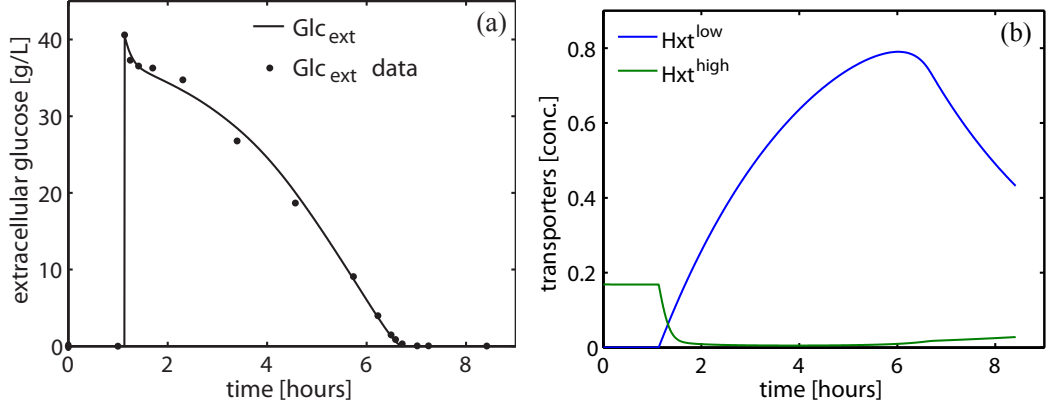


Figure 3.3.: Simulations of the dynamics of glucose concentration for Experiment A (see Table 3.1) considering high and low affinity transporters. (a) Simulation of Eq. (3.2) (line) and experimental data of external glucose (dots). The simulation is in good agreement with the experimental data. The noticeably faster consumption rate of glucose following a pulse can be reproduced by the model. (b) Simulations of Eqs. (3.5) and (3.6) describing the dynamic change in composition of low (blue line) and high (green line) affinity transporters. In high glucose concentrations, the low affinity transporters increase, whereas in low glucose concentrations, the high affinity transporters increase. A maximum has been reached here, since the cells have been exposed to glucose poor conditions.

concentrations increase, the low affinity transporters reach a limit of saturation at the value $Hxt^{\text{low}} = k_{\text{synth}}^{\text{low}}/k_{\text{degr1}}^{\text{low}} \approx 1.1961$ as shown in Figure 3.5. *Vice versa*, as glucose concentrations decrease, the high affinity transporters reach a saturation limit, at the value $Hxt^{\text{high}} = k_{\text{synth}}^{\text{high}} / (k_{\text{degr1}}^{\text{high}} \cdot K^{\text{high}}) \approx 0.1688$. The derivations of these numbers are shown in detail in the next paragraph. Interestingly, the estimated value of the parameter k^{high} for high affinity transporters reveals an about 30-fold higher value compared to the value of its analogical parameter k^{low} for low affinity transporters (Table 3.2). This indicates, that the lower concentration of high affinity transporters (about 10-fold lower, as shown in Figure 3.5) is compensated through a higher efficiency of the transporters, whereas in comparison the highly concentrated low affinity transporters operate less efficiently.

Derivation of the transporters concentrations in steady state

For derivation of the concentration of high and low affinity transporters at steady state as shown in Figure 3.5, we use Eqs. (3.5) and (3.6), setting these equations equal to zero. In general, this system can be solved numerically only. However, for limiting cases, a solution can be calculated analytically. In the following, the steps are shown.

- **The limiting case $Glc_{\text{ext}} \ll K^{\text{low}}, K^{\text{high}}$**

- For low affinity transporters, the case $Glc_{\text{ext}} \ll K^{\text{low}}$ leads to the cancellation

3. Mathematical modelling of the Snf1 pathway

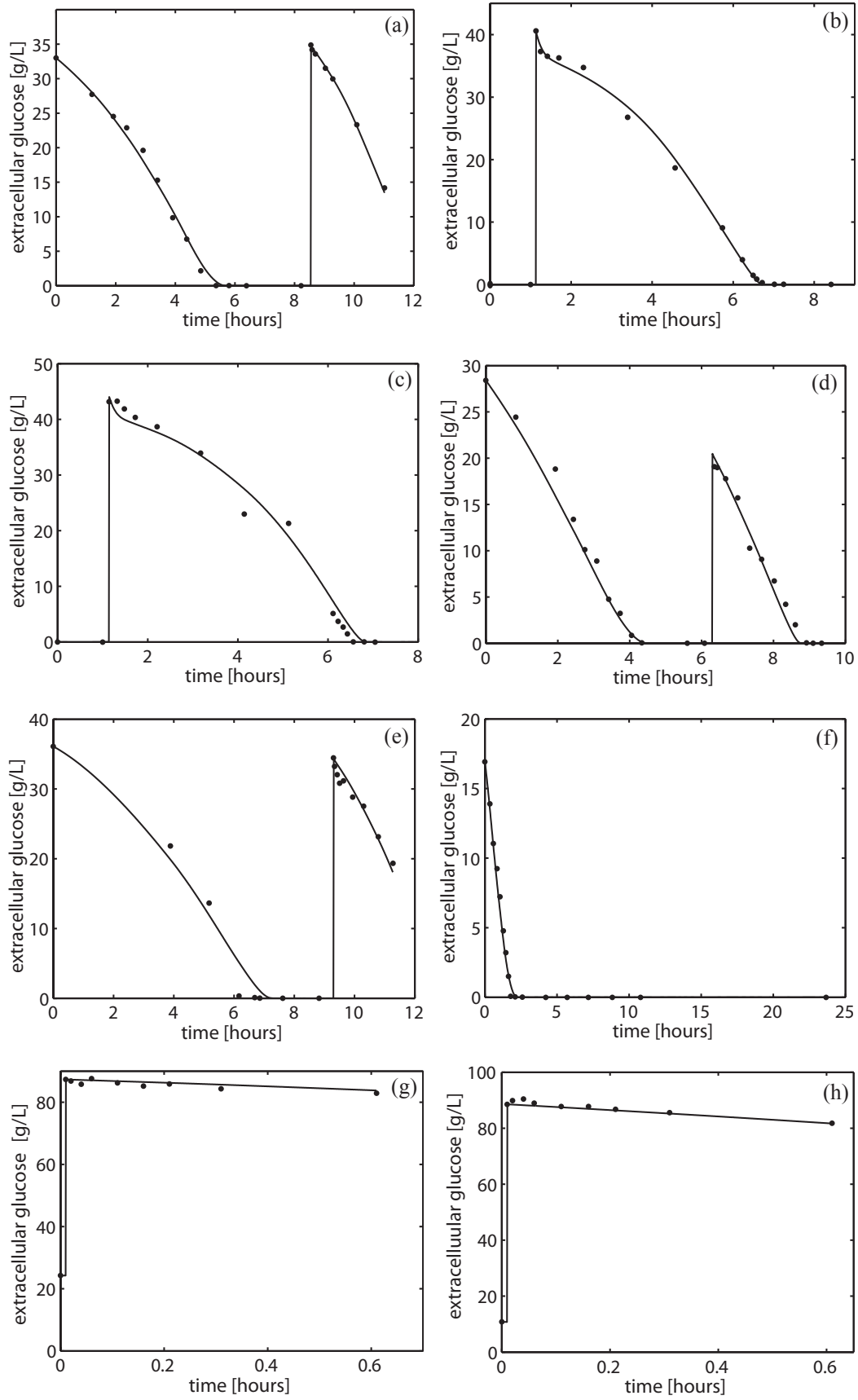


Figure 3.4.: Comparison of simulations of Eq. (3.4) representing glucose consumption to data of extracellular glucose (dots) for all experiments (in order: A, B, C, D, E, F, G, H, compare Table 3.1).

3.1. Dynamics of hexose transporters in *S. cerevisiae* upon glucose pulses

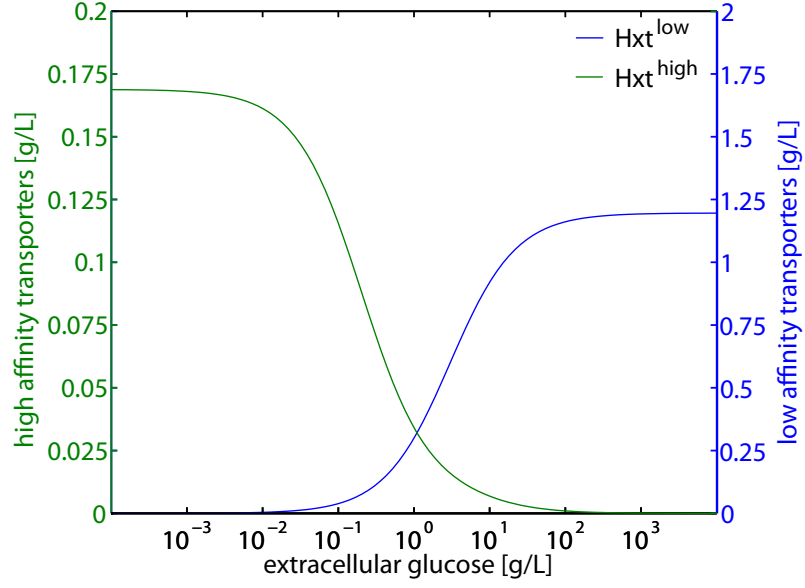


Figure 3.5.: High and low affinity transporters as function of glucose concentration at steady-state conditions. A reciprocal relationship between the high and low affinity transporters as reported in [Ramos *et al.* 1988] as glucose concentrations increase, the low affinity transporters reach a limit of saturation at the value $Hxt^{\text{low}} \approx 1.1961$ g/L. *Vice versa*, as glucose concentrations decrease, the high affinity transporters reach a saturation limit, at $Hxt^{\text{high}} \approx 0.1688$ g/L.

of the synthesis term, with only the degradation terms remaining

$$\begin{aligned} -k_{\text{degr1}}^{\text{low}} \cdot Hxt^{\text{low}} - k_{\text{degr2}}^{\text{low}} \cdot Hxt^{\text{high}} \cdot Hxt^{\text{low}} &= 0 \\ \Leftrightarrow Hxt^{\text{low}} \left(-k_{\text{degr1}}^{\text{low}} - k_{\text{degr2}}^{\text{low}} \cdot Hxt^{\text{high}} \right) &= 0. \end{aligned}$$

This equation can only be fulfilled for $Hxt^{\text{low}} = 0$.

- For high affinity transporters, the case $Glc_{\text{ext}} \ll K^{\text{high}}$ results in

$$\frac{k_{\text{synth}}^{\text{high}}}{K^{\text{high}}} - k_{\text{degr1}}^{\text{high}} \cdot Hxt^{\text{high}} - k_{\text{degr2}}^{\text{high}} \cdot Hxt^{\text{high}} \cdot Hxt^{\text{low}} = 0$$

and inserting the expression $Hxt^{\text{low}} = 0$ g/L derived above, leads to

$$Hxt^{\text{high}} = \frac{k_{\text{synth}}^{\text{high}}}{k_{\text{degr1}}^{\text{high}} \cdot K^{\text{high}}}.$$

Taking the estimated parameter values, which are shown in Table 3.2, we obtain the value for amounts of high affinity transporters

$$Hxt^{\text{high}} = \frac{k_{\text{synth}}^{\text{high}}}{k_{\text{degr1}}^{\text{high}} \cdot K^{\text{high}}} \approx 0.1688 \text{ g/L}.$$

3. Mathematical modelling of the *Snf1* pathway

- The limiting case $Glc_{\text{ext}} \gg K^{\text{low}}, K^{\text{high}}$

- For high affinity transporters, the case $Glc_{\text{ext}} \gg K^{\text{high}}$ leads to the cancellation of the synthesis term, with only the degradation terms remaining

$$\begin{aligned} -k_{\text{degr1}}^{\text{high}} \cdot Hxt^{\text{high}} - k_{\text{degr2}}^{\text{high}} \cdot Hxt^{\text{high}} \cdot Hxt^{\text{low}} &= 0 \\ \Leftrightarrow Hxt^{\text{high}} \left(-k_{\text{degr1}}^{\text{high}} - k_{\text{degr2}}^{\text{high}} \cdot Hxt^{\text{low}} \right) &= 0. \end{aligned}$$

This equation can only be fulfilled for $Hxt^{\text{high}} = 0$ g/L.

- For low affinity transporters, the case $Glc_{\text{ext}} \gg K^{\text{low}}$ results in

$$k_{\text{synth}}^{\text{low}} - k_{\text{degr1}}^{\text{low}} \cdot Hxt^{\text{low}} - k_{\text{degr2}}^{\text{low}} \cdot Hxt^{\text{high}} \cdot Hxt^{\text{low}} = 0$$

and inserting the expression $Hxt^{\text{high}} = 0$ derived above gives

$$\begin{aligned} k_{\text{synth}}^{\text{low}} - k_{\text{degr1}}^{\text{low}} \cdot Hxt^{\text{low}} &= 0 \\ \Leftrightarrow \frac{k_{\text{synth}}^{\text{low}}}{k_{\text{degr1}}^{\text{low}}} &= Hxt^{\text{low}}. \end{aligned}$$

In contrast to the value for high affinity transporters, this term is independent of the affinity constants K^{low} and K^{high} , respectively. Taking the estimated parameter values from Table 3.2, we obtain the value for the amount of low affinity transporters

$$Hxt^{\text{low}} = \frac{k_{\text{synth}}^{\text{low}}}{k_{\text{degr1}}^{\text{low}}} \approx 1.1961 \text{ g/L.}$$

3.1.5. Applications of the model

The model including the dynamics of high and low affinity transporters can be used to deduce a stimulus for a glucose dependent signalling pathway. We assume that the difference between the rate of glucose consumption per cell and its conversion to glucose-6-phosphate (rate of glycolysis) is proportional to the rate of change of internal glucose concentration. Whereas the external glucose consumption was related to all cells in the fermentor ($OD \cdot k_{\text{OD}}$), we now relate the internal glucose concentration to an average single cell by dividing by the approximate number of all cells per litre, $OD \cdot k_{\text{OD}}$

$$\frac{d}{dt}Glc_{\text{int}} = \frac{k^{\text{high}} \cdot Hxt^{\text{high}}(t) \cdot Glc_{\text{ext}}}{K_{\text{M}}^{\text{high}} + Glc_{\text{ext}}} + \frac{k^{\text{low}} \cdot Hxt^{\text{low}}(t) \cdot Glc_{\text{ext}}}{K_{\text{M}}^{\text{low}} + Glc_{\text{ext}}} - \hat{k}_{\text{glycolysis}} \cdot Glc_{\text{int}}. \quad (3.7)$$

3.1. Dynamics of hexose transporters in *S. cerevisiae* upon glucose pulses

Assuming steady-state conditions, we obtain an approximation for the glycolytic rate coefficient

$$k_{\text{glycolysis}} \approx \frac{Glc_{\text{ext}}}{Glc_{\text{int}}} \cdot \left(\frac{k^{\text{high}} \cdot Hxt^{\text{high}}(t)}{K_{\text{M}}^{\text{high}} + Glc_{\text{ext}}} + \frac{k^{\text{low}} \cdot Hxt^{\text{low}}(t)}{K_{\text{M}}^{\text{low}} + Glc_{\text{ext}}} \right). \quad (3.8)$$

The rate of glycolysis depends on the ratio of extra- and intracellular glucose concentrations and the contribution of the high and low affinity transporters. Under standard conditions, the intracellular glucose concentration in wild-type cells consuming glucose has been taken to be very, if not negligibly, low [Teusink *et al.* 1998]. This rate can then be used as an input in glucose signalling, e.g. as the signal controlling the Snf1 pathway [Gancedo 1998; Santangelo 2006]. Snf1 is activated through phosphorylation upon glucose limitation and inhibited through dephosphorylation upon glucose presence [Wilson *et al.* 1996; McCartney and Schmidt 2001]. We establish a mathematical model for Snf1 dynamics by integrating the variable for the glycolytic rate, $k_{\text{glycolysis}}$, derived from the model for high and low affinity transporters

$$\frac{d}{dt} Snf1^{\text{P}} = a \cdot Snf1 - k_{\text{glycolysis}} \cdot Snf1^{\text{P}}$$

with the total number of molecules staying constant:

$$Snf1_{\text{total}} = Snf1^{\text{P}} + Snf1.$$

The Snf1 Western blot data are composed of phosphorylated Snf1 divided by the total concentration:

$$Snf1_{\text{ratio}}^{\text{P}} = Snf1^{\text{P}} / Snf1_{\text{total}}.$$

Implementing this model into the *SBToolbox2* [Schmidt and Jirstrand 2006] and performing a parameter estimation with the *pswarm-algorithm* [Vaz and Vicente 2007], we achieve the simulations shown in Figures 3.6(a) and 3.6(b). The good agreement of the data and simulation support our model development to the point of high and low affinity contribution and the derivation of the glycolytic rate following thereon.

3.1.6. Conclusions

Glucose is the main energy and carbon source for the yeast, *S. cerevisiae*. The abundance of this sugar is carefully sensed by the cells, adapting the mode of metabolism accordingly. In its natural habitat, yeast is exposed to a wide range of glucose concentrations [Greatrix and Vuuren 2006]. In order to control glucose uptake rate, yeast features transporters with high and low affinities towards glucose. Modelling approaches for transmembrane glucose transport comprise carrier models. We demonstrated that a carrier model, which assumes a constant contribution of high and low affinity transporters, is not sufficient to

3. Mathematical modelling of the Snf1 pathway

Parameter	Unit	Values for the carrier model (Eq. (3.1))	Values for the dynamic transporter model (Eqs. (3.2)+(3.3))	Values for the dynamic high and low affinity model (Eqs (3.4)–(3.6))
k_{OD}	–	10^{10}	10^{10}	10^{10}
K_M	g/L	5	1	–
V_{max}	g/(L · h)	$1.6 \cdot 10^{-10}$	–	–
k	1/h	–	$1 \cdot 10^{-10}$	–
k_{synth}	g/ (L · h)	–	0.27	–
k_{degr}	1/h	–	0.19	–
K	g/L	–	8.86	–
K_M^{low}	g/L	–	–	5
K_M^{high}	g/L	–	–	0.2
k^{low}	1/h	–	–	$1.2 \cdot 10^{-10}$
k^{high}	1/h	–	–	$30.8 \cdot 10^{-10}$
Hxt^{low}	g/L	–	–	dynamic
Hxt^{high}	g/L	–	–	dynamic
k_{synth}^{low}	g/ (L · h)	–	–	0.36
k_{synth}^{high}	g ² / (L ² · h)	–	–	7.52
k_{degr1}^{low}	1/h	–	–	0.3
k_{degr2}^{low}	L/ (g · h)	–	–	$6 \cdot 10^{-6}$
k_{degr1}^{high}	1/h	–	–	5
k_{degr2}^{high}	L/ (g · h)	–	–	57
K_{Hxt}^{high}	g/L	–	–	2.9
K_{Hxt}^{low}	g/L	–	–	8.8

Table 3.2.: Overview of the parameters, units, and their estimated values of the models described in the text. The values in bold style highlight parameter values taken from literature.

3.1. Dynamics of hexose transporters in *S. cerevisiae* upon glucose pulses

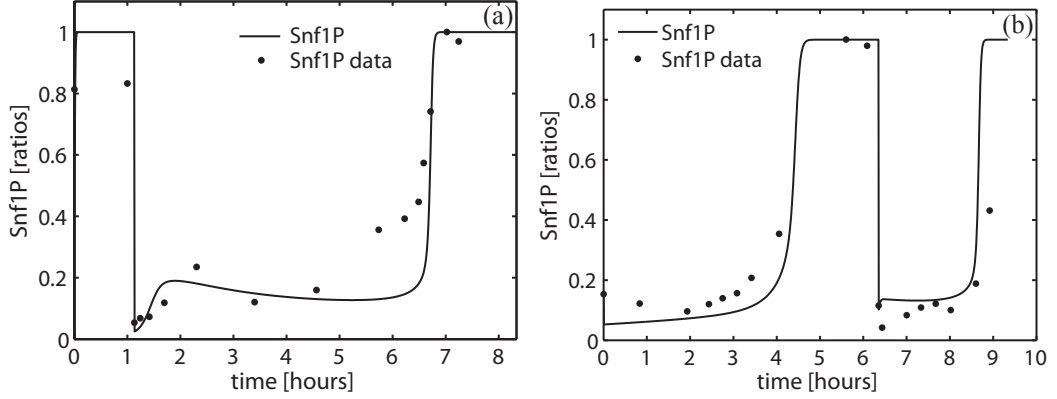


Figure 3.6.: Simulation of phosphorylated Snf1 (denoted Snf1P) compared to Snf1 Western blot data for (a) Experiments B and (b) Experiment D, as detailed in Table 3.1.

describe the glucose uptake in yeast for different batch experiments. We hypothesised that these poor agreements are a consequence of neglecting the dynamic changes of the transporters composition in the cell membrane. We showed the need to account for both, high and low affinity transporters. While high affinity transporters enhance the uptake of glucose in very low glucose concentrations, their pronounced presence in high glucose concentrations can be harmful to the cell. A too fast uptake of glucose can result in an accumulation of toxic waste products during glycolysis. Thus, high affinity transporters must be downregulated in high glucose concentrations in order to keep a healthy intracellular environment. Our results show that the consideration of the dynamic contribution of high and low affinity transporters leads to an explanation of the experimental data. These results point towards a significant reorganisation of the membrane transporters upon pulsing with glucose, in order to achieve an efficient glucose uptake while maintaining a healthy intracellular environment. Our analysis of high and low affinity transporters as function of glucose concentration at steady-state conditions supports the finding of a reciprocal relationship between the high and low affinity transporters as reported in [Ramos *et al.* 1988]. As glucose concentrations increase, the low affinity transporters reach a limit of saturation and *vice versa* as glucose concentrations decrease, the high affinity transporters reach a limit of saturation. We calculated these limits analytically. Our estimated value for the rate of transport efficiency in a high affinity transporter reveals an about 30-fold higher value compared to the value of its analogical parameter in low affinity transport. This indicates that the lower concentration of high affinity transporters (about 10-fold lower) is compensated through a higher efficiency of the transporters, whereas in comparison the highly concentrated low affinity transporters operate less efficiently. For mathematical models of glucose-regulated signalling pathways in yeast, such as the Snf1 pathway, our model serves as a template for the input function, i.e. glycolytic rate.

3.2. Data processing for the Snf1 pathway component Mig1

The hereon following text has been published in [Frey *et al.* 2011b]. The data were generated by the group of Mattias Goksör² from the University of Gothenburg.

How can fluorescent microscopy data, exposed to bleaching and affected by background noise, be processed to extract the information of the protein of interest?

In systems biology, mathematical modelling of signal transduction pathways aims at understanding of biological networks. Therefore, high quality quantitative time course data are necessary [Phillips and Milo 2009]. Fluorescence microscopy and related imaging techniques have, together with the development of fluorescent probes, become a powerful tool to assay biological structures and processes in the physiological context of intact living cells [Pepperkok and Ellenberg 2006]. However, the imaging process induces both reversible quenching and irreversible photobleaching of the fluorophores. Consequently, the target molecule is still present but not detectable. Shaner *et al.* [Shaner *et al.* 2008] addressed this problem by developing highly photostable fluorophores of mOrange and TagRFP. Yet, those derivatives are not always useful nor available. In order to address the problem of photobleaching, we use mathematical modelling. In our case study we compare the model to experimental data on Mig1-GFP shuttling. Acting as a transcription factor in the Snf1-pathway, Mig1 plays a crucial role in the energy metabolism of *S. cerevisiae* during the regulation of glucose [Carlson *et al.* 1984]. Mig1 is controlled by its kinase Snf1 and its phosphatase Glc7/Reg1. As introduced in Chapter 2.3, in the presence of glucose, Snf1 is in an inactive dephosphorylated state and Mig1 represses genes such as SUC2, which encode for proteins converting other carbon sources than glucose as the primary source of energy. In this state, Mig1 resides in the nucleus. If glucose is absent, Snf1 is activated through phosphorylation and in turn phosphorylates Mig1 [Östling and Ronne 1998; Treitel *et al.* 1998; Smith *et al.* 1999]. Mig1 is then transported out of the nucleus into the cytosol [DeVit and Johnston 1999] so that alternative carbon sources can be used in the metabolism of the cell [Santangelo 2006]. Our model describes Mig1-GFP shuttling into and out of the nucleus when the cells are repeatedly deprived and exposed to glucose. This procedure gives us an insight into the shuttling of fluorescently tagged Mig1 proteins using time lapse microscopy [Eriksson *et al.* 2010]. Our method of analysis allows for a stepwise extraction of the information on the background and Mig1-GFP bleaching rates, the background-to-Mig1-GFP ratio, and the rates of Mig1-GFP phosphorylation and dephosphorylation. Hereby, it is possible to predict Mig-GFP shuttling as it would occur without bleaching. Our analysis demonstrates how data acquired using an optical

²Department of Physics, University of Gothenburg, SE-41296 Göteborg, Sweden.

3.2. Data processing for the *Snf1* pathway component Mig1

microscope can be processed and used for mathematical modelling of signal transduction pathways.

3.2.1. Materials and methods

Microscope setup

The microscope used in the experiments was an inverted epi-fluorescence microscope, Leica DMI6000B, equipped with a motorised xy stage and a motorised microscope objective. The images were acquired using a 14 bit dynamic range EMCCD camera (C9100-12, Hamamatsu Photonics) together with a fluorescence light source, EL 6000 (Leica Microsystems), a GFP filter cube (472/30 nm exciter, 520/35 nm emitter and 495LP, Semrock IDEX Corporation) and an mCherry filter cube (560/40x exciter, 630/75m emitter and 585LP, ET-*TexRed*, Chroma). The optical tweezers were formed by expanding a laser beam ($\lambda = 1070$ nm, IPG Photonics) to slightly overfill the back aperture of the microscope objective (100x, NA1.3 oil, HCX PL FLUOTAR, Leica Microsystems). The same objective was also used to image the yeast cells. The trapping laser beam was introduced to the microscope via a dichroic mirror (Omega Optical Inc.) inserted between the microscope objective and the filter cube cassette (for details regarding our optical tweezers setup see Sott *et al.* [Sott *et al.* 2009]). The power in the laser focus was calculated to be 240 mW by measuring the transmission through the microscope objective using the dual-objective technique as described by Misawa *et al.* [Misawa *et al.* 1991]. The flow rates in the microchannels were controlled by syringe pumps (CMA 400, CMA Microdialysis AB). The microscope, the camera, and the microfluidic pumps were all controlled from the computer through the software OpenLab (Improvision Inc.) with custom written programs in the extension OpenLab Automator.

Microfluidic device

In order to allow for precise and reversible changes of glucose concentration around single yeast cells, a microfluidic device was constructed, on which three inlet channels were merged into one single channel containing the measurement region wherein the cells were positioned (depicted in Figure 3.7). The lower inlet channel was used to introduce cells suspended in growth medium into the system. The medium flowing in the middle channel was the same growth medium as the cells were suspended in, while the medium flowing in the top channel was pure growth medium without glucose (except for the GFP bleaching experiments, see below). The two lower inlets were connected to the same syringe pump, while the upper inlet was connected to a second pump. Thus, the flow rate could be controlled independently, enabling environmental changes of the cells positioned in the measurement region. Two different flow settings were used, referred to as flow configu-

3. Mathematical modelling of the Snf1 pathway

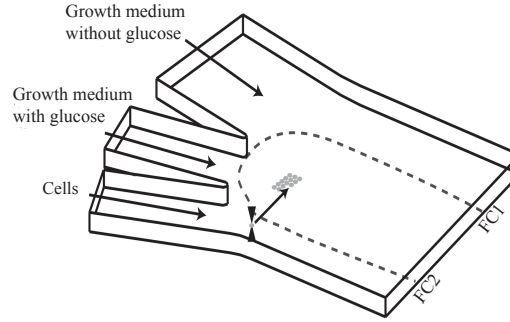


Figure 3.7.: Schematic representation of the microfluidic flow system. The lowermost channel introduces the cells, the middle channel neutral medium, and the uppermost stress medium, in this case medium without glucose. FC1 and FC2 denotes flow configuration 1 and 2, respectively.

ration 1 (FC1) and flow configuration 2 (FC2), respectively, as shown in Figure 3.7. In FC1, the flow rate in the larger inlet was set to 40 nl/min, while the flow rates in the two smaller inlets were set to 80 nl/min. This configuration was used when positioning the cells on the surface and whenever glucose should be present in the measurement region. In FC2, the flow rates were instead 480 nl/min in the larger inlet and 40 nl/min in each of the two smaller inlets. This configuration was used to expose the cells positioned in the measurement region to stress, i.e. to remove glucose.

Fabrication and preparation of the microfluidic device

The microfluidic device was fabricated using soft lithography. For specific details regarding the fabrication process, we refer to Sott *et al.* [Sott *et al.* 2009]. The microfluidic device was moulded in poly(dimethylsiloxane), PDMS, and sealed to a cover glass by exposing both the PDMS and the cover glass to oxygen plasma using a plasma cleaner (Harrick Scientific). Holes were punched in the PDMS structure allowing the channels to be connected to polytetrafluoroethylene (PTFE) tubings, which in turn were attached to 250 μ l glass syringes (Hamilton Company). To enable attachment of cells, Concanavalin A (ConA), dissolved in buffer (10 mM Tris-HCl and 100 mM NaCl at pH 8.0) at a concentration of 1 mg/ml, was allowed to adsorb to the cover glass surface for one hour before the experiments.

Yeast strain, plasmid and growth conditions

The yeast strain used in all experiments was YSH2346 (BY4741 125 MAT α NRD1-mCherry-hphNT1), transformed with the plasmid BM3315 [DeVit *et al.* 1997]. The strain carries its native copy of the MIG1 gene and its only genomic alteration is the insertion of a mCherry-hphNT1 fragment, constructed using plasmid pBS35 (gift from Prof. Roger Y. Tsien) as PCR template, behind the NRD1 gene. The NRD1-mCherry construct allows

3.2. Data processing for the *Snf1* pathway component *Mig1*

for detection of the nucleus in experiments using fluorescence microscopy. BM3315 is a centromeric, URA3 plasmid for expression of Mig1-GFP, driven by the endogenous MIG1 promoter. Cells were grown in synthetic drop-out medium (Yeast Nitrogen Base, YNB, 6.7 g/l, Complete Supplement Mixture (CSM-Uracil) 0.77 g/l pH 6), supplemented with either glucose 4% *m/v* plus ethanol 3 % *v/v* or with ethanol 3 % *v/v* as sole carbon source [DeVit *et al.* 1997]. Yeast cultures were grown to $OD_{600} = 0.6 - 1.0$, corresponding to mid log phase, at 30°C in an 15 incubation shaker (220 rpm), collected and concentrated by centrifugation (30 s, 6000 rpm).

Positioning the cells

To position the cells inside the measurement region of the microfluidic device, the microscope stage and the objective were controlled by an OpenLab automation [Eriksson *et al.* 2010]. The coordinates of the first positioned cell, the total number of cells and the spacing between the cells were all determined by the user. Then, the automation positioned the trapped cells in an array one by one, by bringing them down towards the bottom surface at the desired positions in order to get attached to the coated surface. The program also allowed the user to visually approve the trapped cell before it was positioned in the measurement region. Here, only morphologically deviating cells and cells in clusters were discarded in the experiments. For each experiment, approximately 25 cells were imaged. However, some cells had to be excluded from further analysis, since they showed lack of GFP, looked unhealthy or dead, or were lost during the course of the experiment. This resulted in approximately 20 successfully analysed cells for each experiment.

Image analysis

For each time point an image stack with seven optical sections was acquired. Each optical section was imaged using three different filter settings in order to acquire the brightfield, Mig1-GFP (green) and mCherry (red) signal. In order to keep the fluorescent labeling to a minimum, we used brightfield images to find the cell contours, while the size and position of the nuclei were determined using the fusion protein Nrd1-mCherry, which is always localised in the nucleus independent of the level of stress. The image analysis was performed using our own software, *CellStress* [Smedh *et al.* 2010], written in MATLAB (MathWorks, Inc.). The contours of the nuclei were found using the mCherry images, while the contours of the cells were identified from the brightfield images using the plug-in tool *CellStat* [Kvarnström *et al.* 2008]. The fluorescence intensity of the Mig1-GFP inside the nucleus was finally measured for each individual cell (see Figure 3.8).

3. Mathematical modelling of the Snf1 pathway

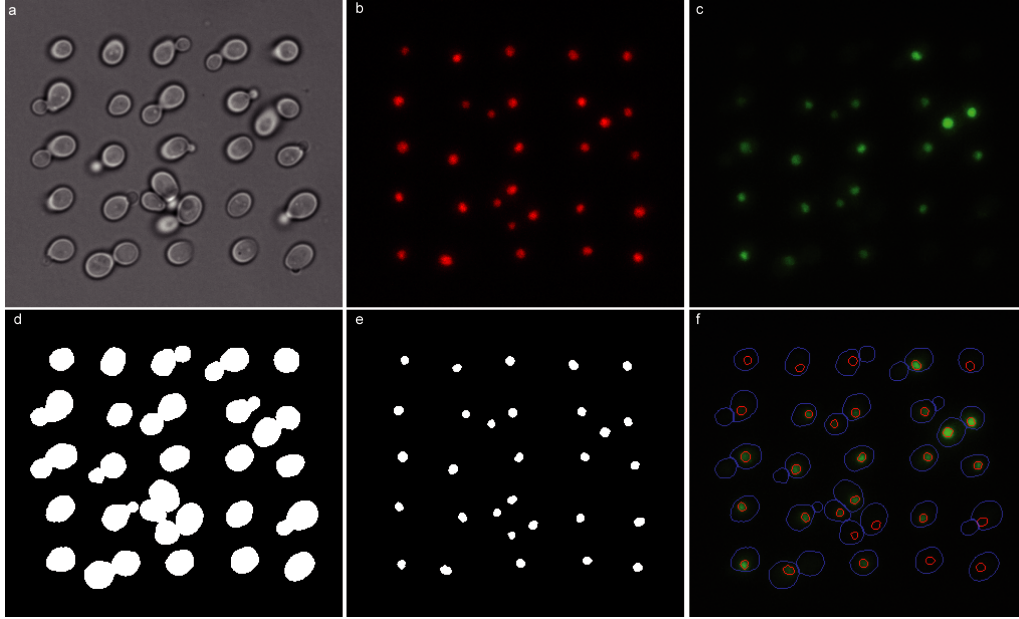


Figure 3.8.: *S. cerevisiae* cells expressing Mig1-GFP and Nrd1-mCherry in 4% glucose media. The image segmentation is performed on (a) the bright field image just below the focal plane and (b) the maximum intensity projection of the mCherry fluorescence channel. In (c) a maximum intensity projection of the GFP channel is shown. (d) and (e) show the segmentation of the bright field and the mCherry images, respectively. In (f) the contours of the cell objects and nuclear objects from the segmentations are shown as an overlay in the GFP image.

Background bleaching experiment

Every cell has autofluorescence, which arises from naturally occurring molecules, such as flavins, NADH and other fluorescing biomolecules [Smedh *et al.* 2010]. The exact mechanism and nature of the background molecules are not known in this case, but bleaching is a widely familiar problem resulting in the destruction of the fluorophore and a decrease in emission intensity over time [Rost 1995]. A background bleaching experiment yields information regarding the bleaching rate of naturally existing fluorescing molecules in the cell. Thus, the experiment was done using the strain BY4741 without the plasmid expressing Mig1-GFP. All other parameters, such as glucose concentration and pulse duration (intervals of 10 minutes only) are as described in the environmental change experiment (see below). Axial stacks (seven images with a spacing of $0.8\mu m$) of brightfield and fluorescence images (GFP and mCherry, respectively) were acquired at intervals of 30 seconds.

GFP bleaching experiment

In order to distinguish between changes in signal intensity due to bleaching of GFP and those due to shuttling kinetics, experiments were performed where cells either remained in a glucose rich medium or in a glucose free medium during the whole course of the experiment. The aim of this experiment was to determine the background-to-Mig1-GFP

3.2. Data processing for the Snf1 pathway component Mig1

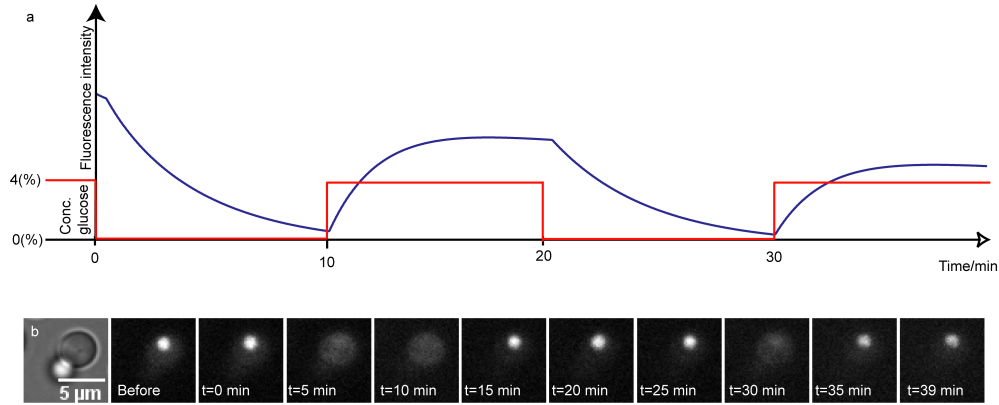


Figure 3.9.: Experiments with a changing environment. (a) Schematic of the change in glucose concentration and the change in GFP signal in the nucleus versus time, respectively. (b) The corresponding microscope images of a selected cell, showing the shuttling of Mig1-GFP into and out of the nucleus as a response of these changes. The leftmost image is a brightfield image and the others are fluorescence images.

ratio and to analyse the rate, by which bleaching of the GFP molecules occurs and how this bleaching rate might differ from that of the naturally occurring fluorescing molecules. Axial stacks (seven images with a spacing of $0.8\mu m$) of brightfield and fluorescence images (GFP and mCherry, respectively) were acquired at intervals of 30 seconds.

Environmental change experiment

Prior to the experiment, cells positioned in the flow chamber were exposed to growth medium containing 3% ethanol and 4% glucose to ensure that they are far away from starvation. Hence, one can assume that the maximum number of Mig1-GFP molecules in the nucleus has been reached prior to the initiation of the experiment. In the course of the experiment, the microfluidic flow settings were shifted such that the cells were exposed to medium containing 3% ethanol as sole carbon source, to only stress the cells by glucose starvation, but not an overall starvation, causing Mig1-GFP to shuttle from the nucleus into the cytosol (see Figure 3.9). Then, shifts between the two media were repeated at different time intervals (5, 10 or 20 minutes) in different experiments. In all cases, the full duration of an experiment was 40 minutes, hence four, two or one complete cycle(s) of shifting could be monitored. Axial stacks (seven images with a spacing of $0.8\mu m$) of brightfield and fluorescence images (GFP and mCherry, respectively) were acquired at intervals of 30 seconds. In order to evaluate the correctness of the model, additional experiments (see Figure 3.15) with image acquisition every 60 seconds were done.

Processing of raw data

Whereas some technologies, like Western blotting, report the average response of a population during the experiment, single cell experiments can instead provide data on individual

3. Mathematical modelling of the Snf1 pathway

cells. To obtain the average dynamic behaviour, it requires an averaging over all cells after the experiment. From all three types of experiments described above, we use the intensity data measured in the nuclei. We first normalise the time series of every cell to its average value over time. The time courses now all share the same average value, which equals one. In a second step, we take the average over all normalised cells at each time point and calculate the standard deviation, thus combining approximately 60 cells out of three experiments. In a last step, we scale this averaged time course to a range between zero and one by dividing with its initial intensity. Hence, for all experiments, the initial time point has the intensity value one.

3.2.2. Results

The intracellular response to the environmental changes results in a shuttling of Mig1-GFP between the nucleus and cytosol and can thus be monitored using fluorescence microscopy. For the mathematical model we used data acquired from time lapse fluorescence microscopy where yeast cells were exposed to repetitive environmental changes between glucose rich and glucose free media. The model takes into account the decrease in intensity over time due to bleaching of Mig1-GFP and autofluorescent molecules. It is based on ODEs and describes the experimental data glucose concentration, background intensities, Mig1-GFP intensities and the sum of background and GFP intensities in a dynamic environment.

Parameter estimation

Numerical simulations were carried out with Matlab (MathWorks, Inc.) and the *Systems Biology Toolbox2* [Schmidt and Jirstrand 2006], using the *particle-swarm-algorithm* [Vaz and Vicente 2007] for parameter estimation. A list of all parameter values is given in Table 3.3.

Background bleaching model

In this experiment, cells without the capability of expressing GFP were used. We describe the bleaching of fluorescing molecules by a decreasing exponential function, implying that the bleaching impact is proportional to the fluorescing molecules available (Figure 3.10a). The experimental data of the background show a rapid initial decline within the first three minutes followed by an almost constant level, as shown in Figure 3.11. Hence, one can assume that the bleaching process of the background molecules is a combination of mainly two different processes: a fast and sensitive process and a slow and insensitive process.

3.2. Data processing for the *Snf1* pathway component Mig1

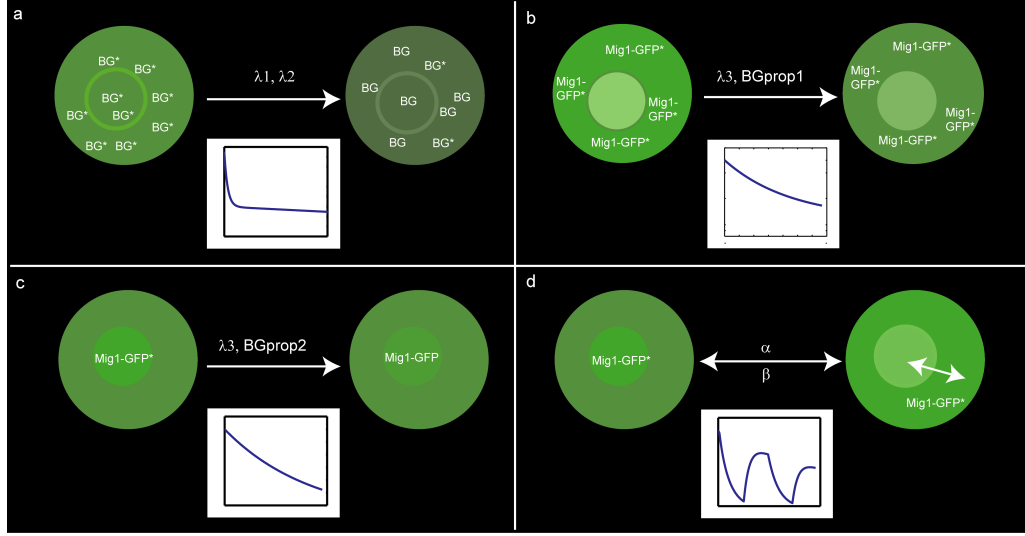


Figure 3.10.: Schematics illustrating the different contributions to the fluorescent signal of the nucleus. (a) Background bleaching with λ_1 denoting the bleaching rate of a fast and sensitive process and λ_2 of a slow and insensitive process. (b) GFP bleaching for cells residing in glucose free media with λ_3 denoting the bleaching rate and BGprop1 denoting the proportion of background to the overall intensity. (c) GFP bleaching for cells residing in glucose rich media, λ_3 and BGprop1 analogously to (b). (d) Nuclear intensity of Mig1-GFP for cells in a dynamic environment, where the surrounding media change between glucose rich and glucose free media, α and β denoting the shuttling rates for Mig1-GFP.

The background noise (BG), described as the sum of two exponentially decaying functions, can be expressed as

$$BG = BG1(0) \cdot e^{-\lambda_1 \cdot t} + BG2(0) \cdot e^{-\lambda_2 \cdot t},$$

where

$$\begin{aligned} \frac{d}{dt}(BG1) &= -\lambda_1 \cdot BG1, \\ \frac{d}{dt}(BG2) &= -\lambda_2 \cdot BG2, \end{aligned}$$

and λ_1 and λ_2 are determined through experimental measurements. The simulation is shown in Figure 3.11. The values for the estimated parameters are given in Table 3.3. The only parameter difference among the background bleaching experiment and the environmental change experiment was the absence of Mig1-GFP. All other parameters were kept constant. The purpose of the background bleaching experiments is to determine the bleaching effect of the autofluorescence, which for normal experiments is hidden in the sum of intensities of GFP and autofluorescence. The change in medium is, however, not considered in the background model. This simplification is reasonable because it is not expected that background molecules are affected by changes in the medium.

3. Mathematical modelling of the Snf1 pathway

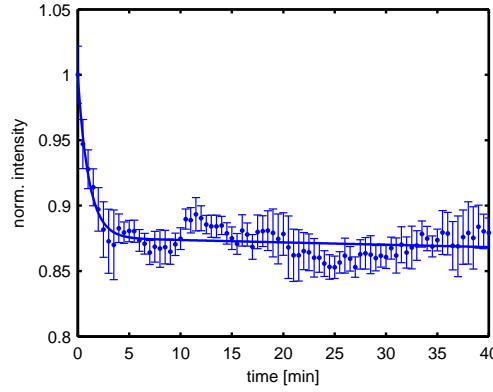


Figure 3.11.: Comparison of simulation and experimental data (intensities in the nucleus) of the autofluorescence in cells without GFP. Images were taken every 30 seconds. Parameter values are listed in Table 3.3.

GFP bleaching model

To analyse GFP bleaching, two different experiments were designed: on the one hand, cells were continuously exposed to a glucose poor medium (0 g/L) resulting in Mig1-GFP residing in the cytosol (Figure 3.10b), on the other hand, cells were continuously exposed to a glucose rich medium (40 g/L) resulting in Mig1-GFP residing inside of the nucleus (Figure 3.10c). The intensity data measured is equal to the sum of the background and Mig1-GFP intensity. The contribution of the background to the overall intensity in the nucleus will be higher when Mig1-GFP is located in the cytosol, and lower when it is located in the nucleus. Since no confocal laser scanning imaging technique is applied, the intensity of the excitation light is assumed to be equal throughout the entire volume of the cell, resulting in a similar bleaching rate λ_3 of Mig1-GFP, regardless of Mig1-GFP localisation within the cell. According to Song *et al.* [Song *et al.* 1995], one can assume an exponential decay of the Mig1-GFP intensity, when exposed to excitation light as illustrated in Figure 3.10b and Figure 3.10c. Any qualitative differences between the two experiments is thus explained by the different contribution of the background to the measured intensity. Furthermore, the decrease of the total excited Mig1-GFP concentration within a cell under bleaching effects can be defined as

$$\frac{d}{dt}(Mig1GFP_{total}) = -\lambda_3 \cdot Mig1GFP_{total}$$

such that

$$BGGFP = Mig1GFP_{total}(0) \cdot e^{-\lambda_3 \cdot t} + BGprop \cdot BG$$

where BGGFP is the intensity composed of background (BG) and Mig1-GFP fluorescent intensity, both decreasing due to bleaching. We define *BGprop* as the local parameter accounting for the background-to-Mig1-GFP ratio (Figure 3.12a and Figure 3.12b). The comparison between the simulation and the experimental data can be seen in Figure 3.12c

3.2. Data processing for the *Snf1* pathway component *Mig1*

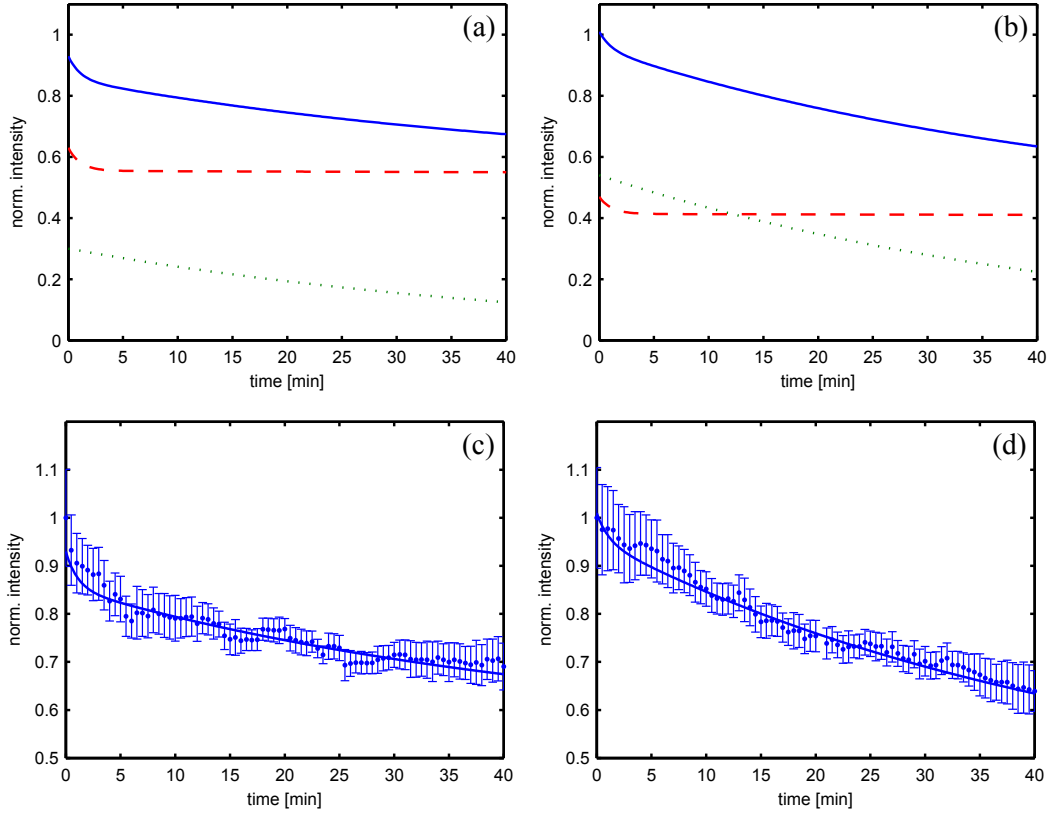


Figure 3.12.: (a), (b) Background (dashed red line) and Mig1-GFP (dotted green line) intensities. Their sum represents the overall measured intensity in the nucleus (solid blue line) in glucose poor medium (left column) and glucose rich medium (right column) as described in the model for the GFP bleaching. Note that under glucose poor conditions the background intensity has a higher portion of the overall measured intensity in the nucleus, since Mig1-GFP is located to the cytosol, compared to glucose rich conditions when Mig1-GFP is located in the nucleus. (c), (d) Comparison of simulation and experimental data of Mig1-GFP and background intensities. Images were taken every 30 seconds. Parameter values are listed in Table 3.3. The GFP bleaching model is described in Section 3.2.2.

and Figure 3.12d. Therefore, it is possible to extract the bleaching rate for Mig1-GFP by using the information from the background bleaching data. Applying this information, it is now possible to start analysing the Mig1-GFP shuttling data.

Environmental change model

This model analyses changes in Mig1-GFP localisation under glucose starvation stress. Fitting the model to the experimental data, the phosphatase and kinase rate constants for Mig1-GFP were determined (Figure 3.10d). As shown in the previous section, the decrease in excited Mig1-GFP concentration due to bleaching can be described as the exponentially decreasing function:

$$Mig1GFP_{total}(t) = Mig1GFP_{total}(0) \cdot e^{-\lambda_3 \cdot t}$$

3. Mathematical modelling of the Snf1 pathway

where λ_3 is the bleaching rate of Mig1-GFP. Then, we finally insert this degradation term into the model for Mig1-GFP shuttling:

$$\frac{d}{dt}(Mig1GFP) = \alpha \cdot (A + \theta_1) \cdot Mig1PGFP - \beta \cdot (B + \theta_2) \cdot Mig1GFP, \quad (3.9)$$

where

$$Mig1PGFP = Mig1GFP_{\text{total}} - Mig1GFP,$$

and α and β are parameters representing the rate of Mig1-GFP dephosphorylation and phosphorylation, respectively. The term within the brackets of Eq. (3.9) is a switch function representing the presence of active phosphatase and kinase of Mig1, respectively. Hence, it can be assumed that the activation of Mig1's kinase and phosphatase is faster than the activation and deactivation of Mig1 itself. The parameters A and B indicate a basal phosphorylation and dephosphorylation of Mig1 regardless of the glucose concentration, respectively. The Heaviside step functions θ_1 and θ_2 [Bracewell 1999] represent the switches among glucose rich and glucose free media:

$$\theta_1 = \begin{cases} 0 & \text{for glucose free medium} \\ 1 & \text{for glucose rich medium} \end{cases}$$

$$\theta_2 = \begin{cases} 1 & \text{for glucose free medium} \\ 0 & \text{for glucose rich medium} \end{cases}$$

The experimental data of the environmental change experiments can be described as the composition of background and Mig1-GFP shuttling:

$$BG_{GFP\text{shuttling}} = Mig1PGFP + BG_{prop} \cdot BG$$

as shown in Figure 3.13(a) to 3.13(c) for the comparison of experimental data and simulation. Figure 3.13(d) shows the composition of background and Mig1-GFP resulting in the overall intensity. Since BG_{prop} is a local parameter, it needs be included into a new estimation for the environmental change experiments. The result of the parameter estimation for A and B indicates that there is in addition to the glucose depending regulation a basal Mig1 (de)phosphorylation, since $A, B \neq 0$. This result is supported by findings in Western blot data indicating that Snf1 is never fully dephosphorylated [Garcia Salcedo 2009]. The values can be found in Table 3.3.

Due to the bleaching process and unlike the Mig1 concentration, the total concentration of excited Mig1-GFP is not constant but decreases over time. In order to predict the rate of change for Mig1 (regardless of GFP-tagging), we use the above equation of Mig1-GFP for Mig1 by replacing $Mig1GFP_{\text{total}}$ with a constant total concentration of Mig1:

$$\frac{d}{dt}(Mig1) = \alpha \cdot (A + \theta_1) \cdot Mig1^P - \beta \cdot (B + \theta_2) \cdot Mig1$$

3.2. Data processing for the *Snf1* pathway component *Mig1*

Parameter	Unit	BG	GFP eth	GFP glc	5min	10min	20min
λ_1	1/min	0.92	“	“	“	“	“
λ_2	1/min	0.0002	“	“	“	“	“
$BG1(0)$	norm.in.	0.12	“	“	“	“	“
$BG2(0)$	norm.in.	0.88	“	“	“	“	“
λ_3	1/min	-	0.022	0.022	“	“	“
$Mig1GFP_{total}(0)$	norm.in.	-	0.30	0.54	0.55	0.55	0.48
$BGprop$	-	-	0.63	0.47	0.57	0.56	0.49
$Mig1GFP(0)$	n.i.	-	-	-	0.41	0.49	0.46
α	$\frac{\text{norm.i.}}{\text{min}}$	-	-	-	0.35	0.35	0.35
β	$\frac{\text{norm.i.}}{\text{min}}$	-	-	-	0.50	0.50	0.50
A	norm.in.	-	-	-	0.03	0.03	0.03
B	norm.in.	-	-	-	0.06	0.06	0.06
$Mig1_{total}$	$\frac{\text{molec.}}{\text{cell}}$	-	-	-	19 000	19 000	19 000

Table 3.3.: Overview of the parameters and values used in the model ordered by the different models in the columns. The parameter values for the background bleaching experiment were taken in order to estimate the parameters for the GFP bleaching experiment, and those values are finally used for the 75 environmental change experiments. The handing down of parameter values is indicated by the quotation marks. The non-existence of a parameter in the model is denoted by a minus. $A, B \neq 0$ indicate a constant level of Mig1 (de)phosphorylation. The gray fields highlight parameter values taken from unpublished data [Garcia Salcedo 2009]. The units for A , B , and the initial conditions are normalised intensities (concentrations), denoted norm.in. the unit of $Mig1_{total}$ is molecules/cell taken from unpublished data [Garcia Salcedo 2009]. $BGprop$ is a scaling factor.

3. Mathematical modelling of the Snf1 pathway

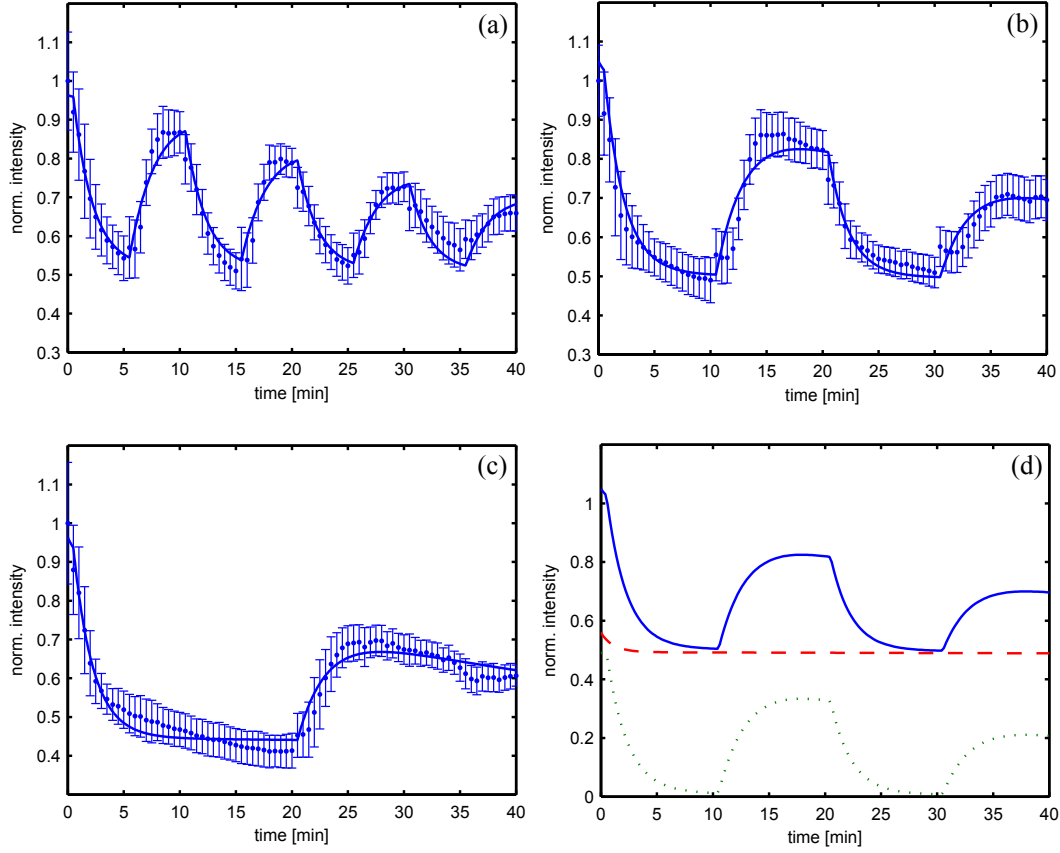


Figure 3.13.: (a) to (c) Comparison of simulation (BGFP shuttling) and experimental data of the environmental change experiment, for pulse durations of (a) 5 minutes, (b) 10 minutes, and (c) 20 minutes, respectively. Images were taken every 30 seconds. (d) Simulation of the intensity in the nucleus of a 10 minutes environmental change experiment. The intensity (solid blue line) is defined as the sum of background (dashed red line) and Mig1-GFP shuttling (dotted green line) both undergoing photobleaching during imaging.

where $Mig1P = Mig1_{total} - Mig1$ and $Mig1_{total}$ represents a constant. So far, our model simulated the normalised data. A more natural view on Mig1 and Mig1-GFP shuttling dynamics is obtained by scaling $Mig1GFP_{total}$ to 19000 ± 3800 , which is an approximate number of Mig1 molecules per cell [Garcia Salcedo 2009]. The simulation can be seen in Figure 3.14(a) for Mig1 and in Figure 3.14(b) for Mig1-GFP.

Model validation

The model was validated using new experimental data acquired at 60 seconds intervals. Hence, a two-fold slower bleaching rate is expected while the values for parameters α , β , A , and B remain the same. Therefore, we divide the bleaching rates λ_1 , λ_2 , and λ_3 by two. New estimates for the local parameter $BGprop$ and the initial conditions are required. As presented in Figure 3.15, the simulation is in good agreement with the experimental data. This supports the assumption that the decrease in the intensity data is due to bleaching

3.2. Data processing for the *Snf1* pathway component Mig1

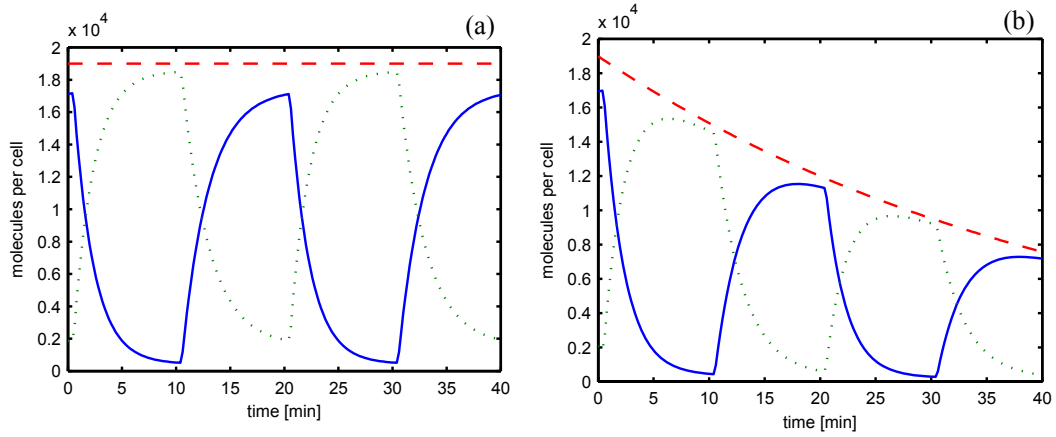


Figure 3.14.: Simulation of Mig1 (solid blue line) and Mig1P (dotted green line). The total concentration (dashed red line) is constant and set to 19 000 molecules per cell. (b) Simulation of Mig1-GFP (solid blue line) and Mig1P-GFP (dotted green line). The total concentration (dashed red line) is decreasing due to photobleaching.

effect during image acquisition.

3.2.3. Discussion

All fluorophores undergo photobleaching during excitation. The lack of photostability is therefore a limiting factor during imaging, especially for time series and single cell experiments. We have developed a mathematical model that successfully describes the decrease of total excited Mig1-GFP due to photobleaching and the shuttling of Mig1-GFP. Our mathematical model takes bleaching and background noise into account and can thus extract the information on Mig1-GFP shuttling in order to predict the dynamic behaviour of Mig1 during changing environmental conditions. The estimated parameter values suggest that the basal phosphorylation and dephosphorylation of Mig1 occur both independently of glucose levels, thereby supporting the findings of Western blot data [Garcia Salcedo 2009]. Furthermore, the estimated parameter values suggest that the kinase has a greater influence on the activation status of Mig1 than the phosphatase. The image acquisition every 60 seconds supports the assumption that the decrease in total excited Mig1-GFP is sufficiently explained by the occurrence of bleaching: Exclusively by dividing the estimated values for bleaching rates by two (since only half the number of images were taken) and assigning the local parameters for background-to-Mig1-GFP ratio, we obtain a satisfying reproduction of the data. Our model suggests that mathematical modelling can be a complement to the extensive development of highly photostable variants of mOrange and TagRFP. It thereby demonstrates how raw data, that were generated in an optical microscope, can be processed and used for mathematical modelling of signal transduction pathways.

The model allows for a stepwise extraction of the information on the background and

3. Mathematical modelling of the Snf1 pathway

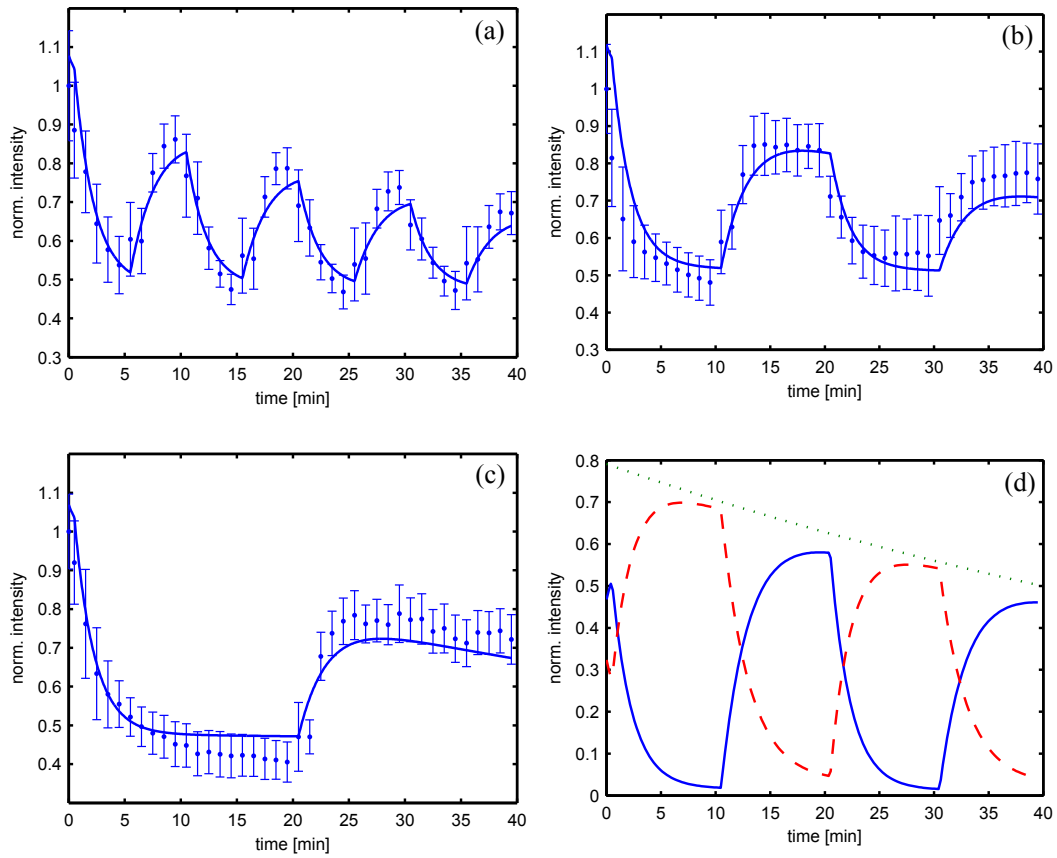


Figure 3.15.: Comparison of simulation and experimental data of the environmental change experiment for pulse durations of (a) 5 minutes, (b) 10 minutes, and (c) 20 minutes. Images were taken every 60 seconds. Dividing the bleaching rates for background and GFP by two and resuming parameters α , β , A , and B as estimated before leads to the successful reproduction of the data.

Mig1-GFP bleaching rates, the background-to-Mig1-GFP ratio, and the rates of Mig1-GFP phosphorylation and dephosphorylation. Hereby, it is possible to predict Mig-GFP shuttling as it would occur without bleaching. The analysis demonstrates how data acquired using an optical microscope can be processed and used for mathematical modelling of signal transduction pathways as shown in Chapter 3.3.

3.3. **Snf1 pathway modelling**

In order to elucidate regulatory mechanisms that comprise interrelations of Snf1 pathway components, in particular, Snf1 and Mig1, we first derived the glucose-regulated stimulus (shown in Section 3.1.5), followed by the processing of Mig1-GFP intensity data (discussed in Section 3.2.2). Experimental data was available generated by the group of Stefan Hohmann¹, University of Gothenburg. Within data-driven modelling and model-driven experimentation cycles, we establish the ODE-based mathematical models describing the Snf1 pathway to investigate the following questions:

- Is the regulation of Snf1 mediated by a glucose-regulated kinase or a glucose-regulated phosphatase, or even both?
- Is the involvement of the Snf4-subunit essential for explaining the experimental observations?
- Is the dephosphorylation of Mig1 controlled by glucose, or could it be constitutive?

This Section is part of an unpublished collaborative manuscript [Garcia Salcedo 2009].

3.3.1. **Alternative Snf1 pathway models**

We now analyse alternative pathway structures of the Snf1 pathway, which include the three hypotheses that Snf1 is regulated through

- a) a constant kinase (UK) and a glucose-regulated phosphatase (PP1),
- b) a constant phosphatase (PP1) and a glucose-regulated kinase (UK), and
- c) both, phosphatase (PP1) and kinase (UK), being glucose-regulated

As described in [McCartney and Schmidt 2001], it was observed that sodium stress lead to Snf1 phosphorylation on the Thr-210 residue, while at the same time Snf1 was unable to phosphorylate Mig1 efficiently. Hence, we also consider two alternative model structures with a glucose-controlled step, that was added to our initial, simple model:

¹Department of Cell and Molecular Biology, University of Gothenburg, SE-40530 Göteborg, Sweden.

3. Mathematical modelling of the Snf1 pathway

- I) initial model (illustrated in Figure 3.16)
- II) a conformational rearrangement that is mediated by the Snf4-subunit (described in [McCartney and Schmidt 2001], network sketched in Figure 3.22)
- III) a complex formation of Mig1 and Hxk2, protecting Mig1 from phosphorylation by Snf1 in glucose presence (suggested in [Ahuatzi *et al.* 2007], network outlined in Figure 3.23).

After describing the integration of the glucose-regulated signal (derived in Section 3.1) and the fluorescence microscopy data for Mig1 (processed in Section 3.2) into the Snf1 models, a detailed discussion and presentation of the nine (Ia), (Ib), (Ic), (IIa), (IIb), (IIc), (IIIa), (IIIb) and (IIIc)) alternative Snf1 network structures is performed.

Integration of the glucose-regulated signal into the mathematical model

Since details of the glucose-regulated signal are still unknown, we do not introduce a new variable, speculating on its degradation, synthesis, and (de)activation processes, but introduce the signal directly into the differential equation system in form of the glucose-dependent glycolysis rate derived in Section 3.1 Eq. (3.8), $k_{\text{glycolysis}}$, as follows

$$\frac{d}{dt}UK_{\text{active}} = -d_{UK} \cdot k_{\text{glycolysis}} \cdot UK_{\text{active}} + a_{UK} \cdot UK_{\text{inactive}} \quad (3.10)$$

$$\frac{d}{dt}PP1_{\text{active}} = a_{PP1} \cdot k_{\text{glycolysis}} \cdot PP1_{\text{inactive}} - d_{PP1} \cdot PP1_{\text{active}}. \quad (3.11)$$

In this way, while the cell subsist on glucose, the upstream kinase of Snf1 (UK) is deactivated and the phosphatase of Snf1 and Mig1 (PP1) is activated leading to the response that genes encoding proteins for the utilisation of alternative carbon sources are repressed via Mig1. In contrast, as glucose availabilities decrease, inactivation of UK slows down and its constant activation prevails, while activation of PP1 slows down and its constant deactivation dominates. Alternative model structures, within every iteration cycle discussed below, include the three different combinations of Eq. (3.10) and Eq. (3.11): (a) a constant kinase and a glucose-regulated phosphatase by cancelling $k_{\text{glycolysis}}$ of Eq. (3.10), (b) a constant phosphatase and a glucose-regulated kinase by cancelling $k_{\text{glycolysis}}$ of Eq. (3.11), and (c) both, phosphatase and kinase, being glucose-regulated without cancelling the rate $k_{\text{glycolysis}}$.

Integration of the Mig1-GFP intensity data into the Snf1 pathway model

The definition of the glucose signal and the processed Mig1 data are now used for modelling the Snf1 pathway. Recalling Eq. (3.9) from the Subsection 3.2.2

$$\frac{d}{dt}(Mig1GFP) = \alpha \cdot (A + \theta_1) \cdot Mig1^P GFP - \beta \cdot (B + \theta_2) \cdot Mig1GFP,$$

the fluorescent microscopy data of Mig1 are comprised into the Snf1 model by adding the following equation

$$\frac{d}{dt}(\text{Mig1}) = \alpha \cdot \text{PP1} \cdot \text{Mig1}^P - \beta \cdot \text{Snf1}^P \cdot \text{Mig1},$$

with the phosphatase Glc7/Reg1 (*PP1*) replacing ($A + \theta_1$) and Snf1^P replacing ($B + \theta_2$). Since A and B have units molecules per cell for normalised Mig1 data, but PP1 and Snf1^P (SNF1^P) are of units molecules per cell for Mig1 numbers per cell, we expect a scaling factor of approximately the size of $\text{PP1}_{\text{total}} \approx 28\,000$ and $\text{Snf1}_{\text{total}} \approx 20\,000$ molecules per cell to be balanced within the parameters α and β .

3.3.2. Snf1 pathway models

The corresponding pathway can be seen in Figure 3.16.

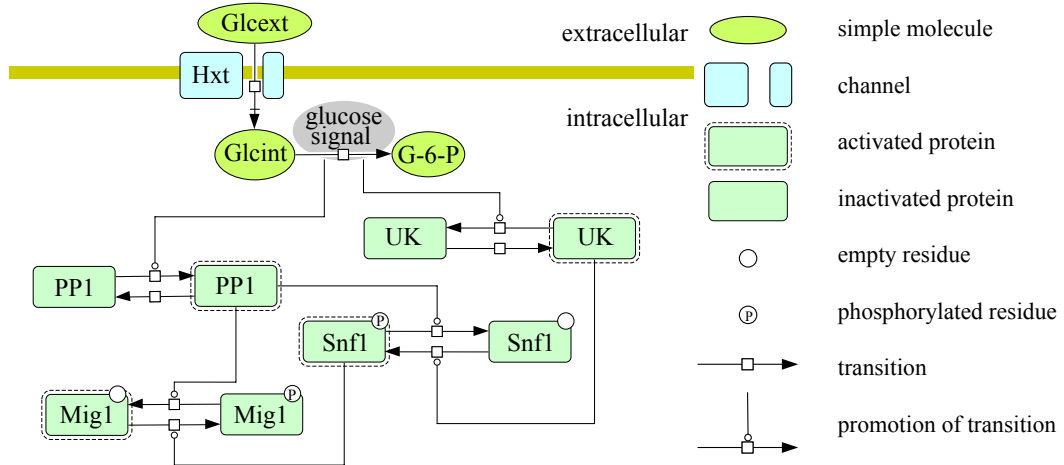


Figure 3.16.: A reaction network suggesting three alternative structures for the Snf1 pathway: (a) a constant kinase and a glucose-regulated phosphatase, (b) a constant phosphatase and a glucose-regulated kinase, as well as (c) a glucose-regulated kinase and phosphatase). In glucose presence, Snf1 is dephosphorylated and Mig1 acts as a transcriptional repressor. In glucose absence, Snf1 is phosphorylated, thereon phosphorylating Mig1, which thereon shuttles to the cytosol. ‘UK’ summarises the three upstream kinases of Snf1. The rate equations are listed in Table 3.4. The image was designed using *CellDesigner* [Funahashi *et al.* 2008] and Adobe Illustrator.

The Snf1 Western blot data

The activation of Snf1, monitored via the phosphorylation state of the Snf1 Thr-210 residue, was studied during controlled batch cultivations (fermentor) as shown in Figure 3.17 and described in detail in Section 3.1.5.

The generated Western blot data present ratios of phosphorylated Snf1 to the overall Snf1 protein. Therefore, we relate

3. Mathematical modelling of the Snf1 pathway

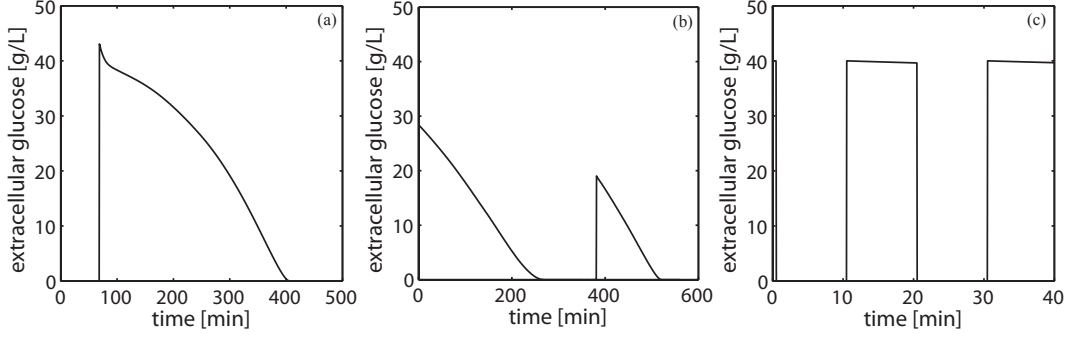


Figure 3.17.: Glucose simulations for Experiments C, D (see Table 3.1) and for a 10 minutes Experiment as shown in Part 3.13(a). These glucose profiles in (a) and (b) are input signals for the Snf1 simulation and the glucose profile in (c) is the input signal for nuclear intensity (taken as a measure for Mig1 intensity).

$$Snf1_{ratio}^P = WB_{scaling\ factor} \cdot \frac{SNF1^P}{Snf1_{total}}$$

for a model that does not consider Snf1 complex formation, and for a model that does take the complex formation into account

$$Snf1_{ratio}^P = WB_{scaling\ factor} \cdot \frac{Snf1^P + SNF1^P}{Snf1_{total}}.$$

The parameter $WB_{scaling\ factor}$ denotes the Western blot scaling factor, which is needed to account for different intensities among different Western blot experiments, e.g. the magnitude of antibody binding. We scale each time series of the different experiments to its maximum value. Snf1 Western blot data of three different overexpression experiments were generated: Overexpression of SAK1, the gene encoding the main kinase of Snf1, overexpression of REG1, the gene encoding the regulatory subunit of the phosphatase of Snf1, and overexpression of SAK1 and REG1 within the same strain. The data of the Sak1 overproduction show, that Snf1 is constitutively phosphorylated, even in high glucose concentrations. At the same time it is observed, that Mig1 remains unphosphorylated. It appears that Snf1 can be activated and perform functions in the presence of glucose (such as in salt tolerance) without targeting Mig1 through phosphorylation. Also overexpressing REG1 did not alter Mig1 (de)phosphorylation dynamics compared to non-overexpressing cells.

Details of the materials and methods for the experimental setups are according to unpublished data [Garcia Salcedo 2009]. The findings of these experiments were as follows:

- For Sak1 overproduction:
 - Constitutive Snf1 phosphorylation
 - In presence of glucose, the artificial Snf1 activation does not have any effect on Mig1 phosphorylation and localisation
- For Reg1 overproduction:
 - In glucose limiting conditions, no significant decrease in the Snf1 phosphorylation level is observed
 - This observation supports the idea that the phosphatase complex Glc7/Reg1 is specifically active toward Snf1 when glucose is abundant
 - Similarly to the conditions of Sak1 overproduction, overexpression of REG1 does not have impact on Mig1 regulation
- For both, Sak1 and Reg1 overproduction:
 - Regulation of Snf1 phosphorylation in cells overexpressing SAK1 is partially restored by overproduction of Reg1

According to unpublished data [Garcia Salcedo 2009], the kinase is approximately 10-fold overexpressed relative to the basal level, whereas the phosphatase is about 35-fold overexpressed. However, since only the gene REG1 encoding for the regulatory subunit was overexpressed without the gene GLC7 encoding for the catalytic subunit, we only act on the assumption that the overproduction is limited to the maximal number of the protein Glc7.

Assumptions

Modelling is limited due to insufficient quantitative and qualitative data on concentrations, reaction and degradation rates, as well as many other parameters that are delicate to measure [Materi and Wishart 2007]. As a consequence, approximations and estimates have to be used. We here assume for all nine model candidates the following:

- The upstream kinases of Snf1 (Elm1, Sak1, Tos3) can be summarised to one kind of upstream kinase (UK).
- The different isoforms of each subunit of Snf1 do not need specification but can be summarised and reduced to just one form.

3. Mathematical modelling of the Snf1 pathway

- All components, especially the Snf1 complexes are well mixed within the cell (no spatial impact due to the β -subunit of Snf1).
- Phosphorylated Mig1, which is located to the nucleus, as well as dephosphorylated Mig1, which is located to the cytosol, can be neglected.

The corresponding reaction rates, kinetic equations, and conservation relations are listed in Table 3.4. We denote the model the Snf1-model. We translated the three alternative

Processes	Reaction rates
UK (Upstream Kinase of Snf1) activation	$R1 = a_{UK} \cdot UK_{\text{inactive}}$
UK deactivation	$R2 = d_{UK} \cdot UK_{\text{active}} \cdot k_{\text{glycolysis}}$
PP1 (phosphatase of Snf1) activation	$R3 = a_{PP1} \cdot PP1_{\text{inactive}} \cdot k_{\text{glycolysis}}$
PP1 deactivation	$R4 = d_{PP1} \cdot PP1_{\text{active}}$
Snf1 phosphorylation/activation	$R5 = a_{Snf1} \cdot Snf1 \cdot UK_{\text{active}}$
Snf1 dephosphorylation/deactivation	$R6 = d_{Snf1} \cdot Snf1^P \cdot PP1_{\text{active}}$
Mig1 phosphorylation/deactivation	$R7 = a_{Mig1} \cdot Mig1 \cdot Snf1^P$
Mig1 dephosphorylation/activation	$R8 = d_{Mig1} \cdot Mig1^P \cdot PP1_{\text{active}}$
Kinetic equations	Conservation relations
$d/dt(UK_{\text{active}}) = R1 - R2$	$UK_{\text{total}} = UK_{\text{active}} + UK_{\text{inactive}}$
$d/dt(PP1_{\text{active}}) = R3 - R4$	$PP1_{\text{total}} = PP1_{\text{active}} + PP1_{\text{inactive}}$
$d/dt(Snf1^P) = R5 - R6$	$Snf1_{\text{total}} = Snf1^P + Snf1$
$d/dt(Mig1) = R8 - R7$	$Mig1_{\text{total}} = Mig1^P + Mig1$

Table 3.4.: Overview of the processes, reaction rates, kinetic equations and conservation relations for models Ia), Ib), and Ic) as depicted in Figure 3.16. The corresponding parameter values are given in Table A.1 in the Appendix.

pathway structures, depicted in Figure 3.16, into ODE-based models. Numerical simulations for all models were carried out with Matlab (MathWorks, Inc.) and the *Systems Biology Toolbox2* [Schmidt and Jirstrand 2006], using the *particle-swarm-algorithm* [Vaz and Vicente 2007] for parameter estimation. A comparison of the model simulations to the experimental Snf1 Western blot data showed that all three investigated models explain the Snf1 data, as can be seen in Figure 3.18.

The results are:

- All three models ((a) a glucose-regulated phosphatase, (b) a glucose-regulated kinase, or (c) both, kinase and phosphatase, glucose-regulated) reproduce the Snf1 Western blot data for wild type cells (compare Figure 3.18).
- Estimating the parameter values for a model with a glucose-regulated phosphatase and a glucose-regulated kinase leads to an optimum displaying almost a constant kinase rate (see Figure 3.19), suggesting that a glucose-regulated phosphatase would be sufficient to regulated Snf1.

These results displays the need for further experimental data.

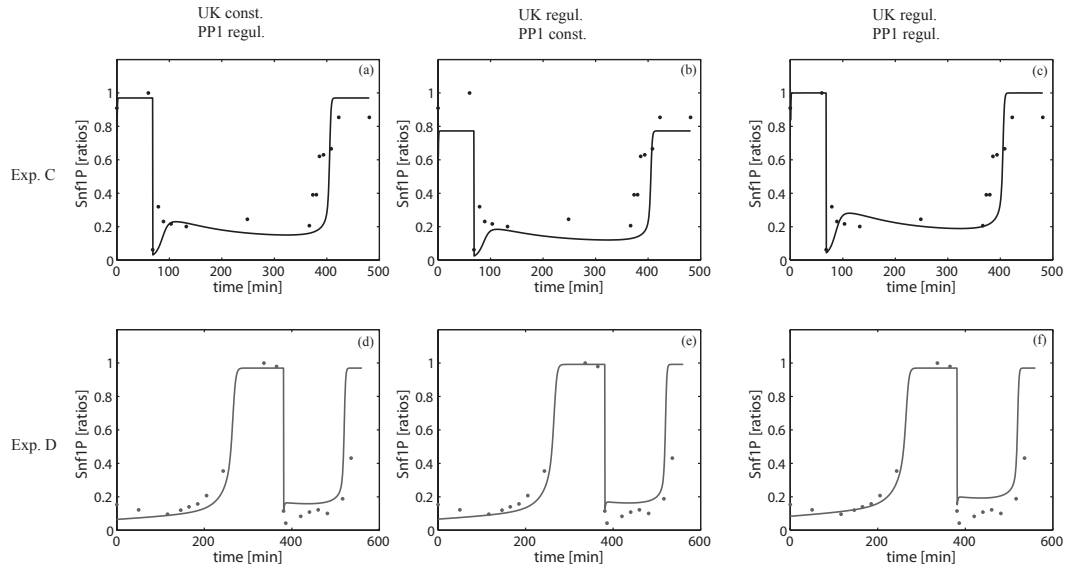


Figure 3.18.: Snf1 data and simulations of three alternative Snf1-models (Ia), Ib), and Ic): (a+d) a constant kinase and a glucose-regulated phosphatase, for two experiments respectively, (b+e) a constant phosphatase and a glucose-regulated kinase, (c+f) a glucose-regulated kinase and a glucose-regulated phosphatase). It can be seen that all pathway structures explain Snf1 (de)phosphorylation dynamics.

As can be seen in Figure 3.20, the Snf1 model introduced above does not explain the mechanisms, that Mig1 phosphorylation and dephosphorylation dynamics remain unaffected. Sak1 overproduction results in a decreased concentration of unphosphorylated Mig1, due to an increased level of phosphorylated Snf1, even in glucose rich media, and as a consequence, an increased process of Mig1 phosphorylation. Also for cells overproducing Reg1, Mig1 is increasingly dephosphorylated but does not remain unaffected as observed in experiments. In particular, the deviations among simulation and experimental data for a Snf1 model with a glucose-regulated kinase (middle column of Figure 3.20) suggest that the regulation of Snf1 alone is not strong enough to compensate for a constitutively active phosphatase to afford the rapid (de)phosphorylation dynamic of Mig1. As follows,

3. Mathematical modelling of the Snf1 pathway

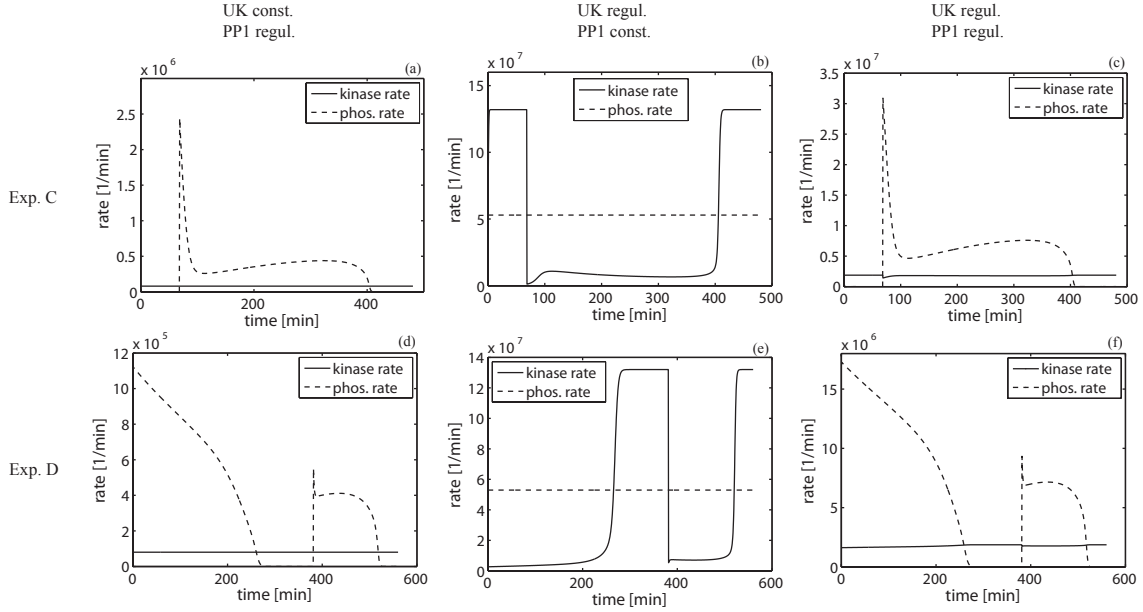


Figure 3.19.: Kinase and phosphatase rates of Snf1 for the Snf1 models Ia), Ib), and Ic). It is notable that a model with both, kinase and phosphatase being glucose-regulated exhibits a pronounced phosphatase rate ($d_{Snf1} \cdot PP1_{active}$) via the phosphatase and a modest, almost constant kinase rate ($a_{Snf1} \cdot UK_{active}$). First row: PP1 regulated model, second row: UK regulated model, third row: both regulate. (a+d) a constant kinase and a glucose-regulated phosphatase, for two experiments respectively, (b+e) a constant phosphatase and a glucose-regulated kinase, (c+f) a glucose-regulated kinase and phosphatase).

we can exclude this model from the list of candidates. As will be shown in the next paragraph, a constitutively active phosphatase may be possible in collaboration with another glucose-stimulated component, such as Hxk2.

In the next two paragraphs, the establishment of two models is shown, which describe the following mechanisms:

- Activation of the Snf1 kinase complex involves two steps: one that requires an upstream kinase and one that is mediated by the γ -subunit of Snf1 [McCartney and Schmidt 2001]. The corresponding regulatory network is shown in Figure 3.21. We denote this model the two-step model for Snf1 regulation.
- Regulation of Mig1 involves a glucose-regulated complex formation with Hxk2. Thereby, Hxk2 binds Mig1 in order to defend it from phosphorylation through Snf1 in glucose presence [Ahuatzi *et al.* 2007]. The corresponding regulatory network is shown in Figure 3.23. We denote this model the Two-step model for Mig1 regulation.

3.3.3. Snf1 pathway models with a two-step regulation for Snf1

McCartney and Schmidt found that while both, glucose stress and sodium ion stress, caused a rapid increase in Snf1 phosphorylation on the residue Thr-210, only glucose

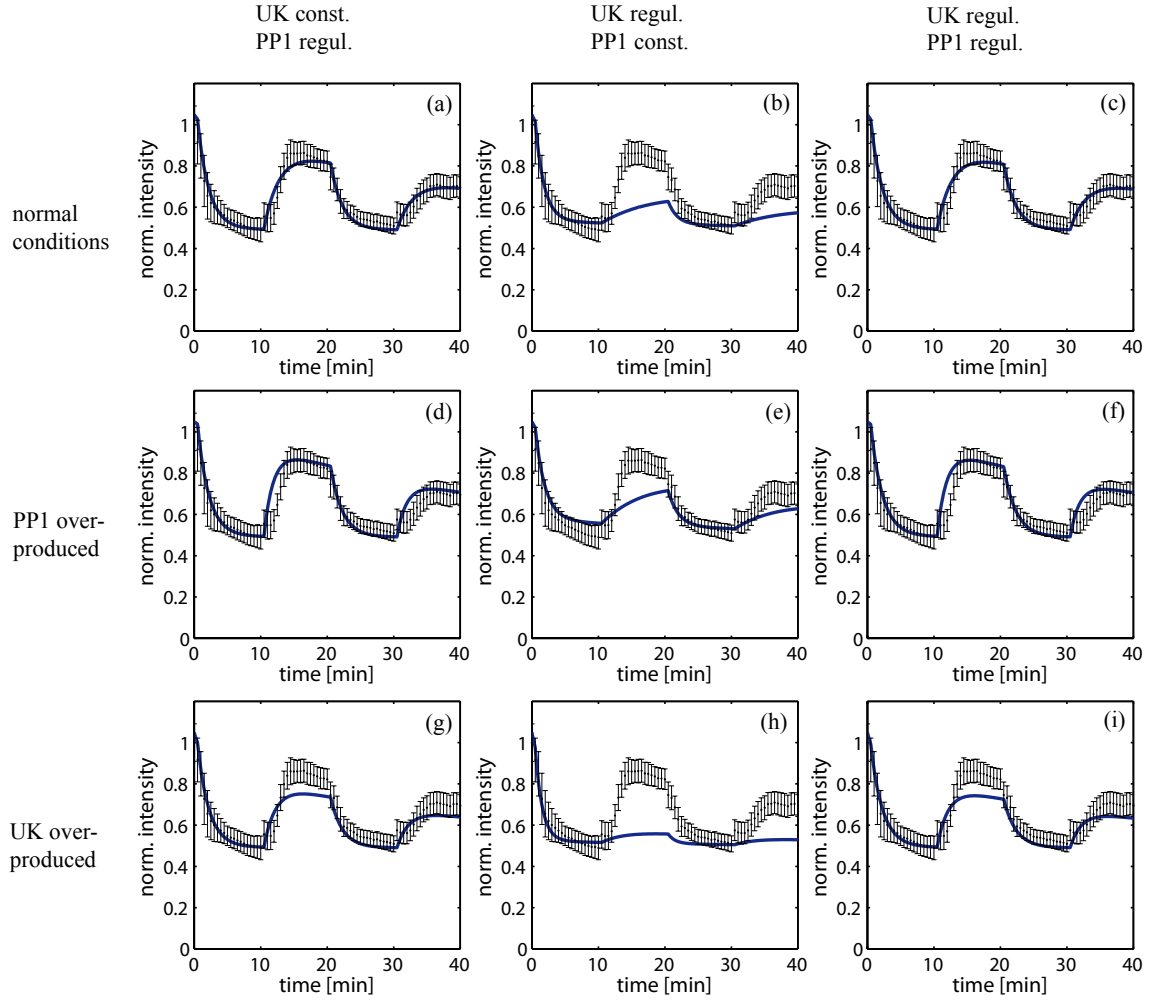


Figure 3.20.: Experimental data and simulations of nuclear intensities, as a measure for Mig1, for the *Snf1* models Ia), Ib), and Ic). First row: normal conditions. Second row: UK overproduced *in silico*. Third row: PP1 overproduced *in silico*. First column: glucose-regulated PP1. Second column: glucose-regulated UK. Third column: both glucose-regulated. It can be seen that a constant phosphatase hampers the abrupt (de)phosphorylation dynamics of Mig1, and thus leads to a poor agreement of simulations and experimental data (see (e) to (h)). Glucose profile as shown in Figure 3.9.

3. Mathematical modelling of the Snf1 pathway

stress triggered the phosphorylation of Mig1 protein [McCartney and Schmidt 2001]. This suggests that activation of the Snf1 kinase complex involves two steps: one that requires an upstream kinase and one that is mediated by the γ -subunit of Snf1 [McCartney and Schmidt 2001], as depicted in Figure 3.21. We establish the corresponding differential

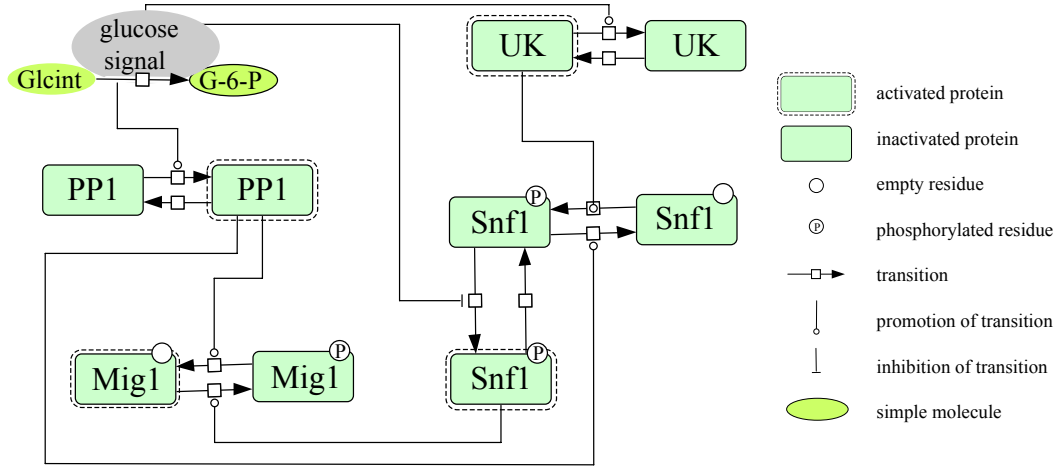


Figure 3.21.: Two-step model for Snf1 regulation, as suggested by McCartney and Schmidt [McCartney and Schmidt 2001] (models IIa), IIb), and IIc)). In glucose presence, Snf1 is dephosphorylated and Mig1 acts as a transcriptional repressor. In glucose absence, Snf1 is phosphorylated, thereon phosphorylating Mig1, which thereon shuttles to the cytosol. Since Snf1 can also be phosphorylated during glucose presence, while Mig1 is not phosphorylated, an additional regulatory step is assumed. In this figure, the Snf1 undergoes a conformational change with the Snf4 subunit while glucose is absence, as suggested by [McCartney and Schmidt 2001].

equations, listed in Table 3.5, and compare the simulations to the experimental data shown in Figure 3.22.

3.3.4. Snf1 pathway models with a two-step regulation for Mig1

In glucose presence, Snf1 is dephosphorylated and Mig1 acts as a transcriptional repressor. In glucose absence, Snf1 is phosphorylated and thereon phosphorylates Mig1 causing the release of transcriptional repression. It appears that Snf1 is phosphorylated during glucose presence, activated by, e.g. salt stress, while Mig1 is not phosphorylated. The Snf1 model neglecting a glucose-regulated step in addition to kinase and phosphatase regulation is not successful in describing the mechanisms, that Mig1 remains unaffected by phosphorylated Snf1 in glucose presence. Figure 3.23 schemes the regulatory network considering a glucose-regulated complex formation of the hexokinase Hxk2 and Mig1, as described by Ahuatzi *et al.* [Ahuatzi *et al.* 2007]. In the presence of glucose, the Mig1Hxk2 complex defends Mig1 from phosphorylation by Snf1. In the absence of glucose, the Mig1Hxk2 complex dissociates, allowing Mig1 to be targeted for phosphorylation by Snf1 [Ahuatzi *et al.* 2007]. The corresponding differential equations are listed in Table 3.6. The simulations are in good agreement with the experimental data for both, normal conditions and *in silico*

3.3. Snf1 pathway modelling

Processes	Reaction rates
UK activation	$R1 = a_{UK} \cdot UK_{\text{inactive}}$
UK deactivation	$R2 = d_{UK} \cdot UK_{\text{active}} \cdot k_{\text{glycolysis}}$
PP1 activation	$R3 = a_{PP1} \cdot PP1_{\text{inactive}} \cdot k_{\text{glycolysis}}$
PP1 deactivation	$R4 = d_{PP1} \cdot PP1_{\text{active}}$
Snf1 phosphorylation	$R5a = a_{Snf1} \cdot Snf1 \cdot UK_{\text{active}}$
Snf1 activation	$R5b = a_{Snf1^P} \cdot Snf1^P$
Snf1 dephosphorylation	$R6a = d_{Snf1} \cdot Snf1^P \cdot PP1_{\text{active}}$
Snf1 deactivation	$R6b = d_{Snf1^P} \cdot Snf1^P_{\text{active}} \cdot k_{\text{glycolysis}}$
Mig1 phosphorylation/deactivation	$R7 = a_{Mig1} \cdot Mig1 \cdot Snf1^P_{\text{active}}$
Mig1 dephosphorylation/activation	$R8 = d_{Mig1} \cdot Mig1^P \cdot PP1_{\text{active}}$
Kinetic equations comprising the Snf1 pathway model	
$d/dt(UK_{\text{active}}) = R1 - R2$	
$d/dt(PP1_{\text{active}}) = R3 - R4$	
$d/dt(Snf1^P) = R5a - R6a$	
$d/dt(Snf1^P_{\text{active}}) = R5b - R6b$	
$d/dt(Mig1) = R8 - R7$	
Conservation relations	
$UK_{\text{total}} = UK_{\text{active}} + UK_{\text{inactive}}$	
$PP1_{\text{total}} = PP1_{\text{active}} + PP1_{\text{inactive}}$	
$Snf1_{\text{total}} = Snf1^P + Snf1 + Snf1^P_{\text{active}}$	
$Mig1_{\text{total}} = Mig1^P + Mig1$	

Table 3.5.: Overview of the reaction rates for two-step models for Snf1 regulation (IIa), IIb), and IIc)) considering an additional step in Snf1 activation towards Mig1 as described by McCartney and Schmidt [McCartney and Schmidt 2001]. The corresponding network structure is depicted in Figure 3.21 and the corresponding parameter values are listed in the Appendix Table A.2.

3. Mathematical modelling of the Snf1 pathway

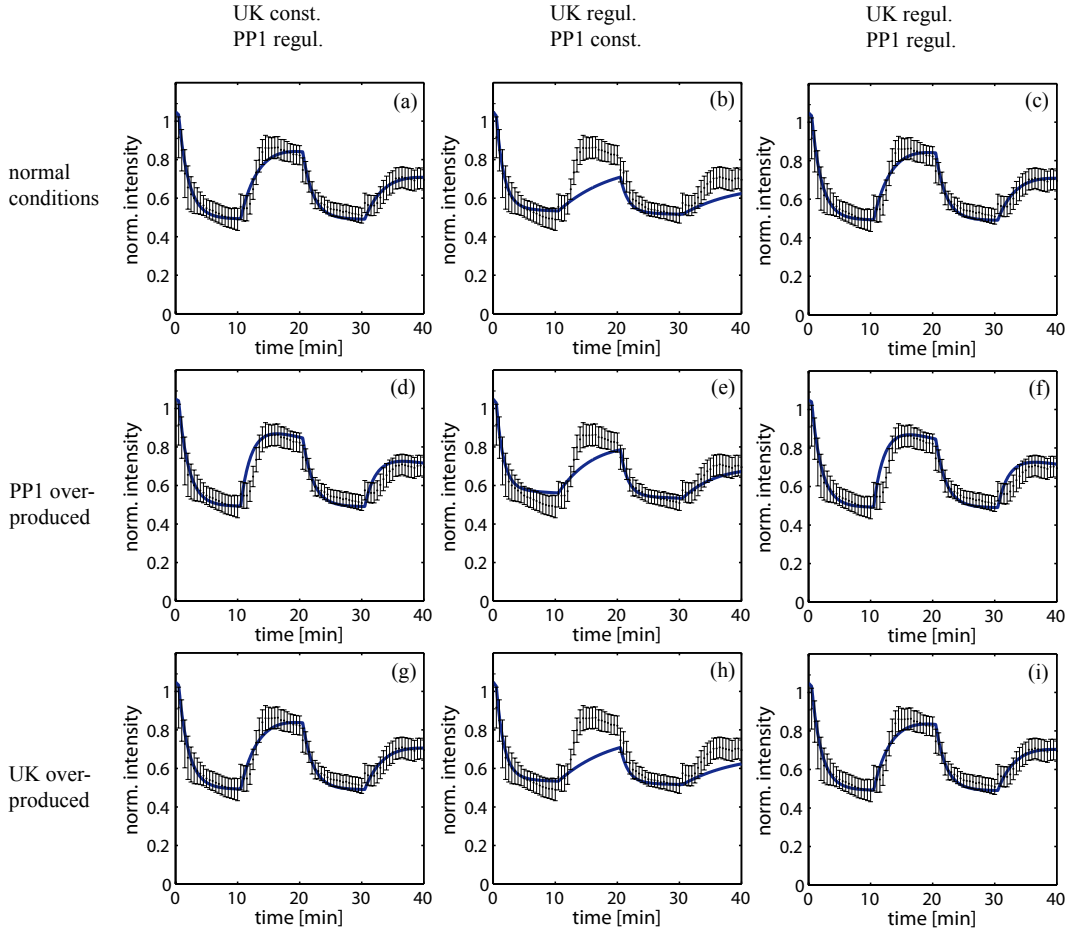


Figure 3.22.: Experimental data and simulations of nuclear intensities, as a measure for Mig1, for two-step models of Snf1 regulation (IIa), IIb), and IIc)). First row: normal conditions. Second row: UK overproduced *in silico*. Third row: PP1 overproduced *in silico*. First column: glucose-regulated PP1. Second column: glucose-regulated UK. Third column: both glucose-regulated. It can be seen that in the same way as the Snf1 model introduced above (see Table 3.4), a constant phosphatase hampers the abrupt (de)phosphorylation dynamics of Mig1, and thus leads to a poor agreement of simulations and experimental data (see middle column). However, in contrast to the Snf1 model, there is no difference between the Mig1 dynamics under normal conditions compared to conditions with UK overproduction. This observation can be explained by the glucose-regulated Snf1-Snf4 conformational rearrangement.

overproduction of the kinase and phosphatase, as can be seen in Figure 3.24.

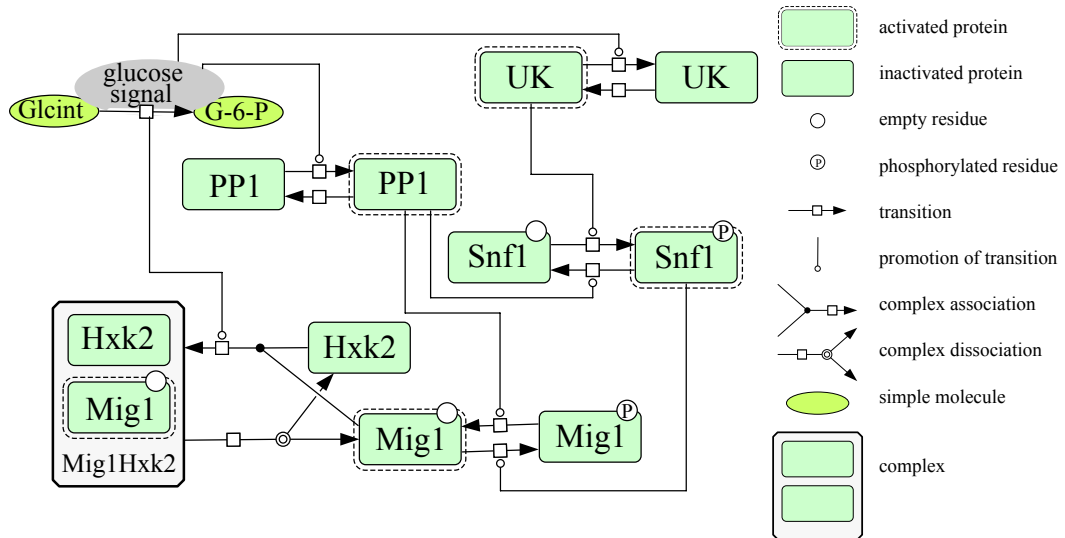


Figure 3.23.: Two-step model for Mig1 regulation. In glucose presence, Snf1 is dephosphorylated and Mig1 acts as a transcriptional repressor. In glucose absence, Snf1 is phosphorylated, thereon phosphorylating Mig1, which thereon shuttles to the cytosol. Since Snf1 can also be phosphorylated during glucose presence, while Mig1 is not phosphorylated, additional regulatory steps are assumed, e.g. the complex formation of Mig1 and Hxk2, which is provoked by glucose, as suggested by Ahuatzi *et al. et al.* [Ahuatzi *et al.* 2007]. The Mig1Hxk2 complex defends Mig1 from being phosphorylated by Snf1 while glucose is present. In the absence of glucose, the Mig1Hxk2 complex dissociates, allowing Mig1 to be targeted and be phosphorylated by Snf1.

The results can be summarised as follows:

- All three mechanisms (i.e. (a) a glucose-regulated phosphatase, (b) a glucose-regulated kinase, and (c) both, kinase and phosphatase, glucose-regulated) reproduce the Snf1 Western blot data for normal conditions (compare Figure 3.18).
- A comparison of the model allowing for glucose regulation of kinase and phosphatase to the experimental data leads to a distinctive phosphatase rate for Snf1 and an almost constant kinase rate. This indicates, that the regulation of the phosphatase would be sufficient to regulate Snf1 dynamics (see Figure 3.19). However, it does not imply that the kinase is likely to be constant.
- Considering the nuclear intensity data, the model with a constant phosphatase shows only a poor agreement of the experimental data and the simulations. This supports the existence of a glucose-regulated phosphatase. (see middle column of Figures 3.20 and 3.22)
- Including a two-step regulation for Snf1 improves the agreement of data and simulations (see Figure 3.22).

3. Mathematical modelling of the Snf1 pathway

Processes	Reaction rates
UK (Upstream Kinase of Snf1) activation	$R1 = a_{UK} \cdot UK_{\text{inactive}}$
UK deactivation	$R2 = d_{UK} \cdot UK_{\text{active}} \cdot k_{\text{glycolysis}}$
PP1 (phosphatase of Snf1) activation	$R3 = a_{PP1} \cdot PP1_{\text{inactive}} \cdot k_{\text{glycolysis}}$
PP1 deactivation	$R4 = d_{PP1} \cdot PP1_{\text{active}}$
Snf1 phosphorylation/activation	$R5 = a_{Snf1} \cdot Snf1 \cdot UK_{\text{active}}$
Snf1 dephosphorylation/deactivation	$R6 = d_{Snf1} \cdot Snf1^P \cdot PP1_{\text{active}}$
Mig1 phosphorylation/deactivation	$R7 = a_{Mig1} \cdot Mig1 \cdot Snf1^P$
Mig1 dephosphorylation/activation	$R8 = d_{Mig1} \cdot Mig1^P \cdot PP1_{\text{active}}$
Mig1 complex association	$R9 = k_1 \cdot Mig1 \cdot Hxk2 \cdot k_{\text{glycolysis}}$
Mig1 complex dissociation	$R10 = k_2 \cdot Mig1Hxk2$
Kinetic equations	Conservation relations
$d/dt(UK_{\text{active}}) = R1 - R2$	$UK_{\text{total}} = UK_{\text{active}} + UK_{\text{inactive}}$
$d/dt(PP1_{\text{active}}) = R3 - R4$	$PP1_{\text{total}} = PP1_{\text{active}} + PP1_{\text{inactive}}$
$d/dt(Snf1^P) = R5 - R6$	$Snf1_{\text{total}} = Snf1^P + Snf1$
$d/dt(Mig1) = R8 - R7 - R9 + R10$	$Mig1_{\text{total}} = Mig1^P + Mig1 + Mig1Hxk2$
$d/dt(Hxk2) = R10 - R9$	$Hxk2_{\text{total}} = Hxk2 + Mig1Hxk2$

Table 3.6.: Overview of the processes, reaction rates, kinetic equations and conservation relations for the two-step models for Mig1 regulation (IIIa), IIIb), and IIIc)), as depicted in Figure 3.23. The list of parameter values is given in the Appendix Table A.3.

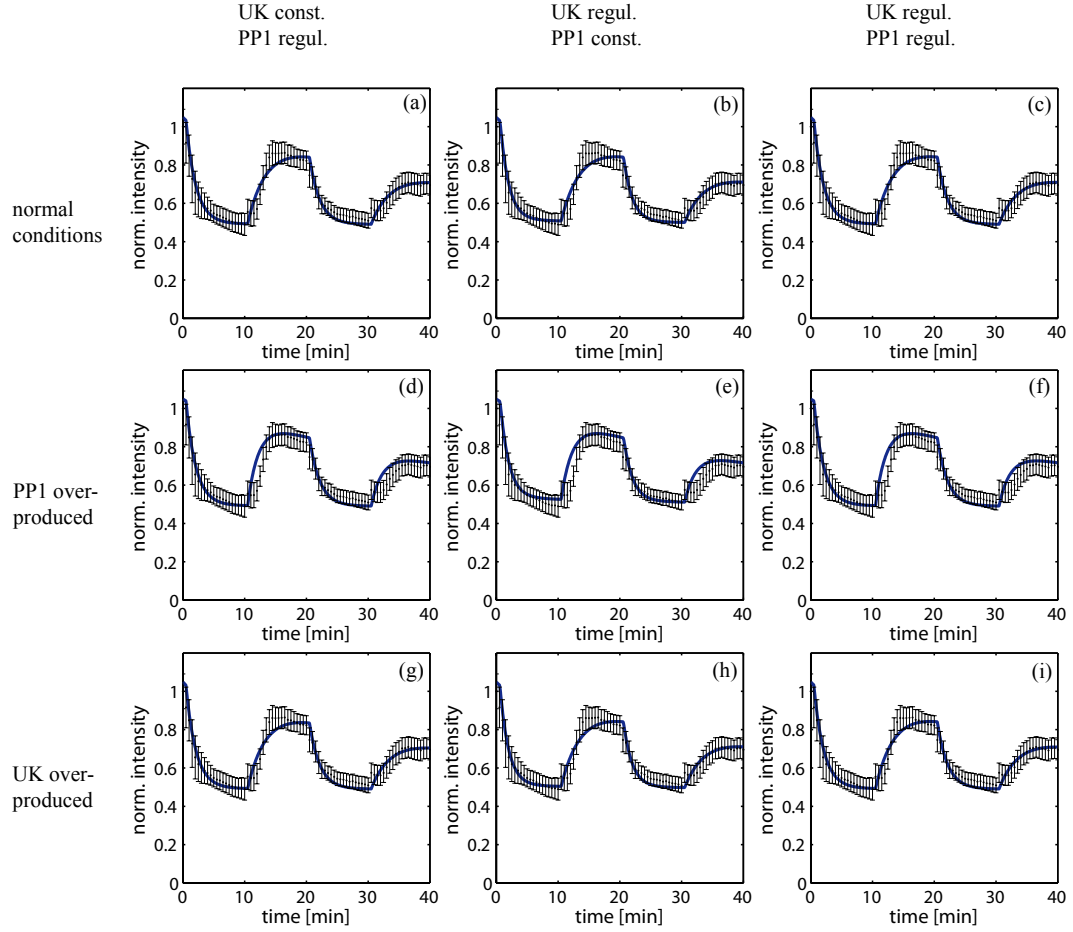


Figure 3.24.: Experimental data and simulations of nuclear intensities, as a measure for Mig1, for a two-step Mig1 regulation model (IIIa), IIIb), and IIIc)). First row: normal conditions. Second row: UK overproduced *in silico*. Third row: PP1 overproduced *in silico*. First column: glucose-regulated PP1. Second column: glucose-regulated UK. Third column: both glucose-regulated. It can be seen that the model with a constant phosphatase reproduces the abrupt (de)phosphorylation dynamics of Mig1 (see middle column). This is due to the interplay with the glucose-regulated complex formation with Hxk2. In contrast, the Snf1 model without this additional step as introduced above (see Table 3.4), displays poor agreement of simulations and experimental data (see middle column of Figure 3.20). Glucose profile as shown in Figure 3.9.

3. Mathematical modelling of the Snf1 pathway

- Including a two-step regulation for Mig1 considerably improves the agreement of data and simulations (see Figure 3.24).

3.4. Summary

Although the details on the mechanisms of the glucose signals responsible for Snf1 regulation remain to be elucidated, so far, it is widely assumed in the literature that the signal leading to glucose-induced Snf1 inactivation is related to the rate of the first step of glycolysis. Thus, in a first approach to modelling the Snf1 pathway, we present the derivation of a glucose-regulated signal by means of the glucose consumption rate per cell. As a basis for this approach, the mechanisms of glucose transport into a yeast cell had to be reviewed. Yeast consumes glucose through facilitated diffusion accomplished by a complex transport system consisting of several different kinds of hexose transporters. Using experimental data for extracellular glucose, we find that for certain experimental setups, the well-known carrier model, which assumes a constant dynamic contribution of transporters, is not sufficient. We develop an ODE-based model considering the high and low affinity contribution on the glucose uptake rate and find that this approach shows a satisfying fit for both, the overall shape and the details comprised after a glucose pulse. On this basis, we derive the glucose-regulated signal, which then is used as the regulatory signal for Snf1 [Frey *et al.* 2011a].

Furthermore, the processing of fluorescent microscopy data of a downstream target of Snf1, the transcriptional repressor Mig1, is presented. Fluorescence microscopy, in combination with optical tweezers and microfluidics, can be used to acquire images with high spatial and temporal resolution that allow quantitative information regarding the response of single cells to environmental changes [Eriksson 2009]. The fluorescent microscopy data for Mig1-GFP had to be processed in order to extract the data of interest (Mig1-GFP) from bleaching effects and background noises. We establish an ODE-based mathematical analysis for Mig1-GFP data processing, which allows a stepwise extraction of the information on the background and Mig1-GFP bleaching rates, the background-to-Mig1-GFP ratio, and the rates of Mig1-GFP phosphorylation and dephosphorylation. Eventually, it is possible to predict Mig-GFP shuttling as it would occur without bleaching. Our analysis demonstrates how data acquired using an optical microscope can be processed and used for mathematical modelling of signal transduction pathways [Frey *et al.* 2011b].

Iterative cycles between data-driven modelling and model-driven experimentation were carried out. The information of the glucose signal, the processed Mig1 data, and Snf1 Western blot data were used for modelling the Snf1 pathway. Additional information was given through the finding, that upon overexpression of SAK1 (the main upstream kinase of Snf1), Snf1 was highly phosphorylated even in high glucose media, while Mig1 remained

unaffected. Also, Mig1 (de)phosphorylation was not influenced by REG1 overexpression. In search of the regulatory mechanisms underlying the Snf1 pathway, several alternative pathway structures are proposed, translated into ODE-based models, and tested by comparing the model simulations to the (processed) experimental data. The Snf1 Western blot data can be reproduced for all model alternatives. In order to describe the Mig1 data, the models comprising a two-step regulation for Snf1 are constricted to those models with a glucose-regulated phosphatase. However, investigating the models comprising a two-step regulation for Mig1 shows that all of them can explain the data. With the given data and the current model assumptions, it is not possible to distinguish between simulations of a pathway, where both, the kinase and the phosphatase of Snf1, are glucose-regulated and where only the phosphatase transmits the glucose signal. Yet, the models show, that Mig1 requires a glucose-regulated step for dephosphorylation, either in form of a directly glucose-regulated phosphatase or a mechanisms involving an additional glucose-regulated component. However, a model with a glucose-regulated kinase and a glucose-regulated phosphatase show the best agreement to the experimental data with an almost constant kinase rate while the phosphatase rate exhibited pronounced dynamics upon glucose availabilities. Indeed, this does not lead to the conclusion that a glucose-regulated phosphatase alone is more favourable or more likely. It would also be a feasible explanation if both, a glucose-regulated kinase and a glucose-regulated phosphatase, are responsible for Snf1 regulation. This redundancy might allow for defending Snf1 from dysfunctions.

Modelling is limited due to insufficient qualitative and quantitative data on concentrations, reaction and degradation rates, as well as many other parameters that are delicate to measure [Materi and Wishart 2007]. With regard to further work, investigating the mechanisms (such as including hexokinases into the model) that eventually lead to the phosphatase activation or kinase deactivation appears to be a promising approach to constrict the remaining possible Snf1 network structures. The phosphatase of Snf1 and Mig1 is a complex, composed of the regulatory Reg1 and the catalytic Glc7 subunit. So far, only REG1 was overexpressed, leading to only a slight increase in the total number of complexes. For this reason, overexpression of both subunits at the same time seems more promising to create a condition of high Snf1 phosphatase overproduction. Also, in order to answer the question of Snf1 regulation, it might be useful to, in addition to the data introduced here, generate different kinds of data, such as spectroscopic data elucidating Snf1 complex formations or Reg1/Glc7 and Snf1 complex formations. Another challenge certainly lies within not only temporal but also spatial considerations of the different locations of the Snf1 complex to the nucleus, cytosol, or vacuole, and the role of the three different kinases of Snf1.

4. Quantitative measures for signalling pathways

In this chapter at first, an introduction to quantitative measures is given in Section 4.1. Next, quantitative measures are established, as defined by Heinrich *et al.* [Heinrich *et al.* 2002] in Section 4.2 and 4.4. These definitions build the basis for the onward analyses: In Section 4.3, extensions of those measures are discussed, which has been submitted for publication in the collaborative manuscript Millat *et al.* [Millat *et al.* 2010]. In Section 4.5, restrictions for a weakly activated system for a single phosphorylation cycle are addressed. In Section 4.6, an optimality criterion as a measure of optimal cascade length concerning average time and average duration of active cascade components is defined. Thereon, consequences of model approximations are discussed in Section 4.7. Main parts of this chapter are published in [Frey *et al.* 2009].

4.1. The need for quantitative measures

To ensure survival, cellular systems continuously need to adapt to changing environmental conditions. The stimuli triggered by those changes are mediated via signalling pathways from specified detection systems to the interior of the cell in order to cause changes in gene expression or enzyme activity [Downward 2001]. As recent experimental and theoretical studies have shown, timing and order of events [Rensing *et al.* 2001; Murphy and Blenis 2006], signal duration [Marshall 1995; Ferrell Jr. 1996; Sabbagh *et al.* 2001; Vaudry *et al.* 2002; Millat *et al.* 2008] as well as signal strength (thresholds) [Behar *et al.* 2008] are key parameters for the cellular response. On the one hand, cells that do not react quickly enough to changing nutrient conditions risk being overgrown by competitors that are quicker on the uptake [Kuttykrishnan *et al.* 2010]. On the other hand, cells that respond too quickly risk wasting energy on the inappropriate response itself and being overgrown by more efficient competitors [Kalisky *et al.* 2007]. This leads to the conclusion that the specific structure of a pathway reflects its specific characteristic dynamical requirements. Signal specificity is determined by the temporal and spatial dynamics of signalling components [Kholodenko 2006]. It was observed in PC12 cells that the duration of signalling through ERK may hold the key to the very different outcomes of EGF and NGF stimulation [Sabbagh *et al.* 2001; Vaudry *et al.* 2002]. As reported in [Marshall 1995],

4. Quantitative measures for signalling pathways

the duration of ERK activation determines whether cells can trigger either proliferation or differentiation. For the cellular response, and therefore, for the specific function of the pathway, the properties of signals are crucial. However, an analysis for comparing different pathway structures requires measures for quantification of properties, such as the timing or duration of activated signal. The application of quantitative measures to components of those pathways provides a tool for their characterisation. The characterisation of dynamic features of signal transduction pathways is hence crucial to describe cellular adaptation. This can also be determined by analysing experimental data without any knowledge about the underlying network. Different attempts were made to define mathematical relations, which extract this information from experimental and theoretical time courses. (For recent reviews see [Klipp 2009; Kholodenko *et al.* 2010].) The meaningful determination of quantitative properties for dynamic signals is not trivial. Over recent years, mathematical theories have been developed to describe the regulation of signalling pathways as a function of key parameters, i.e. phosphatase or kinase rate constants. The notion of characteristic times is an approach frequently used to determine signal properties. Well-known examples are the transition time [Easterby 1981, 1986; Llorens *et al.* 1997], and the t_{99} magnitude [Easterby 1973; Storer and Cornish-Bowden 1974; Torres *et al.* 1991], which is the time necessary to reach 99% of the final steady state. The t_{99} magnitude has the physical meaning of the relaxation time of a system [Schwarz 1968; Atkins and de Paula 2002], which is related to the eigenvalues of the system. This measure is well-defined from a theoretical point of view, but difficult to determine from data and complex systems. For this reason, Llor  ns *et al.* [Llorens *et al.* 1999] introduced a geometrical approach to estimate the magnitude of the average time, taken by any observable of a metabolic pathway, to reach a new state, when either a perturbation or a persistent variation was applied. Heinrich *et al.* defined measures to quantify signalling time τ , signal duration ϑ , and signal amplitude S using three different integrals over the dynamic signal $X(t)$ [Heinrich *et al.* 2002]. These integrals sum over the signal with different orders (order $n = 0, 1, 2$), with respect to time t^n . This approach excludes signals, which do not return to a zero basal level, and thus also those, which are in non-phosphorylated protein forms. In the analyses following below, we use the approach of Heinrich *et al.* [Heinrich *et al.* 2002], where integrals of different orders are used to characterise signals for a general system (see Section 4.2) and a weakly activated system (in Section 4.4).

4.2. Quantitative measures for general systems

Heinrich *et al.* [Heinrich *et al.* 2002] introduced a general model¹, denoted Hg model, that describes a sequential kinase-phosphatase-cascade, as depicted in Figure 4.1. The change of concentration of a phosphorylated protein X_i^P is described by the rate equation [Heinrich *et al.* 2002]

$$\frac{d}{dt}X_i^P = \tilde{\alpha}_i(X_i)(X_{i-1}^P) - \beta_i X_i^P, \quad (4.1)$$

where $\tilde{\alpha}_i = \alpha_i/X_i^{\text{tot}}$ and X_i^{tot} denotes the total concentration, X_i the dephosphorylated form of the proteins, X_0 the receptor concentration, and α and β denote the kinase and phosphatase rate constants, respectively. For a detailed derivation of this equation we refer to [Heinrich *et al.* 2002] or the Appendix B.3.

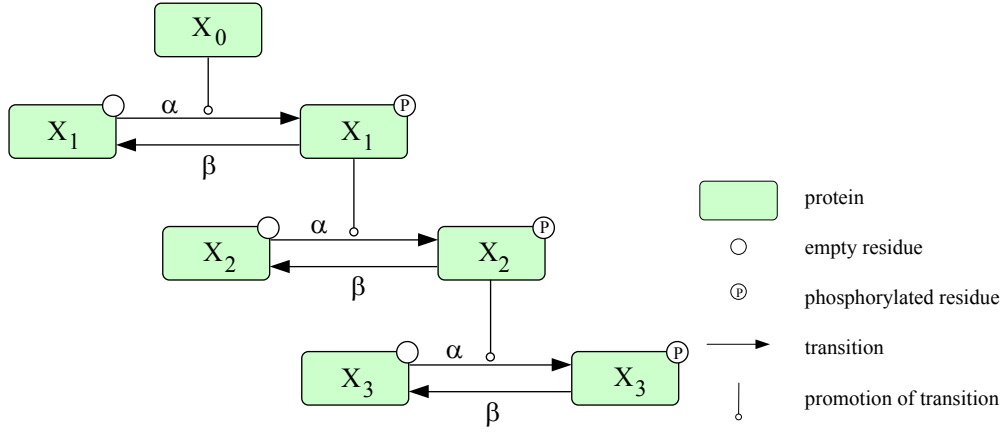


Figure 4.1.: The sequential kinase-phosphatase-cascade model of Heinrich *et al.* [Heinrich *et al.* 2002]. The dephosphorylated form of the proteins is denoted as X_i and the phosphorylated as X_i^P . X_0 denotes the receptor concentration, α and β denote the kinase and phosphatase rate constants, respectively.

For such a system, Heinrich *et al.* [Heinrich *et al.* 2002] introduced the following quantitative measures: The signalling time of a pathway defined as

$$\tau_i := \frac{\int_0^\infty t X_i^P dt}{\int_0^\infty X_i^P dt}. \quad (4.2)$$

The signalling time of a pathway is thus defined as the average time for the signal of the i -th component X to become activated (Figure 4.2). The denominator integrates over the entire signal $X_i^P(t)$ and corresponds to the total amount of all X_i^P molecules generated during the signalling period. More generally, it can be interpreted as signal power or

¹The naming convention ‘general’ is chosen in contrast to a ‘weakly activated’ model discussed in Section 4.4.

4. Quantitative measures for signalling pathways

dosage of the considered signal. The quantitative measure signal duration is defined as

$$\vartheta_i := \sqrt{\frac{\int_0^\infty t^2 X_i^P dt}{\int_0^\infty X_i^P dt} - \tau_i^2} \quad (4.3)$$

and characterises for how long a signal of component X_i^P remains active. With quantitative measures given in Eqs. (4.2) and (4.3), we can generate information about signal strength and signal amplification. The quantitative measure signal amplitude is then given by

$$S_i := \frac{\int_0^\infty X_i^P dt}{2\vartheta_i}. \quad (4.4)$$

Due to the averaging involved, the signal amplitude S is smaller than the maximal signal strength. All three definitions include integrals that sum over the signal with different orders with respect to time t . This approach therefore excludes signals, which do not return to a zero basal level.

Finally, [Heinrich *et al.* 2002] define the amplification ratio A as

$$A_{i,i-1} = \frac{S_i}{S_{i-1}}, \quad i = 1, \dots, n$$

comparing the signal amplitude of the i -th component with its precursor. Thereby, A_1 denotes the amplification of the stimulus and its successor. If $A_{i,i-1} > 1$ the signal is amplified, and damped for $A_{i,i-1} < 1$. The overall amplification of a signalling pathway can thus be measured as

$$A_{n,0} \equiv A_n = \frac{S_n}{S_0}, \quad (4.5)$$

where S_0 denotes the signal amplitude of the stimulus and S_n of the most downstream and phosphorylated protein. It describes the course of the signal amplitude S on its way from receptors to the nucleus. Heinrich *et al.* found that in short pathways, signal amplification can be achieved only with slow signal propagation and prolonged signal duration. This might be biologically undesirable, and could explain why signalling cascades generally consist of multiple steps. The series of components in a cascade can afford amplification of the signal, e.g. binding of one hormone molecule to the cell can potentially lead to the activation of hundreds of signalling molecules inside of the cell, so that relatively small amounts of a certain extracellular signal can have drastic intracellular effects [Hancock 2010].

Within this study, we assume an exponential decreasing function for the stimulus

$$X_0(t) = \mathcal{X}_0 e^{-\lambda t},$$

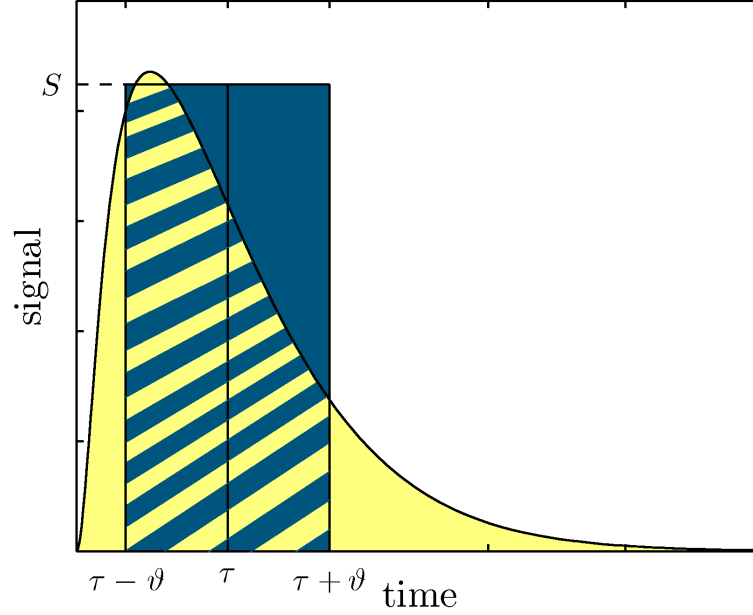


Figure 4.2.: Illustration of signalling time τ , signal duration ϑ , and signal strength S for a hypothetical time-dependent signal [Heinrich *et al.* 2002]. Note that the signalling time τ does not necessarily coincide with the maximum level of the signal. This would only be the case for a symmetric function. By definition of S , the area under the curve is equal to the area of the rectangle.

where \mathcal{X}_0 is the initial concentration, that is the ‘concentration’ of activated receptors. How fast the stimulus decreases is determined by the rate constant λ . The greater λ the faster the stimulus tends to zero. Due to this special choice, the integrals in Defs. (4.2)-(4.4) can be solved analytically. The signalling time for the receptor is then $\tau_0 = 1/\lambda$, which coincides with the relaxation time or characteristic time. The signal duration is also $\vartheta_0 = 1/\lambda$. Finally, it is $S_0 = \mathcal{X}_0/2$ for the signal amplitude as shown in Heinrich *et al.* and in the Appendix B.5.

4.3. Extension to signals with a non-zero basal level

In previous studies [Heinrich and Rapoport 1975], the application of quantitative measures was restricted to signals that eventually return to a value of zero. In [Millat *et al.* 2010], we extend previous definitions in order to allow for signals approaching a non-zero basal level, which will be presented here. The restriction to transient signals, which return to zero, is a limitation that can be avoided by the measures based on Llorens [Llorens *et al.* 1999].

For example, the characteristics of non-phosphorylated proteins in a cascade, as shown in Figure 4.1, cannot be computed using the definitions of [Heinrich *et al.* 2002]. This case is illustrated with the simulations shown in Figure 4.3. For the simulations, we used a sequential phosphorylation cascade (Figure 4.1), which is a simplified representation of

4. Quantitative measures for signalling pathways

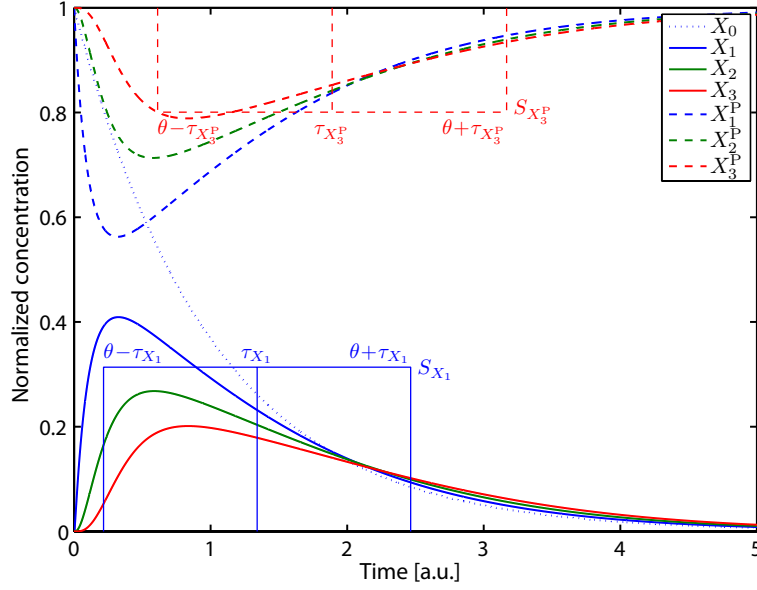


Figure 4.3.: Time course of selected components of a sequential phosphorylation cascade. The behaviour of phosphorylated proteins (X_1^P , X_2^P , and X_3^P (solid lines)) can be described with the original approach of [Heinrich *et al.* 2002], the behaviour of the non-phosphorylated proteins (X_1 , X_2 , and X_3 (dashed lines)) with the approach of [Millat *et al.* 2010]. Exemplary, we show the values for the quantitative measures τ , ϑ and S for protein X_3 . Figure from [Millat *et al.* 2010]. ‘a.u.’ denote arbitrary units.

the MAPK cascade [Seger and Krebs 1995; Schlessinger 2000; Avruch 2007].

For this case study, the integrals defining τ , ϑ , and S have to be redefined. To incorporate signals, which do not tend to zero but to a basal level \tilde{X} for $t \rightarrow \infty$, we replace the integral kernel of the original representation [Heinrich *et al.* 2002] by the difference $X(t) - \tilde{X}$. In contrary to the definitions in [Llorens *et al.* 1999; Klipp 2009], we do not use the absolute value of the difference. As discussed below, the algebraic sign of the integrals is important for the interpretation of quantitative measures and contains information about the components of signalling pathways.

Using the extended integral kernels we obtain the zero-order integral

$$I = \int_0^{\infty} (X(t) - \tilde{X}) dt , \quad (4.6)$$

the first-order integral

$$T = \int_0^{\infty} t (X(t) - \tilde{X}) dt , \quad (4.7)$$

and finally the second-order integral

$$Q = \int_0^{\infty} t^2 (X(t) - \tilde{X}) dt . \quad (4.8)$$

4.3. Extension to signals with a non-zero basal level

These integrals coincide with the original definitions of [Heinrich *et al.* 2002] if the basal level is equal to zero. Due to the consideration of the basal level \tilde{X} , the integrals are finite for signals tending to a non-zero final value for $t \rightarrow \infty$. The integrals for signals with a zero basal level are always positive. However, signals with a non-zero basal level may result in negative integrals because of the difference $X(t) - \tilde{X}$. A positive integral I represents the total amount of produced/phosphorylated proteins [Heinrich *et al.* 2002] and a negative integral describes the total amount of consumed/dephosphorylated proteins during the dynamic signal transduction process.

Following the approach of [Heinrich *et al.* 2002] and inserting the extended integral kernels, the signalling time is calculated as the ratio of the integrals (4.7) and (4.6):

$$\tau = \frac{T}{I} = \frac{\int_0^{\infty} t[X(t) - \tilde{X}]dt}{\int_0^{\infty} [X(t) - \tilde{X}]dt} . \quad (4.9)$$

The denominator integrates over the entire signal of phosphorylated protein $X_i^P(t)$ and corresponds to the total amount of all X_i^P molecules generated during the signalling period. More generally, the area under the curve can be interpreted as the total amount of activated protein X_i^P . This formula is an analogous to the mean value of a statistical distribution. It may be interpreted as the average time required to activate or deactivate the considered protein. Since for the same signal $X(t)$ the integrals T and I always have the same algebraic sign, the signalling time is positive definite.

The signal duration is given as

$$\vartheta = \sqrt{\frac{Q}{I} - \tau^2} = \sqrt{\frac{\int_0^{\infty} t^2[X(t) - \tilde{X}]dt}{\int_0^{\infty} [X(t) - \tilde{X}]dt} - \tau^2} \quad (4.10)$$

and corresponds to a standard deviation. It indicates the average duration the signal is active or inactive, respectively. The ratio of the integrals (4.8) and (4.6), as used in the above definition (4.10), is always positive because the integrals are of the same algebraic sign.

In order to develop the definition for the average signal concentration S , Heinrich *et al.* consider the area under the curve $X_i^P(t)$, $\int_0^{\infty} X_i^P dt$, (Figure 4.2). Then, the average concentration S is chosen the way that $2\vartheta \cdot S$ spans a rectangle, such that its area has the same size as the area under the curve [Heinrich *et al.* 2002]. Thus, combining the quantitative measures as defined in Eq. (4.2) and Eq. (4.3), the signal strength or signal amplitude is given by

$$S = \tilde{X} + \frac{I}{2\vartheta} . \quad (4.11)$$

4. Quantitative measures for signalling pathways

Equations (4.9)-(4.11) coincide with the definitions in [Heinrich *et al.* 2002] for a basal level equal to zero.

The application of the integrals defining the introduced quantitative measures of Eqs. (4.2)–(4.4) is restricted to a special class of signal shapes: The signal has to be finite at initial time t_0 (in our investigations we assume a value of zero). In addition, the term $\int_0^\infty t^2 X_i^P dt$ of Eq. (4.3) requires that the limit of the signal disappears for $t \rightarrow \infty$ faster than t^{-2} . According to these limitations, the introduced formalism can be applied to a cascade, where the initial concentrations of the phosphorylated proteins, the non-phosphorylated proteins, intermediates and the external stimulus are finite.

4.4. Quantitative measures for weakly activated systems

Heinrich *et al.* [Heinrich *et al.* 2002] apply a simplification of Eq. (4.1) that arises if one assumes ‘weak activation’, i.e. only a small fraction of protein X_i is activated during the process of signal transduction. This assumption implies that the concentration of the phosphorylated form of protein X is much smaller than the concentration of the unphosphorylated form, i.e.

$$\frac{X_i^P}{X_i^{\text{tot}}} \ll 1 \quad (4.12)$$

for each component of the considered cascade, denoted as the Hw model. This occurs for high phosphatase rates $\hat{\beta}_i \cdot P_i = \beta_i, P_i = 1$ and low kinase rates $\alpha_i \cdot X_{i-1}^P$. We can then neglect the contribution of the activated form of protein X_i in Eq. (4.1) and obtain the simplified rate equation

$$\frac{d}{dt} X_i^P = \alpha_i X_{i-1}^P - \beta_i X_i^P. \quad (4.13)$$

Note that the law of conservation of mass is not considered here. Consequences of this neglect are discussed in Section 4.5.

The linear differential equation (4.13) allows analytical solutions for the quantitative measures signalling time τ in Eq. (4.2), signal duration ϑ in Eq. (4.3), and signal strength S in Eq. (4.4), as shown in [Heinrich *et al.* 2002]. Thus, the signalling time for the activated protein X_i^P in a weakly activated system is defined as

$$\tau_i = \frac{1}{\lambda} + \sum_{j=1}^i \frac{1}{\beta_j}. \quad (4.14)$$

Interestingly, the definition of the signalling time is independent of the kinase rate constant. Since all summands are positive, the signalling time is an increasing function with increasing number of cascade levels. This means that for the same set of kinetic parameters, the more elements are combined in a cascade, the longer the transfer of information

4.5. Restrictions for weakly activated systems

in terms of way and time. To reach the same signalling time of two cascades of different lengths (i.e. number of tiers), every step of the longer cascade has to be accelerated through an appropriate choice of kinetic parameters. However, the range of those kinetic parameters is restricted due to physical properties of the molecules. According to [Heinrich *et al.* 2002], the signal duration of X_i^P is

$$\vartheta_i = \sqrt{\frac{1}{\lambda^2} + \sum_{j=1}^i \frac{1}{\beta_j^2}}. \quad (4.15)$$

Also, the signal duration is independent of the kinase rate constant α . Both, signalling time and signal duration, increase with longer signalling cascades. For the signal amplitude of X_i^P one obtains [Heinrich *et al.* 2002]

$$S_i = \frac{S_0 \prod_{k=1}^i \frac{\alpha_k}{\beta_k}}{\sqrt{1 + \lambda^2 \sum_{j=1}^i \frac{1}{\beta_j^2}}}. \quad (4.16)$$

S_0 is equal to $\mathcal{X}_0/2$ with \mathcal{X}_0 describing the concentration of activated receptor at time zero, as shown in the Appendix B.5. In contrast to the signalling time and signal duration, the average concentration depends on all pathway components, i.e. receptor, kinases and phosphatases [Heinrich *et al.* 2002]. The definition agrees with the intuitive idea that high amplification can be reached through high kinase rates and low phosphatase rates.

In the next section, it is shown that a model for a weakly activated pathway does not reflect the biological context appropriately, unless it is restricted to certain parameter combinations. Using a simple example of a cascade with one activation cycle, the parameter value interval is calculated.

4.5. Restrictions for weakly activated systems

Which parameter values do still allow for a sensible description of the biological system while applying a weakly activated system?

As introduced in Section 4.4, a sequential kinase-phosphatase-cascade is called ‘weakly activated’ if there is a low level of phosphorylation and a high level of dephosphorylation. The relevance for weak activation in natural systems is disputable. For adapting their gene expression to actual demands, cells respond to environmental changes and stimuli. In order to avoid responses towards noise, this process most likely requires strong activation. However, several analyses, such as [Chaves *et al.* 2004] and [Nakabayashi and Sasaki 2004], concerning optimal lengths and phosphorylation numbers are based on weakly activated systems. Since the law of conservation of mass is not taken into account in Eq. (4.13),

4. Quantitative measures for signalling pathways

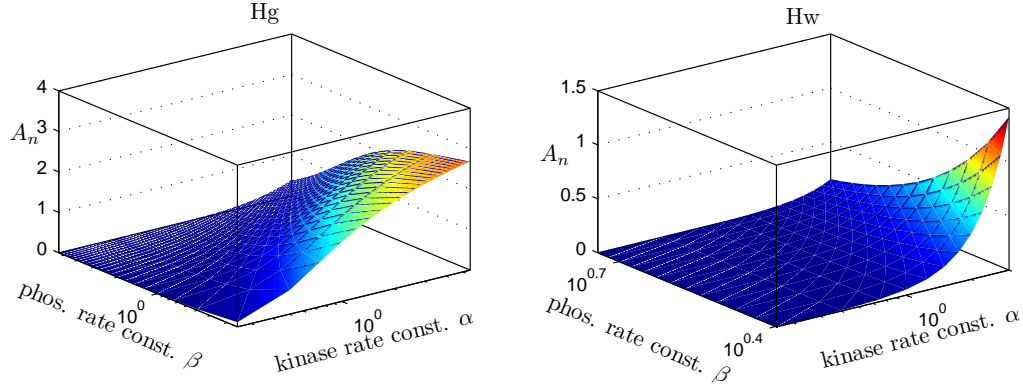


Figure 4.4.: Amplification A_n in the Hg and Hw model [Heinrich *et al.* 2002] as a function of the phosphatase rate constant β and the kinase rate constant α (plotted in logarithmic scale). The results are shown for cascade length three. (Hg model: $0 < \beta < 5.5$ and $0 < \alpha < 5.5$, Hw model: $2.5 < \beta < 5.5$ and $0 < \alpha < 3$). It can be seen in the Hg model that with an increasing kinase rate constant the amplification converges to a limiting value. It is noticeable for the Hw model that amplification increases as the kinase rate constant is increased. This cannot be achieved for the Hg model and does not seem to be realistic since obviously the number of available proteins in a biological system is finite.

the solutions of the ODEs describing non-phosphorylated proteins become negative for certain values of the parameters α and β , while the phosphorylated proteins exceed the overall total concentrations. In order to determine the exact limiting values, we analysed a cascade of length one. The analysis described below stresses that weakly activated systems are restricted to certain parameter combinations only and that beyond these values they perform nonsensical behaviour from a biological point of view [Frey *et al.* 2008].

We compare the Hg model (Eq. (4.1)) and the Hw model (Eq. (4.13)) by applying the quantitative measure signal amplitude of Def. (4.4) and Def. (4.16), respectively. More precisely, we examine the amplification ratio (Def. (4.5)) as a function of kinase and phosphatase rate constants.

A comparison of the Hg model and the Hw model examining the amplification A_n as a function of kinase and phosphatase rate constants shows striking deviations between the two models as can be seen in Figure 4.4. For real systems, the finite amount of molecules available restricts the overall amplification. In the Hg model the amplification reaches a limit, shown with the occurrence of a plateau in Figure 4.4 on the left. By contrast, in the Hw model, a signal can theoretically be amplified up to infinity by increasing the kinase rate constant as shown in Figure 4.4 on the right. We insert the signal amplitude of Eq. (4.16) into the overall amplification Eq. (4.5), restricting the values to $\lambda = 1$, $\beta_1 = \beta_2 = \dots = \beta_n$, and $\alpha_1 = \alpha_2 = \dots = \alpha_n$. The limit as $\alpha \rightarrow \infty$ leads to

$$\lim_{\alpha \rightarrow \infty} A_n = \lim_{\alpha \rightarrow \infty} \frac{\alpha^n}{\beta^n} \left(1 + \frac{n}{\beta^2}\right)^{-1/2} = \infty,$$

which is practically not possible for biological systems. For a weakly activated system, the

4.5. Restrictions for weakly activated systems

key parameters such as phosphatase or kinase rate constants can be calculated explicitly, as can be seen in Defs. (4.14), (4.15), and (4.16).

We calculate the range of parameter values for α and β , for which a biologically nonsensical behaviour is avoided. For the sake of simplicity, we use a single activation/deactivation cycle. This system can be described in the formalism of a weak activation as

$$\begin{aligned}\frac{d}{dt}X_1 &= -\lambda X_1, \\ \frac{d}{dt}X_2 &= -\alpha X_1 + \beta X_3, \\ \frac{d}{dt}X_3 &= \alpha X_1 - \beta X_3,\end{aligned}$$

where X_1 is the receptor concentration, X_2 the concentration of the unphosphorylated protein, and X_3 the phosphorylated protein. Again, the deactivation of the receptor is determined by the time constant λ and the (de)activation of the protein by the kinase rate constant α and the phosphatase rate constant β . This system of coupled differential equations can be solved analytically (for instance using DSolve function from Mathematica) and we obtain

$$\begin{aligned}X_1(t) &= \mathcal{X}_1 \cdot e^{-\lambda t}, \\ X_2(t) &= \frac{\mathcal{X}_1 \cdot \alpha}{\beta - \lambda} \cdot (e^{-\beta t} - e^{-\lambda t}) - \mathcal{X}_3 \cdot e^{-\beta t} + \mathcal{X}_2 + \mathcal{X}_3, \\ X_3(t) &= -\frac{\mathcal{X}_1 \cdot \alpha}{\beta - \lambda} \cdot (e^{-\beta t} - e^{-\lambda t}) + \mathcal{X}_3 \cdot e^{-\beta t}.\end{aligned}$$

For demonstration purposes, we choose the parameters as follows: rate constant $\lambda = 1$, initial concentrations $\mathcal{X}_1 = 1$, $\mathcal{X}_2 = 1$, and $\mathcal{X}_3 = 0$, which leads to the following equations:

$$\begin{aligned}X_1(t) &= e^{-t}, \\ X_2(t) &= \frac{\alpha}{\beta - 1} (e^{-\beta t} - e^{-t}) + 1, \\ X_3(t) &= -\frac{\alpha}{\beta - 1} (e^{-\beta t} - e^{-t}).\end{aligned}\tag{4.17}$$

Note that this value choice for \mathcal{X}_1 , \mathcal{X}_2 , \mathcal{X}_3 , and λ requires the phosphatase rate constant β to have a value unequal to one. If the minimal values of $X_2(t)$ are smaller than zero, the approximation of weakly activated cascades becomes unphysical. Therefore, we calculate

4. Quantitative measures for signalling pathways

the minimum of Eq. (4.17) as follows

$$\begin{aligned}
X_2(t) &= \frac{\alpha}{\beta - 1} \left(e^{-\beta t} - e^{-t} \right) + 1 \\
\frac{d}{dt} X_2(t) &= \frac{\alpha}{\beta - 1} \cdot \left(e^{-t} - \beta \cdot e^{-\beta t} \right) \\
&= 0 \\
\Leftrightarrow t &= \frac{\ln \beta}{\beta - 1} \\
X_2 \left(\frac{\ln \beta}{\beta - 1} \right) &= \frac{\alpha}{\beta - 1} \left(\beta^{\frac{1}{1-\beta}} - \beta^{\frac{\beta}{1-\beta}} \right) + 1.
\end{aligned} \tag{4.18}$$

Eq. (4.18) contains the values for the minimum of X_2 in dependency of α and β . Combinations of the parameters leading to a minimum ≤ 0 are parameter combinations, which are not possible in biological systems and therefore, are not allowed. We solve Eq. (4.18) ≥ 0 for kinase rate constant α and obtain the combination of parameters, for which the minimum is non-negative:

$$\alpha \leq (\beta - 1) / (\beta^{1/(1-\beta)} - \beta^{\beta/(1-\beta)}).$$

For a cascade with one activation cycle, we found that the values of α and β must follow the inequality $\alpha \leq (\beta - 1) / (\beta^{1/(1-\beta)} - \beta^{\beta/(1-\beta)})$ in order to allow for biological meaningful considerations only.

4.6. An optimality criterion

How to define a plausible optimisation criterion for comparing different pathway structures?

Previous works [Chaves *et al.* 2004; Nakabayashi and Sasaki 2004] investigated the average time τ as a function of the number of phosphorylation steps. An optimal surviving strategy might be to transmit a signal fast. Additionally, the duration should be long enough to be distinguishable from noise, while not impeding the signal transmission longer than needed. Since both, the signal duration as well as the signalling time are crucial for the response of the system [Sabbagh *et al.* 2001; Vaudry *et al.* 2002], we include both into our optimality criterion [Frey *et al.* 2008]. Assuming that the structure of a pathway is the result of a multivariate optimisation process, an optimality criterion is defined using the quantitative measures introduced above. We expect that structures, which enable a fast response to a stimulus, by exerting a sufficiently long duration to be distinguishable from noise, are of advantage. It is therefore reasonable to define the optimality criterion

as follows:

$$O_n = \min_n (\tau_n \cdot \vartheta_n), \quad (4.19)$$

τ_n = average time until a protein is activated,

ϑ_n = average duration a protein remains activated.

The level of the cascade is denoted with n . Thus, n represents the most downstream and phosphorylated protein. τ and ϑ are defined by Defs. (4.2) and (4.3).

Based on these definitions, we test the hypothesis, whether the structure of the MAPK cascade is the result of such an optimisation process. This analysis is presented in Chapter 5.

4.7. Consequences of approximations

The analysis of signal transduction pathways often requires simplifying reductions. There is an ongoing discussion how the applied approximations change the system's behaviour. Approximations can change the system's behaviour qualitatively and quantitatively [Millat *et al.* 2007]. Several studies [Blüthgen *et al.* 2006; Flach and Schnell 2006; Millat *et al.* 2007] demonstrate that approximations can strongly influence the response of the considered system. Therefore, the question arises:

What are the consequences of three different model approximations with respect to time and duration describing the same pathway structure?

The different models to be compared here, are summarised in Table 4.1, introduced in detail in the Appendix B, and briefly listed as follows:

1. The mechanistic model by Huang and Ferrell (hereafter denoted HF model) was developed using an enzyme kinetic model of 18 non-linear ODEs [Huang and Ferrell 1996].
2. Assuming that the intermediate complexes operate at a quasi-steady state, this model is reduced to nine ODEs, introduced by Heinrich *et al.* (denoted Hg model) [Heinrich *et al.* 2002].
3. A further simplification leads to the the model by Kholodenko (denoted K model) [Kholodenko 2000].

The starting point is the mechanistic HF model, for which we exemplarily chose six different sets of parameters. The compatible parameters for the Hg model and K model were derived as described in [Millat *et al.* 2007], assuming a quasi steady state, a formal bimolecular reaction and constant concentration of phosphatase, as shown in Appendix B.4. For

4. Quantitative measures for signalling pathways

Model by	Example equation	Parameters
HF [Huang and Ferrell 1996]	$\frac{d}{dt} X_i^P = \{d_{i+1} + k_{i+1}\} (X_{i+1} X_i^P) + k_i (X_i X_{i-1}^P) - a_{i+1} X_{i+1} X_i^P$	a_i, d_i, k_i
K [Kholodenko 2000]	$\frac{d}{dt} X_i^P = \frac{k_i X_{i-1}^P X_i}{K_M + X_i} - \frac{V_i X_i^P}{K_M + X_i^P}$	$K_M^i = \frac{d_i + k_i}{a_i}$ $V_i = k_i P$
Hg [Heinrich <i>et al.</i> 2002]	$\frac{d}{dt} X_i^P = \alpha_i X_{i-1}^P \{1 - X_i^P / X_i^{\text{tot}}\} - \beta_i X_i^P$	$\alpha_i = \frac{k_i}{K_M^i}$ $\beta_i = \frac{k_i}{K_M^i} P$

Table 4.1.: Overview of the three models used for analysis in this chapter. The first column indicates the reference of the literature, the second column shows one example equation of each model, and the third column shows the specific parameters and their derivation from the mechanistic HF model. Table from [Frey *et al.* 2009].

simplicity, the number of parameters is reduced by examining only cascades with identical cycles.

In case the mechanistic interactions, approximations or intermediate steps of a signalling pathway are still unknown or uncertain, modelling of the pathway becomes precarious. Among others, quantitative measures can be used to characterise the effect of different approaches, such as different mechanistic interactions, approximations and of different intermediate steps. Here, a structural analysis is performed by comparing alternative structures for signalling cascades, as shown in Figure 4.5, using the quantitative measures described in Section 4.2. The different intermediate steps include single, double and triple phosphorylations of a three level cascade.

Figure 4.5 shows that the Hg and K models, which both assume that intermediate complexes operate at a quasi-steady state, have a similar behaviour, in contrast to the HF model, which considers the formation of complexes. Interestingly, those parameter value sets, where association constant a is bigger than dissociation constant d and catalytic constant k , Figures 4.5(e), 4.5(f), 4.5(k), 4.5(l), show huge deviations of the HF model compared to the Hg and K model. This can be explained by the increased complex formation in the HF model, which emphasises the neglect of complexes in the Hg and K models even more. For values of dissociation constant d bigger than a and k , the concentration of complexes in the HF model is small. This fact leads to a similar behaviour compared to the Hg and the K models, which both neglect the formation of complexes, Figures 4.5(b), 4.5(h), and 4.5(i). When the sum of catalytic constant k and dissociation constant d is much bigger than association constant a , this leads to small concentrations of complexes in the HF model, and thus, to similar behaviour among the three model approximations, Figures 4.5(a), and 4.5(g).

4.7. Consequences of approximations

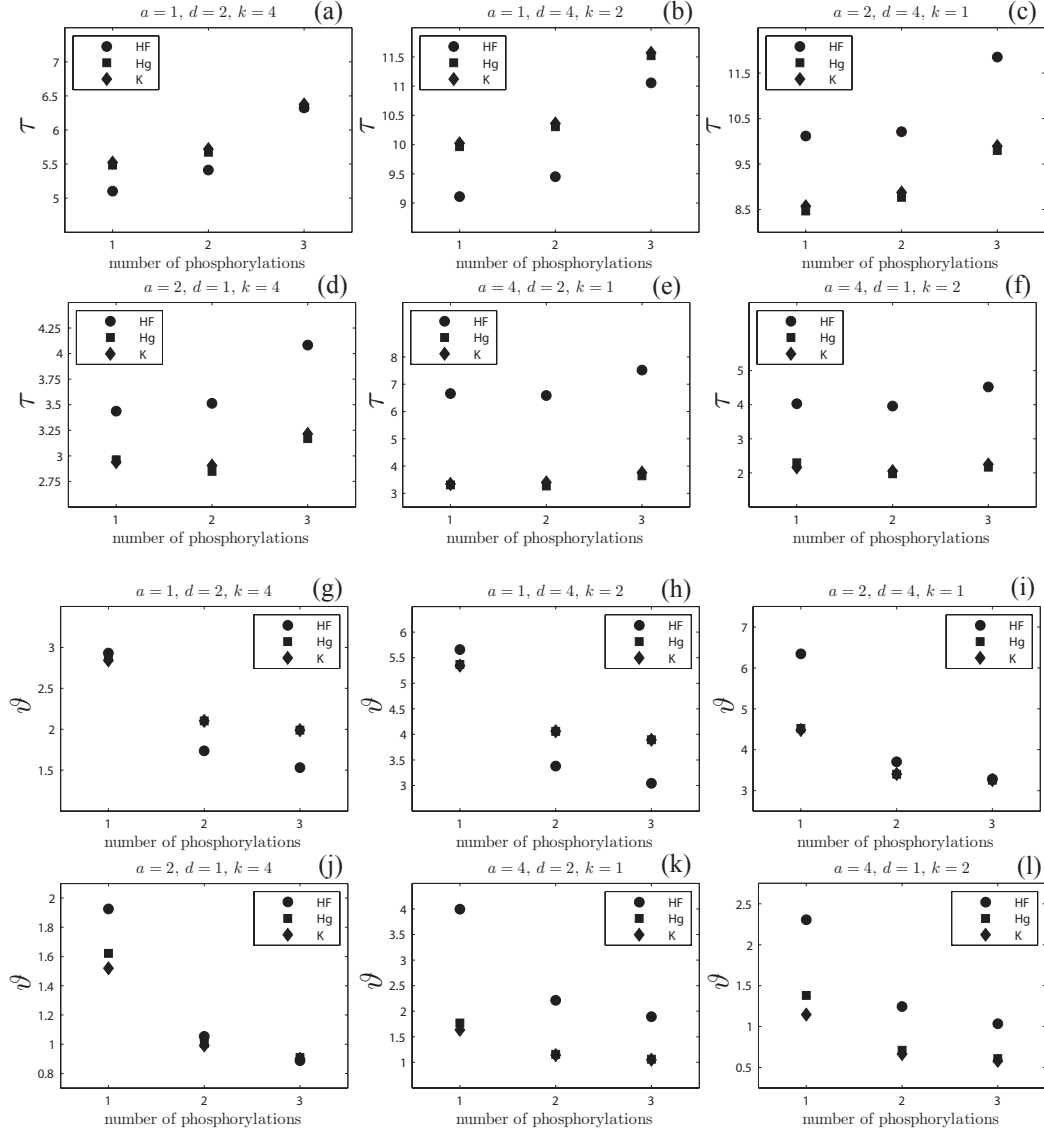


Figure 4.5.: Comparing the different model approaches Hg, HF and K for a cascade with three tiers over a range of single, double, and triple phosphorylation applying signalling time τ and signal duration ϑ . Parameters, namely association constant a , dissociation constant d , and catalytic constant k , are indicated above each subfigure. The quantitative measures unravel deviations of the HF model (considering complex formation) on the one hand and of the Hg and K model (both neglecting complex formations) on the other hand. Figures are taken from [Frey *et al.* 2009].

4.8. Summary

Once a model of signal transduction pathways has been determined fulfilling plausible assumptions of the biological background and reproducing the experimental data, the question still remains disregarded, why this specific kind of structure has evolved. The application of quantitative measures to components of those pathways provides a tool for their characterisation and can thus be used for comparison among different pathway structures.

Definitions of quantitative measures by [Heinrich *et al.* 2002] are restricted to signals that eventually approach zero. Depending on the kinds of signals, a redefinition for signals with a non-zero basal level becomes necessary. We redefined quantitative measures to make applicable for a broader class of signals [Millat *et al.* 2010]. We define an optimality criterion that allows for a multivariate optimisation process.

Amplification as a function of the kinase rate constant α and phosphatase rate constant β exposes huge deviations between the Hg model and the Hw model. The amplification defined by the Hg model is limited to the overall concentration, the amplification of a Hw model, however, is not. In order to satisfy the mass conservation in the Hw model, the values of those parameters were determined for a single phosphorylation cycle.

Comparing three different model approximations, the quantitative measures mirror that the underlying assumptions are more similar among the Hg and K model than between them and the HF model. Interestingly, it depends on the choice of parameters, whether or not the HF model shows faster responses to a stimulus than the Hg and K model. This is a consequence of the used quasi-steady state approximation in the Hg and K model. On the one hand, those two models neglect the time to establish the quasi-steady state of the complexes, which is fully described in the HF model. On the other hand, if no quasi-steady state is established, the quasi-steady state approximation used in the two other models is not valid and adds an artificial bottleneck in the dynamics of the system. Consequently, the more detailed HF model becomes faster than the Hg and K models. As shown in investigations of enzyme kinetic reactions, the choice of parameters determines the validity of the quasi-steady state assumption [Schnell and Mendoza 1997].

5. Application of quantitative measures to the MAPK cascade

In this chapter, the optimality criterion of Eq. (4.19) is applied to three MAPK pathway models, which differ in their underlying approximations, and consequences of approximations are discussed. Also, applying the optimality criterion, we compare the characteristic MAPK structure to alternative structural designs. The work presented here includes main contents published in [Frey *et al.* 2008] and [Frey *et al.* 2009].

5.1. The two double phosphorylations within the MAPK cascade

The ubiquitous *Mitogen Activated Protein Kinase cascades* (MAPK cascade) are well-conserved from yeast to mammals [Widmann *et al.* 1999]. They relay signals from diverse stimuli and receptors to the nucleus and are involved in many crucial processes of cellular development [Pearson *et al.* 2001; Avruch 2007], e.g. proliferation, differentiation [Raman *et al.* 2007] and apoptosis [Lamkanfi *et al.* 2007]. Many oncogenes have been shown to encode proteins that transmit mitogenic signals upstream of this cascade, so that the MAPK pathway provides a simple unifying explanation for the mechanism of action of many non-nuclear oncogenes [Seger and Krebs 1995]. Consequently, these signalling pathways play an important role in many diseases [Kyriakis and Avruch 2001; Lawrence *et al.* 2008], e.g. their role in cancer is of special interest.

The MAPK cascade consists of a system of at least three activation steps [Bardwell 2005] as shown schematically in Figure 1.2. It is assumed that the corresponding kinase and phosphatase activities do not depend on the number of added phosphate groups. The first protein kinase (MAPKKK) activates the second kinase (MAPKK), the second one then activates the third kinase (MAPK) through double phosphorylation [Anderson *et al.* 1990; Alessi *et al.* 1994]. Active MAPK thus can enter the nucleus and regulate transcription factors that control gene expression.

For about a decade, the MAPK cascade has been subject to mathematical modelling. The mathematical analyses unravel many interesting features of this fundamental structure in cellular signalling. The sequential alignment of (de)phosphorylation cycles amplifies their inherent ultrasensitivity [Goldbeter and Koshland, Jr. 1981] in such a way that

5. Application of quantitative measures to the MAPK cascade

the cascades are presumed to be a very sensitive, highly nonlinear, biochemical switch [Ferrell Jr. 1996; Ferrell and Machleder 1998]. Additional combination with positive and/or negative feedback brings about further interesting nonlinear behaviour, as bistability and oscillations [Kholodenko 2000; Xiong and Ferrel Jr. 2003; Wang *et al.* 2006]. Due to the specific structure of the MAPK cascade, which consists of two double phosphorylations and a cascade length three, the question arises: Do certain structures realise a design principle with respect to the quantitative measures [Frey *et al.* 2008]?

5.2. Applying quantitative measures to the MAPK cascade

Is the characteristic structure of a MAPK pathway, comprising two double phosphorylations, of advantage for signal transmission with respect to the average time and average duration of active signal?

There are more complex structures of MAPK pathways discussed in the literature, such as single or multiple negative feedback loops [Dougherty *et al.* 2005; Dhillon *et al.* 2007]. However, for this study, the analysis is done for a sequential multi-stage phosphorylation cascade, whereas the analyses of more complex structures are kept for future work. The present work performs a structural analysis by comparing alternative structures for those cascades by using quantitative measures for signalling time, signal duration and signal amplitude. Such measures were first introduced in [Heinrich *et al.* 2002]. An analysis of optimal cascade lengths was published in [Chaves *et al.* 2004] and [Nakabayashi and Sasaki 2004]. They performed their analysis based on a weakly activated system assuming the structure of a cascade is the outcome of a univariate optimisation process. Simulating the model for a weakly activated system, we found that certain parameter combinations led to a violation of the mass conservation, as shown in Section 4.5. This can lead to solutions of the differential equations with negative concentrations, which is obviously not possible in biological systems. Therefore, we focus on a the general model, and compare alternative structures with respect to a multivariate optimisation criterion introduced in Section 4.6. We compare different lengths of a cascade keeping the amplification ratio at a constant value.

The optimality criterion in Eq. (4.19) shows a minimum for structures with double phosphorylations, as shown in Figure 5.1. This result matches the structure of the MAPK cascade. For the parameter value sets of the second row, the products show a huge deviation among a structure with single and structure with double phosphorylations. Here, the optimum lies at a triple phosphorylation, but compared to the very large decrease from a single to a double phosphorylation there is no noteworthy improvement of the structure when changing a double to a triple phosphorylation. In addition, a structure with three phosphorylations would imply an increased complexity and additional processes to

5.2. Applying quantitative measures to the MAPK cascade

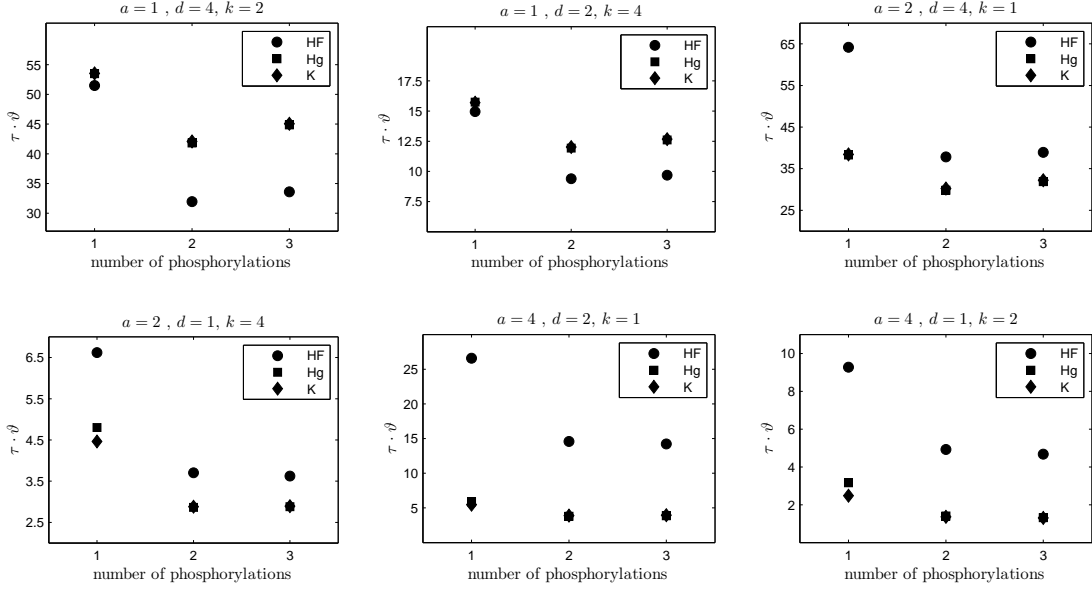


Figure 5.1.: Product of signalling time and signal duration: Comparison over a range of single, double, and triple phosphorylation of the Hg, K, and HF model for a cascade with three tiers. Parameters are indicated above each figure. We consider the most downstream and phosphorylated protein of the cascade. The optimality criterion of Eq. (4.19) is fulfilled for double and triple phosphorylated structures. Parameter values are indicated above each figure. The corresponding τ and ϑ are shown in Figure 4.5. See text for further explanation or [Frey *et al.* 2009].

realise them compared to a structure with double phosphorylations. To allow a reasonable comparison among different pathway structures of the Hg model, we kept the amplification A_n at a constant value. This way, the pathways may differ in their structure, but still realise the same function (amplification). We investigate the consequences of structural changes within the Hg model under constant amplification and the consequences of changes in amplification. Figure 5.2 shows the influence of the amplification A_n on the quantitative measures τ , ϑ and their product for three amplification factors, $A_n = 1$, $A_n = 2$, and $A_n = 6$. The speed of the response τ correlates with its duration ϑ . Our optimality criterion is satisfied for high amplifications ($A_n = 2$ and $A_n = 6$) and a cascade length of two and three, respectively, which includes the case of the MAPK cascade structure. Nakabayashi and Sasaki *et al.* [Nakabayashi and Sasaki 2004] found that the optimum number of kinase cascade steps increases approximately linearly with the logarithm of the amplification. They suggested that multi-step phosphorylations would have evolved to accelerate τ of weak signals. For that purpose they focus on the speed of signal transduction (τ) as the criterion for determining the optimal response. In our simulations not only τ , but also our multivariate optimality criterion supports this idea, (compare Figure 5.2). The length of the MAPK cascade is of at least three protein kinases [English *et al.* 1999] and its amplification lies within three to ten [Blüthgen 2007]. An overview of the concentrations

5. Application of quantitative measures to the MAPK cascade

is given in [Fujioka *et al.* 2006] showing that the input signal of a MAPK cascade (Raf) is a weak signal compared to the final product concentration (ERK).

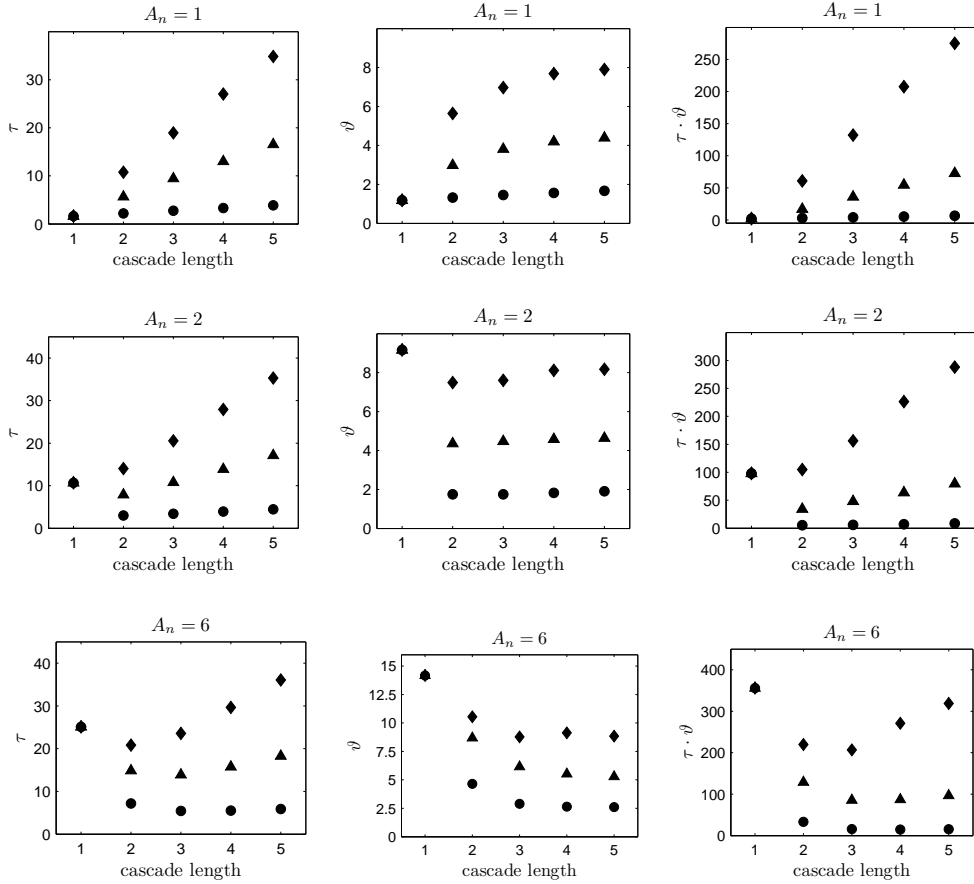


Figure 5.2.: Hg model for cascade lengths up to five. The number of phosphorylations is depicted the following way: single (circle), double (triangle), and triple phosphorylation (diamond). Left column: average time until a signal is activated τ . Middle column: average duration, which a signal remains activated φ . Right column: optimality criterion $\tau \cdot \varphi$. A_n denotes the amplification factor of the cascade element located most downstream. Note that for an increased amplification, the minimum according to our optimality criterion appears for longer cascades. For an amplification $A_n = 6$, the minimum can be found at length three for double phosphorylation, which is the structure of the MAPK cascade. (The receptor concentration was chosen to equal one, the concentration of the more downstream proteins to equal ten, $\alpha = 2$; β was chosen to obtain the specific amplification A_n).

Binder and Heinrich [Binder and Heinrich 2004] presented a first step towards an approach that investigates the interrelation between dynamics and the structural design of pathways. In contrast to [Binder and Heinrich 2004], we here consider short cascades with single, double, and triple phosphorylations.

We show how a double phosphorylated structure, which exists in MAPK cascades, changes the properties of the transduced signal in a favourable way comparing it to single phosphorylated structures. In general, the average time until a signal is activated (τ) becomes slower with increasing number of phosphorylations and the average duration a

signal remains activated (ϑ) becomes shorter. This means that multiple phosphorylations could have evolved to generate slow signals of short duration. A signal with a fast response might be of disadvantage because a biological system might need a certain time to proof its validity. On the other hand, the proof of validation should be fast enough to realise protection against damage or intake of nutrients when exposed to high availabilities. We also considered the product of τ and ϑ . If a minimum of this product exists, it shows an optimal trade-off between both. Indeed, as can be seen in Figure 5.1, a minimum most often exists for structures with double phosphorylations. This structure matches the design of the MAPK cascade, which suggests that the MAPK cascade is in favour to trigger a fast response of short duration. For a few parameter combinations the product of the average time τ (see Eq. (4.2)) and the average duration ϑ (see Eq. (4.3)) shows a minimum at triple phosphorylation. Yet, in those cases, the minimal value of the triple phosphorylation is similar to that of a double phosphorylation. Moreover, there is a huge deviation among a structure with single compared to a structure with double or triple phosphorylations. Although for some parameter value combinations, the minimum lies at a triple phosphorylation, there is no noteworthy deviation and thus improvement compared to a double phosphorylation. A double phosphorylated structure could still be favoured since a structure with three phosphorylations would imply an increased complexity and additional processes to realise and fuel them with energy, compared to a structure with only double phosphorylations. Besides the importance of the timing and duration of the transmitted signal, another crucial characteristic for the correct functioning of a pathway lies in the ability to amplify signals.

5.3. Summary

Quantitative measures can be used to characterise the properties of signalling molecules, and thus, of signalling pathways. Here, pathways of single, double, and triple phosphorylated structures of different model approximations are compared in terms of average time and average duration of activation. The application of the previously defined optimality criterion suggests, that a double phosphorylated structure, which matches the design of the MAPK cascade, is in favour to trigger a fast response of short duration. A minimum of the optimality criterion indicates an optimal trade-off between a fast signal response accompanied with a sufficiently long duration, e.g. to be distinguishable from noise while at the same time remain quickly responsive to changes in the environment or the interior.

6. Conclusions

Cells are permanently exposed to changes in their environment. The process of adaption has been proven to be a promising and necessary survival strategy of the cell realised by signal transduction pathways of interacting proteins. They detect extracellular signals, translate, and transmit their information to the interior of the cell and eventually trigger the specific and appropriate response. One focus of this thesis comprises a systems biology approach to dynamic modelling of the AMP-activated kinase pathway. This pathway plays a key role in energy sensing and metabolism by keeping an appropriate balance between the energy-producing catabolic and energy-consuming anabolic processes. Activated by metabolic stresses that cause depletion of ATP, AMPK switches off ATP-consuming anabolic processes that are not essential for the immediate survival of the cell and stimulates catabolic processes that generate ATP.

In this research, a systems biology approach is realised through an iterative cycle between data-driven modelling and model-driven experimentation. Using ordinary differential equations, mathematical modelling is established for the AMPK pathway homologue in the yeast *S. cerevisiae*, the Snf1 pathway. As a basis for the model development, the underlying biological background of both pathways is introduced in detail. Then, steps of model developments including the derivation of the glucose-regulated signal, Mig1-GFP data processing, and the analysis of the Snf1 pathway are presented and discussed.

So far, the mechanisms leading to Snf1 regulation upon glucose availabilities are still elusive, however, it appears to be related to the first step of glycolysis. Therefore, a first essential step for developing a mathematical model of the Snf1 pathway is the deviation of a glucose-regulated stimulus [Frey *et al.* 2011a] that ultimately determines Snf1 regulation. Thereby, we find that the carrier model, which describes the transport of molecules through the cellular membrane and considers only a constant contribution of transporters, is not able to explain the experimental data of glucose consumption in batch experiments. We show, that the dynamics of high and low affinity hexose transporters within the cell membrane of *S. cerevisiae* are essential and need to be considered and incorporated into the model. Thereon, a meaningful and precise reproduction of the glucose data is accomplished. The derived glucose-regulated signal is then supplied to serve as input function for Snf1 regulation.

Furthermore, Mig1-GFP fluorescence microscopy data, which suffer from bleaching effects and background noise, have to be processed in order to become suitable for modelling.

6. Conclusions

Therefore, a mathematical approach is discussed. It allows for a stepwise extraction of the data of interest (Mig1-GFP) by subtracting the background noise and accounting for the decrease of intensity due to bleaching effects. Therefore, the bleaching rates of the background noises and the Mig1-GFP itself and the background to Mig1-GFP ratios are determined. Eventually, this approach allows for the extraction of information on Mig1-GFP and for the prediction of Mig1 shuttling as it would occur without bleaching and background noise during changing environmental conditions [Frey *et al.* 2011b].

The derived glucose-regulated signal and the processed Mig1-GFP data are then used, combined with Snf1 Western blot data, to compare and analyse alternative pathway structures underlying the Snf1 pathway. We encode different hypotheses by ODE-based models. Iterative cycles between data-driven modelling and model-driven experimentation are carried out. We find that an additional glucose-regulated involvement is essential for explaining the experimental observations of unaffected Mig1 (de)phosphorylation in SAK1 and REG1 overexpressing cells. The models suggest, that Mig1 requires a glucose-regulated step for dephosphorylation, either in form of a directly glucose-regulated phosphatase or in case of a constantly active phosphatase, a mechanisms involving an additional glucose-regulated component. With regard to the Snf1 data, all three model alternatives ((a) regulation via the phosphatase, (b) regulation via the kinase, and (c) regulation via both) lead to a good agreement of Snf1 Western blot data and simulations, and thus all underlying mechanisms remain possible candidates for Snf1 regulation. The models also indicate that the regulation of Snf1 can be realised by a glucose-regulated phosphatase alone. However, a combination of both regulatory mechanisms allows for more subtle ways to adapt to changing environmental conditions and cannot be excluded from the list of Snf1 pathway candidates.

In order to describe the dynamic properties of signalling pathways, the application of quantitative measures, such as the average time until activation or the average duration of remaining in an activated state, can be used. They are useful to compare different pathway structures, providing insights, why a certain structure is favoured to another one. Also, the quantification of a signal might unravel crucial differences among healthy and diseased cells. The second focus of this thesis lies on the analysis of the characteristic structure of the MAPK cascade. Quantitative measures are assigned to investigate signalling pathway structures that are optimal in terms of a fast signal propagation, which stays active only for a short duration. Comparing single, double, and triple phosphorylated structures, we find that an optimum of the optimality criterion appears for the double phosphorylated structure of the MAPK cascade with respect to its characteristic amplification. For an increased amplification, the optimum appears for longer cascades, supporting the idea that multi-step phosphorylations could have evolved to accelerate the speed of weak signals.

With regard to further work, provided that additional data, as spectroscopic data,

are available, the considerations of complex dynamics might be useful to constrict the remaining candidates for Snf1 network structures. Another challenge certainly lies not only within temporal but also spatial considerations, especially, as determined by the different isoforms of the β -subunit of Snf1, the different locations of the Snf1 complex to the nucleus, cytosol, or vacuole. For the conditions of the experiments considered here, the phosphatase regulation might be sufficient to regulate Snf1, however, for other environmental conditions the contribution of a glucose-regulated kinase might be essential. Thus, designing new experiments might find a scenario that provides a way to distinguish between a glucose-regulated phosphatase model and a model, in which kinase and phosphatase are glucose-regulated. This raises new questions that require further research.

Appendix

A. Parameters for the Snf1 models

Parameter	UK const. PP1 regul. Model Ia)	UK regul. PP1 const. Model Ib)	UK regul. PP1 regul. Model Ic)
a_{Snf1}	$1 \cdot 10^3$	$1 \cdot 10^4$	$1 \cdot 10^2$
d_{Snf1}	$6 \cdot 10^3$	$2 \cdot 10^3$	$3 \cdot 10^3$
a_{PP1}	$6 \cdot 10^5$	$3 \cdot 10^5$	$2 \cdot 10^6$
d_{PP1}	$3 \cdot 10^6$	$1 \cdot 10^3$	$3 \cdot 10^5$
d_{UK}	$1 \cdot 10^6$	$5 \cdot 10^6$	$5 \cdot 10^6$
a_{UK}	$1 \cdot 10^4$	$4 \cdot 10^3$	$1 \cdot 10^6$
d_{Mig1}	$2 \cdot 10^{-3}$	$1 \cdot 10^{-6}$	$7 \cdot 10^{-5}$
a_{Mig1}	$2 \cdot 10^{-5}$	$4.7 \cdot 10^{-5}$	$2 \cdot 10^{-5}$
$WB_{s.f.}$ (Exp. C)	0.97	1.08	1
$WB_{s.f.}$ (Exp. D)	0.97	1.39	0.97
UK_{tot}	$1.5 \cdot 10^4$	$1.5 \cdot 10^4$	$1.5 \cdot 10^4$
$PP1_{tot}$	$2.8 \cdot 10^4$	$2.8 \cdot 10^4$	$2.8 \cdot 10^4$
$Snf1_{tot}$	$2 \cdot 10^4$	$2 \cdot 10^4$	$2 \cdot 10^4$
$Mig1_{tot}$	$1.9 \cdot 10^4$	$1.9 \cdot 10^4$	$1.9 \cdot 10^4$

Table A.1.: Overview of the parameters and values used in models Ia), Ib), and Ic). The total numbers of molecules per cell are taken from unpublished data [Garcia Salcedo 2009].

A. Parameters for the *Snf1* models

Parameter	UK const. PP1 regul. Model IIa)	UK regul. PP1 const. Model IIb)	UK regul. PP1 regul. Model IIc)
a_{Snf1}	$1 \cdot 10^3$	$1 \cdot 10^4$	$1 \cdot 10^2$
d_{Snf1}	$6 \cdot 10^3$	$2 \cdot 10^3$	$3 \cdot 10^3$
a_{PP1}	$6 \cdot 10^5$	$3 \cdot 10^5$	$2 \cdot 10^6$
d_{PP1}	$3 \cdot 10^6$	$1 \cdot 10^3$	$3 \cdot 10^5$
d_{UK}	$1 \cdot 10^6$	$5 \cdot 10^6$	$5 \cdot 10^6$
a_{UK}	$1 \cdot 10^4$	$4 \cdot 10^3$	$1 \cdot 10^6$
a_{Snf1^P}	$3 \cdot 10^4$	$1 \cdot 10^4$	$1 \cdot 10^4$
d_{Snf1^P}	$4 \cdot 10^7$	$8 \cdot 10^7$	$6 \cdot 10^6$
d_{Mig1}	$1.7 \cdot 10^{-3}$	$2 \cdot 10^{-6}$	$6 \cdot 10^{-5}$
a_{Mig1}	$2 \cdot 10^{-5}$	$2 \cdot 10^{-5}$	$2 \cdot 10^{-5}$
$WB_{s.f.}$ (Exp. C)	0.97	1.08	1
$WB_{s.f.}$ (Exp. D)	0.97	1.39	0.97
UK_{tot}	$1.5 \cdot 10^4$	$1.5 \cdot 10^4$	$1.5 \cdot 10^4$
$PP1_{tot}$	$2.8 \cdot 10^4$	$2.8 \cdot 10^4$	$2.8 \cdot 10^4$
$Snf1_{tot}$	$2 \cdot 10^4$	$2 \cdot 10^4$	$2 \cdot 10^4$
$Mig1_{tot}$	$1.9 \cdot 10^4$	$1.9 \cdot 10^4$	$1.9 \cdot 10^4$

Table A.2.: Overview of the parameters and values used in the with a two-step *Snf1* regulation (models IIa), IIb), and IIc)). The parameter values for PP1 and UK were taken from models Ia), Ib), and Ic). The total numbers of molecules per cell are taken from unpublished data [Garcia Salcedo 2009].

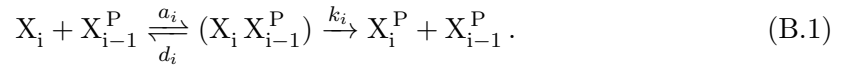
Parameter	UK const. PP1 regul. Model IIIa)	UK regul. PP1 const. Model IIIb)	UK regul. PP1 regul. Model IIIc)
a_{Snf1}	$1 \cdot 10^3$	$1 \cdot 10^4$	$1 \cdot 10^2$
d_{Snf1}	$6 \cdot 10^3$	$2 \cdot 10^3$	$3 \cdot 10^3$
a_{PP1}	$6 \cdot 10^5$	$3 \cdot 10^5$	$2 \cdot 10^6$
d_{PP1}	$3 \cdot 10^6$	$1 \cdot 10^3$	$3 \cdot 10^5$
d_{UK}	$1 \cdot 10^6$	$5 \cdot 10^6$	$5 \cdot 10^6$
a_{UK}	$1 \cdot 10^4$	$4 \cdot 10^3$	$1 \cdot 10^6$
d_{Mig1}	$1.72 \cdot 10^{-3}$	$2 \cdot 10^{-6}$	$6 \cdot 10^{-5}$
a_{Mig1}	$2 \cdot 10^{-5}$	$2 \cdot 10^{-5}$	$2 \cdot 10^{-5}$
k_1	$4 \cdot 10^4$	$2 \cdot 10^3$	$2 \cdot 10^6$
k_2	$4 \cdot 10^6$	0.7	$1 \cdot 10^7$
$WB_{s.f.}$ (Exp. C)	0.97	1.08	1
$WB_{s.f.}$ (Exp. D)	0.97	1.39	0.97
UK_{tot}	$1.5 \cdot 10^4$	$1.5 \cdot 10^4$	$1.5 \cdot 10^4$
$PP1_{tot}$	$2.8 \cdot 10^4$	$2.8 \cdot 10^4$	$2.8 \cdot 10^4$
$Snf1_{tot}$	$2 \cdot 10^4$	$2 \cdot 10^4$	$2 \cdot 10^4$
$Mig1_{tot}$	$1.9 \cdot 10^4$	$1.9 \cdot 10^4$	$1.9 \cdot 10^4$
$Hxk2_{tot}$	$1 \cdot 10^5$	$1 \cdot 10^5$	$1 \cdot 10^5$

Table A.3.: Overview of the parameters and values used in the models IIIa), IIIb), and IIIc). The total numbers of molecules per cell are taken from unpublished data [Garcia Salcedo 2009]. The parameter values for PP1 and UK were taken from models Ia), Ib), and Ic).

B. Models of the MAPK cascade

B.1. Huang and Ferrell

The MAPK cascade model developed by Huang and Ferrell [Huang and Ferrell 1996] (here denoted HF model) analyzes the intrinsic ultrasensitivity of the stimulus response curve of the cascade. It assumes that each activation/deactivation of proteins follows an enzyme kinetic reaction [Segel 1993; Cornish-Bowden 2004]. For a protein X_i and its upstream active kinase X_{i-1}^P , that catalyzes the phosphorylation of X_i to X_i^P , we have



The bimolecular reaction of X_i and X_{i-1}^P results in an intermediary complex $(X_i X_{i-1}^P)$, which can dissociate into the reactants or the activated form X_i^P and the unchanged enzyme X_{i-1}^P . The three involved reactions are determined by rate coefficients: association constant a_i , dissociation constant d_i , and catalytic constant k_i . X_{i-1}^P is assumed to be an ideal catalyst. Furthermore, it is assumed that all other participants, e.g. H_2O , ATP, are constant over the whole observation period, which leads to a formal equivalent reaction scheme as for an enzymatic reaction [Millat *et al.* 2007]. Additionally, there are some conservation laws for proteins and enzymes, see [Huang and Ferrell 1996]. This system of differential equations describes the time course of the proteins and their different activation states as well as the time course of the formed intermediary complexes as shown in the example of complex formed in Reaction (B.1)

$$\frac{d}{dt}(X_i X_{i-1}^P) = a_i (X_i) (X_{i-1}^P) - \{d_i + k_i\} (X_i X_{i-1}^P).$$

Note that there is an additional equation for the time-dependent stimulus in comparison to the original system in [Huang and Ferrell 1996] where the stimulus is a constant external parameter. The term $(X_i X_{i-1}^P)$ denotes a complex. Note that for our investigation, we introduce an additional equation for the time-dependent stimulus

$$X_0(t) = \mathcal{X}_0 e^{-\lambda t} \quad (\text{B.2})$$

in comparison to the original system in [Huang and Ferrell 1996], where the stimulus is a constant external parameter. This equation describes the receptor deactivation as a consequence of a pulse-like stimulus. For the sake of simplicity we choose a simple

B. Models of the MAPK cascade

monomolecular deactivation mechanism. We assume a receptor concentration of \mathcal{X}_0 at initial time $t_0 = 0$. This assumption guarantees that the final signal of the phosphorylated protein approaches zero for $t \rightarrow \infty$, as required for calculating the quantitative measures.

B.2. Kholodenko

Also in the MAPK model by Kholodenko [Kholodenko 2000], all involved biochemical reactions follow the enzyme kinetic reaction of Eq. (B.1). Again we use the quasi-steady-state approximation to simplify the system of coupled differential equations. In contrast to the above discussed models, the conservation law for the proteins is used to express the level of upstream kinases. Due to this explicit transformation, the model is a simplification of the Hg model (see Eq. (4.1)) [Millat *et al.* 2007]. The resulting rate equation for activation/deactivation of a protein

$$\frac{d}{dt}X_i^P = \frac{k_i X_{i-1}^P X_i}{K_M + X_i} - \frac{V_i X_i^P}{K_M + X_i^P} \quad (\text{B.3})$$

contains two Michaelis-Menten like expressions and is similar to the result of Goldbeter and Koshland [Goldbeter and Koshland, Jr. 1981]. The limiting rate V_i results again from the assumption of a constant phosphatase concentration. Note that neglecting the complex concentration within the model is crucial [Blüthgen *et al.* 2006; Millat *et al.* 2007]. The structure of the used differential equations and the required kinetic parameters and their relation to the mechanistic constants are summarised in Table 4.1.

B.3. Heinrich et al.

The mechanistic model can be simplified if one assumes that the intermediate complexes operate at a quasi-steady state. This assumption converts the differential equation of the complexes into an algebraic equation, e.g.

$$0 = a_i X_i X_{i-1}^P - \{d_i + k_i\} (X_i X_{i-1}^P), \quad (\text{B.4})$$

which can be transformed with respect to the complex concentration ($X_i X_{i-1}^P$). Insertion into the enzyme kinetic reaction reduces it formally to a bimolecular reaction [Millat *et al.* 2007]. If one further assumes a constant phosphatase concentration, the dephosphorylation reaction further reduces to a pseudo-monomolecular reaction [Millat *et al.* 2007]. The change of concentration of a protein can then be described by the differential equation

$$\frac{d}{dt}X_i^P = \tilde{\alpha}_i X_i X_{i-1}^P - \beta_i X_i^P \quad (\text{B.5})$$

as introduced before in the main text as Eq. 4.1, where $\tilde{\alpha}_i = \alpha_i/X_i^{\text{tot}}$ and X_i^{tot} denotes the total concentration of protein X_i [Heinrich *et al.* 2002]. The rate equation Eq. (4.1) can

B.4. Relation between the kinetic parameters

be further simplified if we apply the conservation laws for the proteins and additionally assume that the concentration of intermediate complexes is negligible with respect to the concentration of proteins, which are not bound in a complex. Then, the conservation law reduces to a simple relation between the protein concentrations

$$X_i^{\text{tot}} = X_i + X_i^{\text{P}}. \quad (\text{B.6})$$

Insertion into Eq. (4.1) leads to the Hg model [Heinrich *et al.* 2002]

$$\frac{d}{dt}X_i^{\text{P}} = \alpha_i X_{i-1}^{\text{P}} \left\{ 1 - \frac{X_i^{\text{P}}}{X_i^{\text{tot}}} \right\} - \beta_i X_i^{\text{P}}. \quad (\text{B.7})$$

Applying the quantitative measures of signal properties (Defs. (4.2), (4.3), and (4.4)) introduced in Chapter 4, shows that a change in X_i^{tot} does not change the values of signalling time τ and signal duration ϑ but the signal strength S . Since X_i^{tot} is the sum of phosphorylated and non-phosphorylated form of protein X_i , it cancels out in the definitions for signalling time (4.2) and signal duration (4.3). The signal strength (4.4), on the other hand depends on the total concentration. This means that signalling time as well as signal duration of a cascade, as in Figure (1.2), do not depend on the total concentrations of the involved proteins. Nevertheless, the choice of the rate constants and a ratio of the initial (receptor) concentration X_0^{tot} to the more downstream elements of the cascade X_i^{tot} affect these quantitative measures as shown in Chapter 5.

The definitions of signalling time τ , signal duration ϑ , signal amplitude S and related quantities depend on the existence of the involved definite integrals. This condition restricts the approach to a special class of dynamic signals. At initial time $t = 0$, all concentrations have to be finite, which is not a serious problem because it is fulfilled automatically by biological systems. A cell cannot produce an infinite amount of molecules resulting in an infinite concentration. (Additionally, the cellular volume cannot be zero.) Since the upper limit of integration is set to infinity it is required for the calculability of the integral that all considered signals tend to zero. The definition of the signal duration, Def. (4.3), further enforces the following requirement. An involved integral is proportional to t^2 . Consequently, the investigated signal X_n^{P} has to decrease faster than t^{-2} for $t \rightarrow \infty$. This restriction excludes signals that tend to a steady state or produce stable oscillations. Also, the inactive protein forms of the MAPK cascade, see left picture of Figure 1.2, cannot be investigated using the introduced approach. However, this framework can be generalised using a similar approach as in [Llorens *et al.* 1999].

B.4. Relation between the kinetic parameters

So far we introduced three models [Huang and Ferrell 1996; Kholodenko 2000; Heinrich *et al.* 2002] and explained their structure and main assumptions. In our analysis, we

B. Models of the MAPK cascade

examined cascades with identical cycles only. This assumption was made for reducing the number of parameters in order to keep the model clearly arranged. An important part of the models, which we have not yet discussed is: their different kinetic parameter sets. For a systematic comparison of the behavior of the models it is required to relate the rate constants. We derive the kinetic parameters of the models and show that the parameters of the simplified models can be related to the mechanistic kinetic parameters. The starting point is again the HF model. In this model the activation and deactivation of a protein X_i is determined by the association constant a_i , the dissociation constant d_i , and the catalytic constant k_i . Due to the quasi-steady state assumption in the Heinrich model, we obtain new kinetic parameters, which contain a combination of the mechanistic parameters of the HF model. The activation is determined by the rate constant α_i , which follows from the balance equation (B.4) as

$$\alpha_i = \frac{k_i}{K_M^i}. \quad (\text{B.8})$$

Due to the assumed constant phosphatase, the rate constant of deactivation β_i is an effective rate constant [Atkins and de Paula 2002; Millat *et al.* 2007]

$$\beta_i = P \frac{k_i}{K_M^i}, \quad (\text{B.9})$$

which is the product of the concentration P of the phosphatase and the mechanistic rate constants. Both rate constants are ratios of the corresponding catalytic constant k_i and the Michaelis constant

$$K_M^i = \frac{d_i + k_i}{a_i}. \quad (\text{B.10})$$

The Kholodenko model contains the limiting rate V_i , which is defined as usual as

$$V_i = k_i P \quad (\text{B.11})$$

where P again is the phosphatase concentration.

By applying these equations the kinetic parameters of the different models are related to each other. If one defines a set of mechanistic parameters a_i , d_i , and k_i the parameters of the Heinrich model and the Kholodenko model are uniquely defined. Note that this is not reversible [Millat *et al.* 2007]. Due to the generated relation between the parameters we are now able to investigate the models' behavior as done for the analysis shown in Section 5. For practical purposes, we have to introduce further restrictions for these models. Since the kinetic parameters are determined by physical constraints, e.g. the atomic configuration of the molecules, temperature or pH-value, each rate coefficient is unique. The parameters span an m -dimensional parameter space. This space is further increased by the total protein concentrations, including signalling proteins, kinases, and phosphatases, and the initial concentrations. A parameter space of this dimension is

intractable for a systematical investigation of the behavior of MAPK cascades, especially if one investigates different structural configurations. Therefore, we have to reduce the dimension. We realise this by using cascades composed of identical activation/deactivation cycles. Furthermore we assume that the coefficients of the deactivation are multiples of the kinetic coefficients of the activation. This means that we have to consider the three rate coefficients of the activation and a constant factor, which determines the coefficients of the deactivation. Furthermore, we use the same total concentration for all involved proteins, except if declared other. Last but not least, we assume that at $t = 0$ all proteins are inactive or non-phosphorylated.

B.5. Properties of the external stimulus

The quantitative measures for the exponential input function can be derived as shown in Heinrich *et al.* [Heinrich *et al.* 2002]:

$$X_0(t) = \mathcal{X}_0 e^{-\lambda t} \quad (\text{B.12})$$

for modeling the external stimulus. \mathcal{X}_0 denotes the initial state at $t = 0$ and λ the inverse time constant. For such a signal, the characteristic quantities can be calculated analytically. The total amount is then simply

$$\begin{aligned} \int_0^\infty X_0 dt &= \int_0^\infty \mathcal{X}_0 e^{-\lambda t} dt \\ &= -\frac{\mathcal{X}_0}{\lambda} \left[e^{-\lambda t} \right]_0^\infty \\ &= \frac{\mathcal{X}_0}{\lambda}. \end{aligned} \quad (\text{B.13})$$

The integral in the nominator of Def. (4.2) can be solved by partial integration

$$\begin{aligned} \int_0^\infty t X_0 dt &= \mathcal{X}_0 \int_0^\infty t e^{-\lambda t} dt \\ &= -\frac{\mathcal{X}_0}{\lambda} \left[t e^{-\lambda t} \right]_0^\infty + \frac{\mathcal{X}_0}{\lambda} \int_0^\infty e^{-\lambda t} dt \\ &= -\frac{\mathcal{X}_0}{\lambda^2} \left[e^{-\lambda t} \right]_0^\infty \\ &= \frac{\mathcal{X}_0}{\lambda^2}. \end{aligned} \quad (\text{B.14})$$

B. Models of the MAPK cascade

Also by partial integration the last remaining integral is solved

$$\begin{aligned}
\int_0^\infty t^2 X_0 dt &= \mathcal{X}_0 \int_0^\infty t^2 e^{-\lambda t} dt \\
&= -\frac{\mathcal{X}_0}{\lambda} \left[t^2 e^{-\lambda t} \right]_0^\infty + \frac{2\mathcal{X}_0}{\lambda} \int_0^\infty t e^{-\lambda t} dt \\
&= \frac{2\mathcal{X}_0}{\lambda} \int_0^\infty t e^{-\lambda t} dt \\
&= -\frac{2\mathcal{X}_0}{\lambda^2} \left(\left[t e^{-\lambda t} \right]_0^\infty + \int_0^\infty e^{-\lambda t} dt \right) \\
&= -\frac{2\mathcal{X}_0}{\lambda^3} \left[e^{-\lambda t} \right]_0^\infty \\
&= \frac{2\mathcal{X}_0}{\lambda^3}.
\end{aligned} \tag{B.15}$$

With these results we then can calculate the characteristic quantities for the external stimulus. Following from Def. (4.2) the signaling time is

$$\tau_0 = \frac{\mathcal{X}_0 \int_0^\infty t e^{-\lambda t} dt}{\mathcal{X}_0 \int_0^\infty e^{-\lambda t} dt} = \frac{\mathcal{X}_0}{\lambda^2} \frac{\lambda}{\mathcal{X}_0} = \frac{1}{\lambda}. \tag{B.16}$$

From Def. (4.3) follows

$$\begin{aligned}
\vartheta_0 &= \sqrt{\frac{\mathcal{X}_0 \int_0^\infty t^2 e^{-\lambda t} dt}{\mathcal{X}_0 \int_0^\infty e^{-\lambda t} dt} - \tau_0^2} \\
&= \sqrt{\frac{2\mathcal{X}_0}{\lambda^3} \frac{\lambda}{\mathcal{X}_0} - \frac{1}{\lambda^2}} = \frac{1}{\lambda}
\end{aligned} \tag{B.17}$$

for the signal duration. Finally, we obtain from Def. (4.4)

$$S_0 = \frac{\mathcal{X}_0 \int_0^\infty e^{-\lambda t} dt}{2\vartheta_0} = \frac{\mathcal{X}_0}{\lambda} \frac{\lambda}{2} = \frac{\mathcal{X}_0}{2} \tag{B.18}$$

for the signal strength. Whereas signaling time and signal duration are determined only by the inverse characteristic time λ , the averaged signal amplitude depends on the initial concentration \mathcal{X}_0 only.

Bibliography

- D. Ahuatzi, A. Riera, R. Peláez, Herrero P., and F. Moreno. Hxk2 regulates the phosphorylation state of mig1 and therefore its nucleocytoplasmic distribution. *J Biol Chem*, 282(7):4485–4493, February 2007.
- B. Alberts, A. Johnson, J. Lewis, M. Raff, K. Roberts, and P. Walter. *Molecular Biology of the Cell*. Garland Science, 4th edition, 2002.
- D.R. Alessi, Y. Saito, D.G. Campbell, P. Cohen, G. Sithanandam, U. Rapp, A. Ashworth, C.J. Marshall, and S. Cowley. Identification of the sites in MAP kinase kinase-1 phosphorylated by p74raf-1. *EMBO J*, 13:1610–1619, 1994.
- N.G. Anderson, J.L. Maller, N.K. Tonks, and T.W. Sturgill. Requirement for integration of signals from two distinct phosphorylation pathways for activation of MAP kinase. *Nature*, 343(6259):651–653, February 1990.
- A.R. Asthagiri and D.A. Lauffenburger. Bioengineering models of cell signaling. *Annu Re. Biomed Eng*, 2:31–53, 2000.
- P.W. Atkins and J. de Paula. *Atkins' Physical Chemistry*. Oxford University Press, 7th edition, 2002.
- J. Avruch. MAP kinase pathways: The first twenty years. *BBA-Mol Cell Res*, 1773(8): 1150–1160, August 2007.
- E. Balsa-Canto, A. Alonso, and J. Banga. An iterative identification procedure for dynamic modeling of biochemical networks. *BMC Syst Biol*, 4(1):11, February 2010.
- L. Bardwell. A walk-through of the yeast mating pheromone response pathway. *Peptides*, 26(2):339–350, February 2005.
- J.U. Becker and A. Betz. Membrane transport as controlling pacemaker of glycolysis in *Saccharomyces cerevisiae*. *Biochim Biophys Acta*, 274:584–597, 1972.
- Z.H. Beg, D.W. Allmann, and D.M. Gibson. Modulation of 3-hydroxy-3-methylglutaryl coenzyme: a reductase activity with cAMP and with protein fractions of rat liver cytosol. *Biochem Biophys Res Co*, 54:1362–1369, 1973.

Bibliography

- M. Behar, N. Hao, H.G. Dohlman, and T.C. Elston. Dose-to-Duration Encoding and Signaling beyond Saturation in Intracellular Signaling Networks. *PLoS Comput Biol*, 4(10):e1000197, October 2008.
- M. Bertilsson, J. Andersson, and G. Liden. Modeling simultaneous glucose and xylose uptake in *Saccharomyces cerevisiae* from kinetics and gene expression of sugar transporters. *Bioprocess Biosyst Eng*, 31:369–377, 2008.
- B. Binder and R. Heinrich. Interrelations between Dynamical Properties and Structural Characteristics of Signal Transduction Networks. *Genome Inform*, 15(1):13–23, January 2004.
- L. Bisson and V. Kunathigan. On the trail of an elusive flux sensor. *Res Microbiol*, 154:603–610, 2003.
- L. Bisson, D.M. Coons, A.L. Kruckeberg, and D.A. Lewis. Yeast Sugar Transporters. *Crit Rev Biochem Mol*, 28:259–308, 1993.
- L.F. Bisson and D.G. Fraenkel. Involvement of kinases in glucose and fructose uptake by *Saccharomyces cerevisiae*. *PNAS*, 80(6):1730–1734, March 1983.
- L.F. Bisson and D.G. Fraenkel. Expression of kinase-dependent uptake in *Saccharomyces cerevisiae*. *J Bacteriol*, 159:1013–1017, 1984.
- N. Blüthgen. Private communication, 2007.
- N. Blüthgen, F.J. Bruggemann, S. Legewie, H. Herzel, H.V. Westerhoff, and B.N. Kholodenko. Effects of sequestration on signal transduction cascades. *FEBS J*, 273(5):895–906, March 2006.
- E. Boles and C.P. Hollenberg. The molecular genetics of hexose transport in yeasts. *FEMS Microbiol Rev*, 21:85–111, 1997.
- J.B. Boudeau, A.F. Baas, M. Deak, N.A. Moorice, A. Kieloch, M. Schutkowski, A.R. Prescott, H.C. Clevers, and D.A. Alessi. MO25 α/β interacts with STRAD α/β enhancing their ability to bind, activate and localize LKB1 in the cytoplasm. *EMBO J*, 22(19):5102–5114, 2003.
- R. Bracewell. *The Fourier Transform and Its Applications*. McGraw Hill, New York, 3rd edition, 1999.
- C. Cantó and J. Auwerx. AMP-activated protein kinase and its downstream transcriptional. *Cell Mol Life Sci*, July 2010.

- D. Carling. The AMP-activated protein kinase cascade – a unifying system for energy control. *Trends Biochem Sci*, 29(1):18–24, January 2004.
- D. Carling and D.G. Hardie. The substrate and sequence specificity of the AMP-activated protein kinase. Phosphorylation of glycogen synthase and phosphorylase kinase. *BBA-Mol Cell Res*, 1012(1):81–86, June 1989.
- D. Carling, K. Aguan, A. Woods, A.J.M. Verhoeven, R.K. Beri, C.H. Brennan, C. Sidebottom, M.D. Davison, and J. Scott. Mammalian AMP-activated protein kinase is homologous to yeast and plant protein kinases involved in the regulation of carbon metabolism. *J Biol Chem*, 269(15):11442–11448, April 1994.
- C.A. Carlson and K.-H. Kim. Regulation of hepatic acetyl coenzyme a carboxylase by phosphorylation and dephosphorylation. *Arch Biochem Biophys*, 163:478–489, 1974.
- M. Carlson. Glucose repression in yeast. *Curr Opin Microbiol*, 2(2):202–207, April 1999.
- M. Carlson, B.C. Osmond, and D. Botstein. Mutants of yeast defective in sucrose utilization. *Genetics*, 98(1):25–40, 25 1981.
- M. Carlson, B.C. Osmond, L. Neigeborn, and D. Botstein. A suppressor of SNF1 mutations causes constitutive high-level invertase synthesis in yeast. *Genetics*, 107:19–32, May 1984.
- J.L. Celenza and M. Carlson. A yeast gene that is essential for release from glucose repression encodes a protein kinase. *Science*, 233(4769):1175 – 1180, September 1986.
- J.L. Celenza and M. Carlson. Mutational analysis of the *Saccharomyces cerevisiae* SNF1 protein kinase and evidence for functional interaction with the SNF4 protein. *Mol Cell Biol*, 9(11):5034–5044, November 1989.
- J.L. Celenza, F.J. Eng, and Carlson. Molecular Analysis of the SNF4 Gene of *Saccharomyces cerevisiae*: Evidence for physical association of the SNF4 protein with the SNF1 protein kinase. *Mol Cell Biol*, 9(11):5045–5054, November 1989.
- M. Chaves, E.D. Sontag, and R.J. Dinerstein. Optimal Length and Signal Amplification in Weakly Activated Signal Transduction Cascades. *J Phys Chem*, 108:15311–15320, 2004.
- R.E. Chen and J. Thorner. Function and Regulation in MAPK Signaling Pathways: Lessons Learned from the Yeast *Saccharomyces cerevisiae*. *Biochim Biophys Acta*, 1773(8):1311–1340, 2007.
- A. Cornish-Bowden. *Fundamentals of Enzyme Kinetics*. Portland Press, 3rd edition, 2004.

Bibliography

- J.M. Corton, J.G. Gillespie, and D. Hardie. Role of the AMP-activated protein kinase in the cellular stress response. *Curr Biol*, 4(4):315–324, 1994.
- S.P. Davies, S.A. Hawley, A. Woods, D. Carling, T.A.J. Haystead, and D.G. Hardie. Purification of the AMP-activated protein kinase on ATP- γ -Sephadrose and analysis of its subunit structure. *FEBS J*, 223(2):351–357, July 1994.
- H. de Jong. Modeling and Simulation of Genetic Regulatory Systems: A Literature Review. *J Comput Biol*, 9(1):67–103, 2002.
- V. De Wever, W. Reiter, A. Ballarini, G. Ammerer, and C. Brocard. A dual role for PP1 in shaping the Msn2-dependent transcriptional response to glucose starvation. *EMBO J*, 24(23):4115–4123, 2005.
- M.J. DeVit and M. Johnston. The nuclear exportin Msn5 is required for nuclear export of the Mig1 glucose repressor of *Saccharomyces cerevisiae*. *Curr Biol*, 9(21):1231–1241, 1999.
- M.J. DeVit, J.A. Waddle, and M. Johnston. Regulated Nuclear Translocation of the Mig1 Glucose Repressor. *Mol Biol Cell*, 8:1603–1618, August 1997.
- A.S. Dhillon, S. Hagan, O. Rath, and W. Kolch. MAP kinase signalling pathways in cancer. *Oncogene*, 26:3279–3290, 2007.
- J.A. Diderich, M. Schepper, P. van Hoek, M.A.H. Luttik, J.P. van Dijken, J.T. Pronk, P. Klaassen, H.F.M. Boelens, M.J. Teixeira de Mattos, K. van Dam, and A.L. Kruckeberg. Glucose uptake kinetics and transcription of hxt genes in chemostat cultures of *saccharomyces cerevisiae*. *J Biol Chem*, 274:15350–15359, 1999.
- J.A. Diderich, J.M. Schuurmans, M.C. van Gaalen, A.L. Kruckeberg, and K. van Dam. Functional analysis of the hexose transporter homologue HXT5 in *Saccharomyces cerevisiae*. *Yeast*, 18:1515–1524, 2001.
- M.K. Dougherty, J. Müller, D.A. Ritt, M. Zhou, X.Z. Zhou, T.D. Copeland, T.P. Conrads, T.D. Veenstra, K.P. Lu, and D.K. Morrison. Regulation of Raf-1 by Direct Feedback Phosphorylation. *Mol Cell*, 17:215–224, January 2005.
- J. Downward. The ins and outs of signalling. *Nature*, 411(6839):759–762, June 2001.
- J.S. Easterby. Coupled enzyme assays: a general expression for the transient. *Biochim Biophys Acta*, 293(2):552–558, February 1973.
- J.S. Easterby. A generalized theory of the transition time for sequential enzyme reactions. *Biochem J*, 199(1):155–161, October 1981.

- J.S. Easterby. The effect of feedback on pathway transient response. *Biochem J*, 233(3): 871–875, February 1986.
- K. Elbing, E.M. Rubenstein, R.R. McCartney, and M.C. Schmidt. Subunits of the Snf1 kinase heterotrimer show interdependence for association and activity. *J Biol Chem*, 281(36):26170–26180, September 2006.
- W.H. Elliott and D.C. Elliott. *Biochemistry and Molecular Biology*. Oxford Univ Press, third edition, 2005.
- J. English, G. Pearson, J. Wilsbacher, J. Swantek, M. Karandikar, S. Xu, and M.H. Cobb. New Insights into the Control of MAP Kinase Pathways. *Exp Cell Res*, 253(1):255–270, November 1999.
- J.R. Erickson and M. Johnston. Genetic and Molecular Characterization of GAL83: Its Interaction and Similarities With Other Genes Involved in Glucose Repression in *Saccharomyces cerevisiae*. *Genetics*, 135:655–664, November 1993.
- E. Eriksson. *Towards quantitative single cell analysis using optical tweezers and microfluidics*. PhD thesis, University of Gothenburg, 2009.
- E. Eriksson, K. Sott, F. Lundqvist, M. Sveningsson, J. Scrimgeour, D. Hanstorp, M. Goksör, and A. Graneli. A microfluidic device for reversible environmental changes around single cells using optical tweezers for cell selection and positioning. *Lab on a Chip*, 10:617–625, 2010.
- J.E. Ferrell, Jr. and E.M. Machleder. The Biochemical Basis of an All-or-None Cell Fate Switch in *Xenopus* Oocytes. *Science*, 280:895–898, May 1998.
- J.E. Ferrell Jr. Tripping the switch fantastic: how a protein kinase cascade can convert graded inputs into switch-like outputs. *TIBS*, 21(12):460–466, December 1996.
- E.H. Flach and S. Schnell. Use and abuse of the quasi-steady-state approximation. *IEE Proc Syst Biol*, 153(4):187–191, July 2006. ISSN 1741-2471.
- K.M. Flick, N. Spielwoy, T. I. Kalashnikova, M. Guaderrama, Q. Zhu, H.-C. Chang, and C. Wittenberg. Grr1-dependent inactivation of Mth1 mediates glucose-induced dissociation of Rgt1 from HXT gene promoters. *Mol Biol Cell*, 14(8):3230–3241, 2003.
- S. Fogarty and D.G. Hardie. Development of protein kinase activators: AMPK as a target in metabolic disorders and cancer. *Biochim Biophys Acta*, 1804(3):581–591, 2010.
- S. Frey, T. Millat, S. Hohmann, and O. Wolkenhauer. How quantitative measures unravel design principles in multi-stage phosphorylation cascades. *J Theor Biol*, 254(1):27–36, September 2008.

Bibliography

- S. Frey, O. Wolkenhauer, and T. Millat. *Control Theory and Systems Biology*, chapter Quantifying properties of cell signaling cascades, pages 69–84. MIT press, 2009.
- S. Frey, T. Millat, R. Garcia Salcedo, D. Bosch, G. Beltran, K. Elbing, G.N. Vemuri, S. Hohmann, and O. Wolkenhauer. Dynamics of hexose transporters in *Saccharomyces cerevisiae* upon glucose pulses. *submitted*, 2011a.
- S. Frey, K. Sott, M. Smedh, T. Millat, P. Dahl, O. Wolkenhauer, and M. Goksör. A mathematical analysis of nuclear intensity dynamics for Mig1-GFP under consideration of bleaching effects and background noise in *Saccharomyces cerevisiae*. *Mol BioSystems*, 7:215–223, 2011b.
- G.F. Fuhrmann, C. Boehm, and A.P.R. Theuvenet. Sugar transport and potassium permeability in yeast plasma membrane vesicles. *BBA-Biomembranes*, 433(3):583–396, 1976.
- A. Fujioka, K. Terai, R.E. Itoh, K. Aoki, T. Nakamura, S. Kuroda, E. Nishida, and M. Matsuda. Dynamics of the Ras/ERK MAPK Cascade as Monitored by Fluorescent Probes. *J Biol Chem*, 281(13):89178926, March 2006.
- A. Funahashi, M. Morohashi, and H. Kitano. CellDesigner: A process diagram editor for gene-regulatory and biochemical networks. *Biosilico*, 1(5):159–162, 2003.
- A. Funahashi, Y. Matsuoka, A. Jouraku, M. Morohashi, N. Kikuchi, and H. Kitano. CellDesigner 3.5: A Versatile Modeling Tool for Biochemical Networks. *Proceedings of the IEEE*, 96(8):1254–1265, 2008.
- J.M. Gancedo. Yeast carbon catabolite repression. *Microbiol Mol Biol R*, 62(2):334–361, June 1998.
- J.M. Gancedo. The early steps of glucose signalling in yeast. *FEMS Microbiol Rev*, 32: 673–704, 2008.
- R. Garcia Salcedo. Private communication, 2009.
- H. Gehart, S. Kumpf, A. Ittner, and R. Ricci. MAPK signalling in cellular metabolism: stress or wellness? *EMBO Rep*, 11(11):834–840, November 2010. ISSN 1469-221X.
- A. Goldbeter and D.E. Koshland, Jr. An amplified sensitivity arising from covalent modification in biological systems. *PNAS*, 78(11):6840–6844, November 1981.
- B.W. Greatrix and H.J.J. van Vuuren. Expression of the HXT13, HXT15 and HXT17 genes in *Saccharomyces cerevisiae* and stabilization of the HXT1 gene transcript by sugar-induced osmotic stress. *Curr Genet*, 49:205–217, 2006.

- A. Gruzman, G. Babai, and S. Sasson. Adenosine Monophosphate-Activated Protein Kinase (AMPK) as a New Target for Antidiabetic Drugs: A Review on Metabolic, Pharmacological and Chemical Considerations. *Rev Diabetic Stud*, 6:13–36, 2009.
- D.M. Gwinn, D.B. Shackelford, D.F. Egan, M.M. Mihaylova, A. Mery, D.S. Vasquez, B.E. Turk, and R.J. Shaw. AMPK phosphorylation of raptor mediates a metabolic checkpoint. *Mol Cell*, 30(2):214–226, April 2008.
- S.R. Hamilton, J.B. O'Donnell Jr., A. Hammet, D. Stapleton, S.A. Habinowski, A.R. Means, B.E. Kemp, and L.A. Witters. AMP-activated protein kinase kinase: detection with recombinant AMPK α 1 subunit. *Biochem Bioph Res Co*, 293:892–898, 2002.
- J.T. Hancock. *Cell Signalling*. Oxford Univ Press, third edition, 2010.
- D.G. Hardie. AMP-activated/SNF1 protein kinases: conserved guardians of cellular energy. *Nat Rev Mol Cell Biol*, 8:774–785, 2007.
- D.G. Hardie and D.A. Pan. Regulation of fatty acid synthesis and oxidation by the AMP-activated protein kinase. *Biochem Soc T*, 30:1064–1070, 2002.
- D.G. Hardie, J.W. Scott, D.A. Pan, and E.R. Hudson. Management of cellular energy by the AMP-activated protein kinase system. *FEBS Lett*, 546:113–120, 2003.
- S.A. Hawley, M. Davison, A. Woods, S.P. Davies, R.K. Beri, D. Carling, and D.G. Hardie. Characterization of the AMP-activated Protein Kinase Kinase from Rat Liver and Identification of Threonine 172 as the Major Site at Which It Phosphorylates AMP-activated Protein Kinase. *J Biol Chem*, 271(44):27879–27887, November 1996.
- S.A. Hawley, J. Boudeau, J.L. Reid, K.J. Mustard, L. Udd, T.P. Mäkelä, D.R. Alessi, and D.G. Hardie. Complexes between the LKB1 tumor suppressor, STRAD α/β and MO25 α/β are upstream kinases in the AMP-activated protein kinase cascade. *J Biol*, 2, 2003.
- S.A. Hawley, D.A. Pan, K.J. Mustard, L. Ross, J. Bain, A.M. Edelman, B.G. Frenuelli, and D.G. Hardie. Calmodulin-dependent protein kinase kinase- β is an alternative upstream kinase for AMP-activated protein kinase. *Cell Met*, 2:9–19, July 2005.
- K. Hedbacker and M. Carlson. SNF1/AMPK pathways in yeast. *Front Bioscience*, 13: 2408–2420, January 2008.
- R. Heinrich and T.A. Rapoport. Mathematical Analysis of multienzyme systems. II. Steady-state and transient control. *BioSystems*, 7:130–136, 1975.
- R. Heinrich, B.G. Neel, and T.A. Rapoport. Mathematical Models of Protein Kinase Signal Transduction. *Mol Cell*, 9(5):957–970, May 2002.

Bibliography

- B.F. Holmes, E.J. Kurth-Kraczek, and W.W. Winder. Chronic activation of 5'-AMP-activated protein kinase increases GLUT-4, hexokinase, and glycogen in muscle. *J Appl Physiol*, 87(5):1990–1995, November 1999.
- S.-P. Hong and M. Carlson. Regulation of Snf1 protein kinase in response to environmental stress. *J Biol Chem*, 282(23):16838–16845, June 2007.
- S.-P. Hong, F.C. Leiper, A. Woods, D. Carling, and M. Carlson. Activation of yeast Snf1 and mammalian AMP-activated protein kinase by upstream kinases. *PNAS*, 100(15):8839–8843, July 2003.
- S.-P. Hong, M. Momcilovic, and M. Carlson. Function of Mammalian LKB1 and Ca^{2+} /Calmodulin-dependent Protein Kinase Kinase α as Snf1-activating Kinases in Yeast. *J Biol Chem*, 280:21804–21809, 2005.
- W. Hoppe, W. Lohmann, H. Markl, and H. Ziegler, editors. *Biophysics*. Springer Verlag, New York, 1983.
- S. Horman, G.J. Browne, U. Krause, J.V. Patel, D. Vertommen, L. Bertrand, A. Lavoinne, L. Hue, C.G. Proud, and M.H. Rider. Activation of AMP-activated protein kinase leads to the phosphorylation of elongation factor 2 and an inhibition of protein synthesis. *Curr Biol*, 12(16):1419–1423, August 2002.
- C.-Y.F. Huang and J.E. Ferrell, Jr. Ultrasensitivity in the mitogen-activated protein kinase cascade. *PNAS*, 93(19):10078–10083, September 1996.
- X. Huang, S. Wulschleger, N. Shpiro, V.A. McGuire, K. Sakamoto, Y.L. Woods, McBurnie W., S. Fleming, and D.R. Alessi. Important role of the LKB1-AMPK pathway in suppressing tumorigenesis in PTEN-deficient mice. *Biochem J*, 412:211–221, 2008.
- R.L. Hurley, K.A. Anderson, J.M. Franzone, B.E. Kemp, A.R. Means, and L.A. Witters. The Ca^{2+} /Calmodulin-dependent protein kinase kinases are AMP-activated protein kinase kinases. *J Biol Chem*, 280:29060–29066, 2005.
- F. Hynne, S. Dan, and P.G. Srensen. Full-scale model of glycolysis in *Saccharomyces cerevisiae*. *Biophys Chem*, 94:121–163, September 2001.
- T. Ideker, T. Galitski, and L. Hood. A New Approach to Decoding Life: Systems Biology. *Annu Rev Genomics Hum Genet*, 2:343–372, 2001.
- K. Inoki, T. Zhu, and K.L. Guan. TSC2 mediates cellular energy response to control cell growth and survival. *Cell*, 115(5):577–590, November 2003.

- S. Ishii, K. Tago, and K. Senoo. Single-cell analysis and isolation for microbiology and biotechnology: methods and applications. *Appl Microbiol Biotechnol*, 86(5):1281–1292, May 2010.
- S.N. Jakobsen, D.G. Hardie, N. Morrice, and H.E. Tornqvist. 5-AMP-activated protein kinase phosphorylates IRS-1 on Ser-789 in mouse C2C12 myotubes in response to 5-Aminoimidazole-4-carboxamide riboside. *J Biol Chem*, 276(50):46912–46916, December 2001.
- R. Jiang and M. Carlson. Glucose regulates protein interactions within the yeast SNF1 protein kinase complex. *Genes Dev*, 10:3105–3115, 1996.
- R. Jiang and M. Carlson. The Snf1 protein kinase and its activating subunit, Snf4, interact with distinct domains of the Sip1/Sip2/Gal83 component in the kinase complex. *Mol Cell Biol*, 17(4):2099–2106, April 1997.
- C. Jin, A. Barrientos, C.B. Epstein, Butow R.A., and A. Tzagoloff. SIT4 regulation of Mig1p-mediated catabolite repression in *Saccharomyces cerevisiae*. *FEBS Lett*, 581(29):5658–5663, December 2007.
- M. Johnston. Feasting, fasting and fermenting: glucose sensing in yeast and other cells. *Trends Genet*, 15(1):29–33, January 1999.
- M. Johnston and J.-H. Kim. Glucose as a hormone: receptor-mediated glucose sensing in the yeast *saccharomyces cerevisiae*. *Biochem Soc T*, 33:247–252, 2005.
- S.B. Jørgensen, J.N. Nielsen, J.B. Birk, G.S. Olsen, B. Viollet, F. Andreelli, P. Schjerling, S. Vaulont, D.G. Hardie, B.F. Hansen, E.A. Richter, and J.F.P. Wojtaszewski. The α 25⁺AMP-Activated Protein Kinase Is a Site 2 Glycogen Synthase Kinase in Skeletal Muscle and Is Responsive to Glucose Loading. *Diabetes*, 53(12):3074–3081, December 2004.
- T. Kalisky, E. Dekel, and U. Alon. Cost-benefit theory and optimal design of gene regulation functions. *Phys Biol*, 4:229–245, 2007.
- B.N. Kholodenko. Negative feedback and ultrasensitivity can bring about oscillations in the mitogen-activated protein kinase cascades. *Eur J Biochem*, 267(6):1583–1588, 2000.
- B.N. Kholodenko. Cell-signalling dynamics in time and space. *Nat Rev Mol Cell Biol*, 7(3):165–176, March 2006.
- B.N. Kholodenko, J.F. Hancock, and W. Kolch. Signalling ballet in space and time. *Nat Rev Mol Cell Biol*, 11:414–426, 2010.

Bibliography

- J-H. Kim, J. Polish, and M. Johnston. Specificity and Regulation of DNA Binding by the Yeast Glucose Transporter Gene Repressor Rgt1. *Mol Cell Biol*, 23(15):5208–5216, August 2003.
- H. Kitano. Computational systems biology. *Nature*, 420(6912):206–210, November 2002. ISSN 0028-0836.
- C.J.L. Klein, L. Olsson, and J. Nielsen. Glucose control in *Saccharomyces cerevisiae*: the role of MIG1 in metabolic functions. *Microbiology*, 144:13–24, 1998.
- E. Klipp. Timing matters. *FEBS Lett*, 583(24):4013–4018, December 2009. ISSN 0014-5793.
- P. Kohl, E.J. Crampin, T.A. Quinn, and D. Noble. Systems biology: an approach. *Clin Pharmacol Ther*, 88(1):25–33, 2010.
- B. Kola, A.B. Grossman, and M. Korbonsits. The role of AMP-activated protein kinase in obesity. *Front Horm Res*, 36:198–211, 2008.
- A.L. Kruckeberg. The hexose transporter family of *Saccharomyces cerevisiae*. *Arch Microbiol*, 166:283–292, 1996.
- A.L. Kruckeberg and L.F. Bisson. The HXT2 Gene of *Saccharomyces cerevisiae* Is Required for High-Affinity Glucose Transport. *Mol Cell Biol*, 10(11):5903–5913, November 1990.
- S. Kuchin, V.K. Vyas, E. Kanter, S.-P. Hong, and M. Carlson. Std1p (Msn3p) positively regulates the Snf1 kinase in *saccharomyces cerevisiae*. *Genetics*, 163:507–514, 2003.
- E.J. Kurth-Kraczek, M.F. Hirshman, L.J. Goodyear, and W.W. Winder. 5'AMP-activated protein kinase activation causes GLUT4 translocation in skeletal muscle. *Diabetes*, 48: 1–5, August 1999.
- S. Kuttykrishnan, J. Sabina, L.L. Langton, M. Johnston, and M.R. Brent. A quantitative model of glucose signaling in yeast reveals an incoherent feed forward loop leading to a specific, transient pulse of transcription. *PNAS*, 107(38):16743–16748, September 2010.
- M. Kvarnström, K. Logg, A. Diez, K. Bodvard, and M. Käll. Image analysis algorithms for cell contour recognition in budding yeast. *Optics Express*, 16(17):12943–12957, August 2008.
- J.M. Kyriakis and J. Avruch. Mammalian Mitogen-Activated Protein Kinase Signal Transduction Pathways Activated by Stress and Inflammation. *Physiol Rev*, 81(2):807–869, April 2001.

- R. Lagunas. Sugar transport in *Saccharomyces cerevisiae*. *FEMS Microbiol Rev*, 104: 229–242, 1993.
- M. Lamkanfi, N. Festjens, W. Declercq, T. Vanden Berghe, and P. Vandenabeele. Caspases in cell survival, proliferation and differentiation. *Cell Death Differ*, 14(1):44–55, January 2007.
- M.C. Lawrence, A. Jivan, C. Shao, L. Duan, D. Goad, E. Zaganjor, J. Osborne, K. McGlynn, S. Stippec, S. Earnest, W. Chen, and M.H. Cobb. The roles of MAPKs in disease. *Cell Res*, 18(4):436–442, April 2008. ISSN 1001-0602.
- A. Levitzki. Targeting signal transduction for disease therapy. *Curr Opin Cell Biol*, 8(2): 239–244, April 1996.
- J.M. Lizcano, O. Göransson, R. Toth, M. Deak, N.A. Moorice, J. Boudeau, S.A. Hawley, L. Udd, T.P. Mäkelä, D.G. Hardie, and D.R. Alessi. LKB1 is a master kinase that activates 13 kinases of the AMPK subfamily, including MARK/PAR-1. *EMBO J*, 23(4):833–843, February 2004.
- M. Llorens, J.C. Nuño, and F. Montero. Transient times in linear metabolic pathways under constant affinity constraints. *Biochem J*, 327(2):493–498, October 1997.
- M. Llorens, J.C. Nuño, Y. Rodríguez, E. Meléndez-Hevia, and F. Montero. Generalization of the Theory of Transition Times in Metabolic Pathways: A Geometrical Approach. *Biophys J*, 77(1):23–36, July 1999.
- K. Ludin, R. Jiang, and M. Carlson. Glucose-regulated interaction of a regulatory subunit of protein phosphatase 1 with the Snf1 protein kinase in *Saccharomyces cerevisiae*. *PNAS*, 95(11):6245–6250, May 1998.
- Z. Luo, M. Zang, and W. Guo. AMPK as a metabolic tumor suppressor: control of metabolism and cell growth. *Future Oncol*, 6(3):457–470, March 2011.
- C.J. Marshall. Specificity of receptor tyrosine kinase signaling: Transient versus sustained extracellular signal-regulated kinase activation. *Cell*, 80(2):179–185, January 1995.
- A.-S. Marsin, L. Bertrand, M.H. Rider, J. Deprez, C. Beauloye, M.F. Vincent, G. van den Berghe, D. Carling, and L. Hue. Phosphorylation and activation of heart PFK-2 by AMPK has a role in the stimulation of glycolysis during ischaemia. *Curr Biol*, 10(20): 1247–1255, October 2000.
- W. Materi and D.S. Wishart. Computational systems biology in drug discovery and development: methods and applications. *Drug Discov Today*, 12(7/8):295–303, April 2007.

Bibliography

- R.R. McCartney and M.C. Schmidt. Regulation of snf1 kinase. *J Biol Chem*, 276(39):36460–36466, September 2001.
- R.R. McCartney, E.M. Rubenstein, and M.C. Schmidt. Snf1 kinase complexes with different beta subunits display stress-dependent preferences for the three Snf1-activating kinases. *Curr Genet*, 47(6):335–344, 2005.
- G.F. Merrill, E.J. Kurth, D.G. Hardie, and W.W. Winder. AICA riboside increases AMP-activated protein kinase, fatty acid oxidation, and glucose uptake in rat muscle. *Am J Physiol Endoc M*, 273(6):1107–1112, 1997.
- T. Millat, E. Bullinger, J. Rohwer, and O. Wolkenhauer. Approximations and their Consequences for Dynamic Modelling of Signal Transduction Pathways. *Math Biosci*, 207(1):40–57, May 2007.
- T. Millat, S.N. Sreenath, R.P. Soebiyanto, J. Avva, K.-H. Cho, and O. Wolkenhauer. The role of dynamic stimulation pattern in the analysis of bistable intracellular networks. *BioSystems*, 92(3):270–281, June 2008.
- T. Millat, S. Frey, and O. Wolkenhauer. Quantitative measures for signalling pathways and signals with non-zero basal levels. *in preparation*, 2010.
- S.E. Mills, D.W. Foster, and J.D. McGarry. Interaction of malonyl-CoA and related compounds with mitochondria from different rat tissues. *Biochem J*, 214(1):83–91, July 1983.
- H. Misawa, M. Koshioka, K. Sasaki, N. Kitamura, and H. Masuhara. Three-dimensional optical trapping and laser ablation of a single polymer latex particle in water. *J Appl Phys*, 70(7):3829–3836, October 1991.
- K.I. Mitchelhill, D. Stapleton, G. Gao, C. House, B. Michell, F. Katsis, L.A. Witters, and B.E. Kemp. Mammalian AMP-activated protein kinase shares structural and functional homology with the catalytic domain of yeast Snf1 protein kinase. *J Biol Chem*, 269(4):2361–2364, January 1994.
- M. Momcilovic, S.-P. Hong, and M. Carlson. Mammalian TAK1 activates Snf1 protein kinase in yeast and phosphorylates AMP-activated protein kinase in vitro. *J Biol Chem*, 281(35):25336–25343, September 2006.
- M. Momcilovic, S.H. Iram, Y. Liu, and M. Carlson. Roles of the Glycogen-binding Domain and Snf4 in glucose inhibition of SNF1 Protein Kinase. *J Biol Chem*, 283(28):19521–19529, July 2008.

- H. Moriya and M. Johnston. Glucose sensing and signaling in *saccharomyces cerevisiae* through the Rgt2 glucose sensor and casein kinase i. *PNAS*, 101(6):1572–1577, February 2004.
- A.L. Mosley, J. Lakshmanan, B.K. Aryal, and S. Özcan. Glucose-mediated phosphorylation converts the transcription factor Rgt1 from a repressor to an activator. *J Biol Chem*, 278:10322–10327, 2003.
- D.M. Muoio and C.B. Newgard. Molecular and metabolic mechanisms of insulin resistance and β -cell failure in type 2 diabetes. *Nat Rev Mol Cell Biol*, 9:193–205, March 2008.
- L.O. Murphy and J. Blenis. MAPK signal specificity: the right place at the right time. *Trends Biochem Sci*, 31(5):268–275, May 2006.
- J. Nakabayashi and A. Sasaki. Optimal phosphorylation step number of intracellular signal-transduction pathway. *J Theor Biol*, 233:413–421, 2004.
- N. Nath, R.R. McCartney, and M.C. Schmidt. Yeast Pak1 kinase associates with and activates Snf1. *Mol Cell Biol*, 23(11):3909–3917, 2003.
- J.S. Oakhill, Z.-P. Chen, J.W. Scott, R. Steel, L.A. Castelli, N. Ling, S.L. Macaulay, and B.E. Kemp. β -Subunit myristoylation is the gatekeeper for initiating metabolic stress sensing by AMP-activated protein kinase (AMPK). *PNAS*, 107:19237–19241, 2010.
- J. Östling and H. Ronne. Negative control of the Mig1p repressor by Snf1p-dependent phosphorylation in the absence of glucose. *Eur J Biochem*, 252(1):162–168, 1998.
- S. Özcan. Two different signals regulate repression and induction of gene expression by glucose. *J Biol Chem*, 277(49):46993–46997, 2002.
- S. Özcan and M. Johnston. Two Different Repressors Collaborate To Restrict Expression of the Yeast Glucose Transporter Genes HXT2 and HXT4 to Low Levels of Glucose. *Mol Cell Biol*, 16(10):5536–5545, October 1996.
- S. Özcan and M. Johnston. Function and regulation of yeast hexose transporters. *Microbiol Mol Biol R*, 63(3):554–569, September 1999.
- S. Özcan, J. Dover, A.G. Rosenwald, S. Wölfl, and M. Johnston. Two glucose transporters in *Saccharomyces cerevisiae* are glucose sensors that generate a signal for induction of gene expression. *PNAS*, 93:12428–12432, 1996.
- S. Özcan, J. Dover, and M. Johnston. Glucose sensing and signaling by two glucose receptors in the yeast *Saccharomyces cerevisiae*. *EMBO J*, 17:2566–2573, 1998.

Bibliography

- G. Pearson, F. Robinson, T.B. Gibson, B. Xu, M. Karandikar, K. Berman, and M.H. Cobb. Mitogen-Activated Protein (MAP) Kinase Pathways: Regulation and Physiological Functions. *Endocr Rev*, 22(2):153–183, April 2001.
- R. Pepperkok and J. Ellenberg. High-throughput fluorescence microscopy for systems biology. *Nat Rev Mol Cell Biol*, 7:690–696, September 2006.
- D. Petranovic, K. Tyo, G.N. Vemuri, and J. Nielsen. Prospects of yeast systems biology for human health: integrating lipid, protein and energy metabolism. *FEMS Yeast Res*, 10:1046–1059, 2010.
- R. Phillips and R. Milo. A feeling for the numbers in biology. *PNAS*, 106(51):21465–21471, December 2009.
- P. Polak and M.N. Hall. mTOR and the control of whole body metabolism. *Curr Opin Cell Biol*, 21(2):209–218, 2009.
- M. Raman, W. Chen, and M.H. Cobb. Differential regulation and properties of MAPKs. *Oncogene*, 26(22):3100–3112, May 2007. ISSN 0950-9232.
- J. Ramos, K. Szkutnicka, and V.P. Cirillo. Relationship between low- and high-affinity glucose transport systems of *Saccharomyces cerevisiae*. *J Bacteriol*, 170(11):5375–5377, November 1988.
- E. Reifengerger, E. Boles, and M. Ciriacy. Kinetic characterization of individual hexose transporters of *Saccharomyces cerevisiae* and their relation to the triggering mechanisms of glucose repression. *Eur J Biochem*, 245:324–333, 1997.
- L. Rensing, U. Meyer-Grahe, and P. Ruoff. Biological timing and the clock metaphor: Oscillatory and hourglass mechanisms. *Chronobiol Int*, 18(3):329–369, May 2001. ISSN 0742-0528.
- M. Rizzi, U. Theobald, E. Querfurth, T. Rohrhirsch, M. Baltes, and M. Reuss. In Vivo Investigations of Glucose Transport in *Saccharomyces cerevisiae*. *Biotechnol Bioeng*, 49:316–327, 1996.
- A.H. Romano. Facilitated Diffusion of 6-Deoxy-D-Glucose in Bakers’ Yeast: Evidence Against Phosphorylation-Associated Transport of Glucose. *J Bacteriol*, 152(3):1295–1297, December 1982.
- F.W.D. Rost. *Fluorescence Microscopy*, volume 2. Cambridge University Press, 1995.
- E.M. Rubenstein, R.R. McCartney, C. Zhang, K.M. Shokat, M.K. Shirra, K.M. Arndt, and Schmidt M.C. Access denied: Snf1 activation loop phosphorylation is controlled by

- availability of the phosphorylated threonine 210 to the PP1 phosphatase. *J Biol Chem*, 283(1):222–230, 2008.
- H. Rubinfeld and R. Seger. The ERK Cascade. *Mol Biotechnol*, 31:151–174, 2005.
- W. Sabbagh, L.J. Flatauer, A.J. Bardwell, and L. Bardwell. Specificity of MAP Kinase Signaling in Yeast Differentiation Involves Transient versus Sustained MAPK Activation. *Mol Cell*, 8, 2001.
- K. Sakamoto, O. Göransson, D.G. Hardie, and D.R. Alessi. Activity of LKB1 and AMPK-related kinases in skeletal muscle: effects of contraction, phenformin, and AICAR. *Am J Physiol Endoc M*, 287(2):319–317, 2004.
- I. Salt, J.W. Celler, S.A. Hawley, A. Prescott, A. Woods, D. Carling, and D.G. Hardie. AMP-activated protein kinase: greater AMP dependence, and preferential nuclear localization, of complexes containing the $\alpha 2$ isoform. *Biochem J*, 334:177–187, 1998.
- I.P. Salt, J.M. Connell, and G.W. Gould. 5-aminoimidazole-4-carboxamide ribonucleoside (AICAR) inhibits insulin-stimulated glucose transport in 3T3-L1 adipocytes. *Diabetes*, 49(10):1649–1656, 2000.
- M.J. Sanders, P.O. Grondin, B.D. Hegarty, M.A. Snowden, and D. Carling. Investigating the mechanism for AMP activation of the AMP-activated protein kinase cascade. *Biochem J*, 403:139–148, 2007.
- G.M. Santangelo. Glucose signaling in *Saccharomyces cerevisiae*. *Microbiol Mol Biol R*, 70(1):253–282, March 2006.
- P. Sanz, G.R. Alms, T.A.J. Haystead, and M. Carlson. Regulatory interactions between the Reg1-Glc7 protein phosphatase and the Snf1 protein kinase. *Mol Cell Biol*, 20(4):1321–1328, February 2000.
- D.B. Savage, K.F. Petersen, and G.I. Shulman. Disordered lipid metabolism and the pathogenesis of insulin resistance. *Physiol Rev*, 87(2):507–520, 2007.
- J.E. Schaffer. Lipotoxicity: when tissues overeat. *Curr Opin Lipidol*, 14(3):281–287, June 2003.
- J. Schlessinger. Cell Signaling by Receptor Tyrosine Kinases. *Cell*, 103(2):211–225, October 2000.
- H. Schmidt and M. Jirstrand. Systems Biology Toolbox for MATLAB: a computational platform for research in systems biology. *Bioinformatics*, 22(4):514–515, February 2006.

Bibliography

- M.C. Schmidt and R.R. McCartney. β -subunits of Snf1 kinase are required for kinase function and substrate definition. *EMBO J*, 19(18):4936–4943, 2000.
- S. Schnell and C. Mendoza. Closed Form Solution for Time-dependent Enzyme Kinetics. *J Theor Biol*, 187(2):207–212, July 1997.
- G. Schwarz. Kinetic Analysis by Chemical Relaxation Methods. *Rev Mod Phys*, 40(1):206–218, January 1968.
- I.H. Segel. *Enzyme Kinetics*. John Wiley and Sons, 1993.
- R. Seger and E.G. Krebs. The MAPK signaling cascade. *FASEB J*, 9(9):726–735, June 1995.
- D.B. Shackelford and R.J. Shaw. The LKB1-AMPK pathway: metabolism and growth control in tumor suppression. *Nat Rev Cancer*, 9:563–575, 2009.
- N.C. Shaner, M.Z. Lin, M.R. McKeown, P.A. Steinbach, K.L. Hazelwood, M.W. Davidson, and R.Y. Tsien. Improving the photostability of bright monomeric orange and red fluorescent proteins. *Nature Methods*, 5(6):545–551, June 2008.
- Y.D. Shaul and R. Seger. The MEK/ERK cascade: From signaling specificity to diverse functions. *Biochim Biophys Acta*, 1773(8):1213–1226, August 2007.
- R.J. Shaw, M. Kosmatka, N. Bardeesy, R.L. Hurley, L.A. Witters, R.A. DePinho, and L.C. Cantley. The tumor suppressor LKB1 kinase directly activates AMP-activated kinase and regulates apoptosis in response to energy stress. *PNAS*, 101(10):3329–3335, March 2004.
- G.I. Shulman. Cellular mechanisms of insulin resistance. *J Clin Invest*, 106(2):171–176, July 2000.
- M. Smedh, C. Beck, K. Sott, and M. Goksör. Cellstress - an open source image-analysis software for single-cell analysis. *Proceedings SPIE*, 2010.
- B. Smets, R. Ghillebert, P. De Snijder, M. Binda, E. Swinnen, C. De Virgilio, and J. Wind-erickx. Life in the midst of scarcity: adaptations to nutrient availability in *Saccharomyces cerevisiae*. *Curr Genet*, 56:1–32, 2010.
- F.C. Smith, S.P. Davies, W.A. Wilson, D. Carling, and D.G. Hardie. The SNF1 kinase complex from *saccharomyces cerevisiae* phosphorylates the transcriptional repressor Mig1p in vitro at four sites within or near regulatory domain 1. *FEBS J*, 453(1-2):219–223, June 1999.

- L. Song, E.J. Hennink, I.T. Young, and H.J. Tanke. Photobleaching Kinetics of Fluorescein in Quantitative Fluorescence Microscopy. *Biophys J*, 68:2588–2600, June 1995.
- K. Sott, E. Eriksson, and M. Goksör. *Lab-on-a-Chip Technology: Biomolecular Separation and Analysis*, volume 2, chapter 9 Acquisition of Single Cell Data in an Optical Microscope. Herold, K.E. and Rasooly, A., Caister Academic Press, 2009.
- D. Stapleton, G. Gao, B.J. Michell, J. Widmer, K. Mitchelhill, T. Teh, C.M. House, L.A. Witters, and B.E. Kemp. Mammalian 5-amp-activated protein kinase non-catalytic subunits are homologs of proteins that interact with yeast Snf1 protein kinase. *J Biol Chem*, 269(47):29343–29346, November 1994.
- S.C. Stein, A. Woods, N.A. Jones, M.D. Davison, and D. Carling. The regulation of AMP-activated protein kinase by phosphorylation. *Biochem J*, 345:437–443, 2000.
- G.R. Steinberg and B.E. Kemp. AMPK in health and disease. *Physiol Rev*, 89:1025–1078, July 2009.
- D.E. Steinmeyer and M.L. Shuler. Structured model for *Saccharomyces cerevisiae*. *Chem Eng Sci*, 44(9):2017–2030, 1989.
- A.C. Storer and A. Cornish-Bowden. The kinetics of coupled enzyme reactions. Applications to the assay of glucokinase, with glucose 6-phosphate dehydrogenase as coupling enzyme. *Biochem J*, 141(1):205–209, July 1974.
- M. Suter, U. Riek, R. Tuerk, U. Schlattner, T. Wallimann, and D. Neumann. Dissecting the role of 5-AMP for allosteric stimulation, activation, and deactivation of AMP-activated protein kinase. *J Biol Chem*, 281:32207–32216, 2006.
- C.M. Sutherland, S.A. Hawley, R.R. McCartney, A. Leech, M.J.R. Stark, M.C. Schmidt, and D.G. Hardie. Elm1p is one of three upstream kinases for the *Saccharomyces cerevisiae* SNF1 complex. *Curr Biol*, 13(15):1299–1305, 2003.
- B. Teusink, J.A. Diderich, H.V. Westerhoff, K. van Dam, and M.C. Walsh. Intracellular Glucose Concentration in Derepressed Yeast Cells Consuming Glucose Is High Enough To Reduce the Glucose Transport Rate by 50%. *J Bacteriol*, 180(3):556–562, February 1998.
- B. Teusink, J. Passarge, C.A. Reijenga, E. Esgalhado, C.C. van der Weijden, M. Schepper, M.C. Walsh, B.M. Bakker, K. van Dam, H.V. Westerhoff, and J.L. Snoep. Can yeast glycolysis be understood in terms of *in vitro* kinetics of the constituent enzymes? Testing biochemistry. *Eur J Biochem*, 267:5313–5329, 2000.

Bibliography

- S. Thompson-Jaeger, J. François, J.P. Gaughran, and K. Tatchell. Deletion of SNF1 affects the nutrient response of yeast and resembles mutations which activate the adenylate cyclase pathway. *Genetics*, 129(3):697–706, 1991.
- N.V. Torres, J. Sicilia, and E. Melendez-Hevia. Analysis and characterization of transition states in metabolic systems. *Biochem J*, 276:231–236, 1991.
- M.C. Towler and D.G. Hardie. AMP-activated protein kinase in metabolic control and insulin signaling. *Circ Res*, 100:328–341, 2007.
- M.A. Treitel, S. Kuchin, and M. Carlson. Snf1 Protein Kinase Regulates Phosphorylation of the Mig1 Repressor in *Saccharomyces cerevisiae*. *Mol Cell Biol*, 18(11):6273–6280, November 1998.
- J. Tu and M. Carlson. The GLC7 type 1 protein phosphatase is required for glucose repression in *Saccharomyces cerevisiae*. *Mol Cell Biol*, 14(10):6789–6796, October 1994.
- J. Tu and M. Carlson. REG1 binds to protein phosphatase type 1 and regulates glucose repression in *Saccharomyces cerevisiae*. *EMBO J*, 14(23):5939–5946, December 1995.
- J. Tu, W. Song, and M. Carlson. Protein phosphatase type 1 interacts with proteins required for meiosis and other cellular processes in *Saccharomyces cerevisiae*. *Mol Cell Biol*, 16(8):4199–4206, August 1996.
- J.J. Tyson, K.C. Chen, and B. Novak. Sniffers, buzzers, toggles and blinkers: dynamics of regulatory and signaling pathways in the cell. *Curr Opin Cell Biol*, 15(2):221–231, April 2003.
- D. Vaudry, P.J.S. Stork, P. Lazarovici, and L.E. Eiden. Signaling Pathways for PC12 Cell Differentiation: Making the Right Connections. *Science*, 296(5573):1648–1649, May 2002.
- A.I.F. Vaz and L.N. Vicente. A particle swarm pattern search method for bound constrained global optimization. *J Global Optim*, 39:197–219, 2007.
- C. Verduyn, E. Postma, W.A. Scheffers, and J.P. Van Dijken. Effect of benzoic acid on metabolic fluxes in yeasts: A continuous-culture study on the regulation of respiration and alcoholic fermentation. *Yeast*, 8(7):501–517, 1992.
- M. Vidal. A unifying view of 21st century systems biology. *FEBS Lett*, 583(24):3891–3894, December 2009. ISSN 0014-5793.
- O. Vincent, R. Townley, S. Kuchin, and M. Carlson. Subcellular localization of the Snf1 kinase is regulated by specific β subunits and a novel glucose signaling mechanism. *Genes Dev*, 15:1104–1114, 2001.

- B. Viollet, R. Mounier, J. Leclerc, A. Yazigi, M. Foretz, and F. Andreelli. Targeting AMP-activated protein kinase as a novel therapeutic approach for the treatment of metabolic disorders. *Diabetes Metab*, 33:395–402, 2007.
- E.O. Voit and M.L. Kemp. So, you want to be a systems biologist? Determinants for creating graduate curricula in systems biology. *IET Syst Biol*, 5(1):70–79, January 2011.
- E.O. Voit, Z. Qi, and G.W. Miller. Steps of Modeling Complex Biological Systems. *Pharmacopsychiatry*, 41(S 01):S78–S84, 2008.
- J.W. Wallis, G. Chrebet, G. Brodsky, M. Rolfe, and R. Rothstein. A Hyper-Recombination Mutation in *S. cerevisiae* Identifies a Novel Eukaryotic Topoisomerase. *Cell*, 58:409–419, 1989.
- Xiao Wang, Nan Hao, Henrik G Dohlman, and Timothy C Elston. Bistability, stochasticity, and oscillations in the mitogen-activated protein kinase cascade. *Biophys J*, 90(6):1961–1978, March 2006.
- S.M. Warden, C. Richardson, J. O'Donnell Jr., D. Stapleton, B.E. Kemp, and L.A. Witters. Post-translational modifications of the β -1 subunit of AMP-activated protein kinase affect enzyme activity and cellular localization. *Biochem J*, 354:275–283, 2001.
- T.F. Weiss. *Cellular Biophysics: Transport*, volume 1 of *Bradford Books*. MIT Press, Cambridge, 1996.
- C. Widmann, S. Gibson, M.B. Jarpe, and G.L. Johnson. Mitogen-Activated Protein Kinase: Conservation of a Three-Kinase Module From Yeast to Human. *Physiol Rev*, 79(1):143–180, January 1999.
- W.A. Wilson, S.A. Hawley, and D.G. Hardie. Glucose repression/derepression in budding yeast: SNF1 protein kinase is activated by phosphorylation under derepressing conditions, and this correlates with a high AMP:ATP ratio. *Curr Biol*, 6(11):1426–1434, 1996.
- W.W. Winder and D.G. Hardie. AMP-activated protein kinase, a metabolic master switch: possible roles in type 2 diabetes. *Am J Physiol Endoc M*, 277:1–10, 1999.
- O. Wolkenhauer. Defining systems biology: An engineering perspective. *IET Syst Biol*, 1(4):204–206, 2007.
- O. Wolkenhauer, H. Kitano, and K.-H. Cho. Systems Biology: Looking at Opportunities and Challenges in Applying Systems Theory to Molecular and Cell Biology. *IEEE Contr Syst Mag*, 23(4):38–48, August 2003.

Bibliography

- A. Woods, M.R. Munday, J. Scott, X. Yang, M. Carlson, and D. Carling. Yeast SNF1 is functionally related to mammalian AMP-activated protein kinase and regulates acetyl-CoA carboxylase in vivo. *J Biol Chem*, 269(30):19509–19515, July 1994.
- A. Woods, P.C.F. Cheung, F.C. Smith, M.D. Davison, J. Scott, R.K. Beri, and D. Carling. Characterization of AMP-activated protein kinase β and γ subunits. *J Biol Chem*, 271(17):10282–10290, April 1996.
- A. Woods, S.R. Johnstone, K. Dickerson, F.C. Leiper, L.G.D. Fryer, D. Neumann, U. Schlattner, T. Wallimann, M. Carlson, and D. Carling. LKB1 is the upstream kinase in the AMP-activated protein kinase cascade. *Curr Biol*, 13(22):2004–2008, November 2003.
- A. Woods, K. Dickerson, R. Heath, S.-P. Hong, M. Momcilovic, S.R. Johnstone, M. Carlson, and D. Carling. Ca²⁺/calmodulin-dependent protein kinase kinase- β acts upstream of AMP-activated protein kinase in mammalian cells. *Cell Met*, 2:21–33, July 2005.
- B. Xiao, R. Heath, P. Saiu, F.C. Leiper, P. Leone, C. Jing, P.A. Walker, L. Haire, J.F. Eccleston, C.T. Davis, S.R. Martin, D. Carling, and S.J. Gamblin. Structural basis for AMP binding to mammalian AMP-activated protein kinase. *Nature*, 449:496–501, September 2007.
- B. Xiao, M.J. Sanders, E. Underwood, R. Heath, F.V. Mayer, D. Carmena, C. Jing, P.A. Walker, J.F. Eccleston, L.F. Haire, P. Saiu, S.A. Howell, R. Aasland, S.R. Martin, D. Carling, and S.J. Gamblin. Structure of mammalian AMPK and its regulation by ADP. *Nature*, 0:1–4, 2011.
- W. Xiong and J.E. Ferrel Jr. A positive-feedback-based bistable 'memory module' that governs a cell fate decision. *Nature*, 426:460–465, November 2003.
- T. Yamauchi, J. Kamon, H. Waki, Y. Terauchi, N. Kubota, K. Hara, Y. Mori, T. Ide, K. Murakami, N. Tsuboyama-Kasaoka, O. Ezaki, Y. Akanuma, O. Gavrilova, C. Vinson, M.L. Reitman, H. Kagechika, K. Shudo, M. Yoda, Y. Nakano, K. Tobe, R. Nagai, S. Kimura, M. Tomita, P. Froguel, and T. Kadowaki. The fat-derived hormone adiponectin reverses insulin resistance associated with both lipoatrophy and obesity. *Nat Med*, 7(8):941–946, August 2001.
- X. Yang, R. Jiang, and M. Carlson. A family of proteins containing a conserved domain that mediates interaction with the yeast SNF1 protein kinase complex. *EMBO J*, 13(24):5878–5886, December 1994.
- T. Ye, K. Elbing, and S. Hohmann. The pathway by which the yeast protein kinase Snf1p controls acquisition of sodium tolerance is different from that mediating glucose regulation. *Microbiology*, 154:2814–2826, 2008.

- G. Zadra, C. Priolo, A. Patnaik, and M. Loda. New Strategies in Prostate Cancer: Targeting Lipogenic Pathways and the Energy Sensor AMPK. *Clin Cancer Res*, 16:3322–3328, 2010.
- S. Zaman, S.I. Lippman, X. Zhao, and J.R. Broach. How *Saccharomyces* responds to nutrients. *Annu Rev Genet*, 42:27–81, 2008.
- L. Zhou, S.S. Deepa, J.C. Etzler, J. Ryu, X. Mao, Q. Fang, D.D. Liu, J.M. Torres, W. Jia, J.D. Lechleiter, F. Liu, and L.Q. Dong. Adiponectin activates AMPK in muscle cells via APPL1/LKB1- and PLC/Ca²⁺/CaMKK-dependent pathways. *J Biol Chem*, 284(33):22426–22435, August 2009.

Publications

S.Frey, T.Millat, R.Garcia Salcedo, D.Bosch, G.Beltran, K.Elbing, G.Vemuri, S.Hohmann, O.Wolkenhauer: Dynamics of hexose transporters in *Saccharomyces cerevisiae* upon glucose pulses. Submitted for publication

S.Frey, K.Sott, M.Smedh, T.Millat, P.Dahl, O.Wolkenhauer, M.Goksör: A mathematical analysis of nuclear intensity dynamics for Mig1-GFP under consideration of bleaching effects and background noise in *Saccharomyces cerevisiae*. Molecular BioSystems 7(1), 215-223 , January 2011

S.Frey, O.Wolkenhauer, T.Millat: Quantifying properties of cell signaling cascades. In ‘Control-Theoretic Approaches in Systems Biology’, P.A.Iglesias and B.Ingalls (editors), MIT press, November 2009

S.Frey, T.Millat, S.Hohmann, O.Wolkenhauer: How quantitative measures unravel design principles in multi-stage phosphorylation cascades. Journal of Theoretical Biology, 254, 27-36, 2008

Selbständigkeitserklärung

Hiermit versichere ich, dass ich diese Arbeit selbständig verfasst habe. Es wurden ausschließlich die angegebenen Quellen und Hilfsmittel benutzt, sowie Zitate kenntlich gemacht.

Theses for the doctoral research

1. The carrier model, which describes the transport of molecules across the cell membrane, assumes a constant contribution of high and low affinity transporters. It is shown that the carrier model is not sufficient to describe the glucose uptake in *S. cerevisiae* for different batch experiments due to the neglect of a dynamic contribution of the transporter in the cell membrane. These results point towards a significant reorganisation of the membrane transporters.
2. An analysis of high and low affinity transporters, as a function of glucose concentration at steady-state, supports the finding of a reciprocal relationship between the high and low affinity transporters as reported by Ramos and co-workers in 1988.
3. The estimated value for the rate of transport efficiency of a high affinity transporter reveals a higher value compared to a low affinity transporter. The lower concentration of high affinity transporters compared to low affinity transporters thus indicates a compensation through a higher efficiency of the transporters, whereas in comparison the highly concentrated low affinity transporters operate less efficiently.
4. The identity of the glucose signal, which regulates Snf1 (de)phosphorylation, still remains elusive. This work shows the derivation of a glucose-regulated stimulus, which can be used as the input function of glucose-regulated signalling pathways, such as the Snf1 pathway. It serves as a template to display and compare alternative pathway structures.
5. Mig1-GFP data, generated by the technique fluorescence microscopy, suffers from bleaching effects and background noises. This work introduces a mathematical approach, which allows for the prediction of Mig1 dynamics as they would occur without bleaching and background noises. The processed data is thereon usable for mathematical modelling of signal transduction pathways.
6. In this research, an iterative cycle of data-driven modelling and model-driven experimentation for the Snf1 pathway was performed. It was found that, in addition to regulation by the kinase and phosphatase, the consideration of a glucose-regulated step is essential in order to explain the dynamics of Mig1 (de)phosphorylations.
7. In addition to establishing a signalling pathway model, the dynamic properties of its pathway components, such as the average time or duration of activation, can be determined. In order to compare different pathway structures, a two-dimensional optimality criterion is defined. It signifies that a cell aims at a fast signal response while keeping the duration of activated signal as short as possible. This strategy may ensure a fast signal transfer while at the same time bordering from noise.
8. Signalling pathways occur in a huge variety of structural designs. Applying quantitative measures for comparison of different pathway structures suggests that the characteristic design of the MAPK pathway favours a fast response to a stimulus in combination with a sufficiently long duration.